Preparation of activated carbon to remove heavy metals Cd(II) and Cr(VI) from aqueous solutions

February 2020

CHU Bei

Graduate School of Science and Engineering

Chiba University

（千葉大学審査学位論文）

水溶液中の二価カドミウムイオンと六価クロムイオンの吸着除去のための活性炭の調製

2020年　2月

褚　備

融合理工学府

先進理化学専攻

共生応用化学コース

Ph.D. thesis submitted in partial fulfillment of the requirements for the degree of Ph.D. in Graduate School of Science and Engineering, Chiba University, Japan.

Affiliation:

Department of Applied Chemistry and Biotechnology, Division of Advanced Science and Technology, Graduate School of Science and Engineering, Chiba University

1-33, Yayoi-cho, Inage-ku, Chiba-shi, Chiba, 263-8522, Japan

Supervisor:

Prof. Motoi Machida, Department of Applied Chemistry and Biotechnology, Graduate School of Engineering, Chiba University

Examiners:

Prof. Shogo SHIMAZU, Department of Applied Chemistry and Biotechnology, Graduate School of Engineering, Chiba University

Prof. Satoshi SATO, Department of Applied Chemistry and Biotechnology, Graduate School of Engineering, Chiba University

Prof. Takashi KARATSU, Department of Applied Chemistry and Biotechnology, Graduate School of Engineering, Chiba University

Prof. Motoi MACHIDA, Department of Applied Chemistry and Biotechnology, Graduate School of Engineering, Chiba University

Assistant Prof. Yoshimasa AMANO, Department of Applied Chemistry and Biotechnology, Graduate School of Engineering, Chiba University

DECLARATION

I hereby declare that this submission is my own work and that, to the best of my knowledge and belief, it contains no material which to a substantial extent has been accepted for the award of any other degree or diploma of the university or other institute of higher learning, except where due acknowledgement has been made in the text.

CHU Bei, Chiba, January 2020

ACKNOWLEDGEMENTS

According to the Chiba University rule, the contents of the "ACKNOWLEDGEMENTS" are not described in the electric file of my doctoral thesis.

ABSTRACT

Heavy metal pollution is harmful to the environment, which seriously endangers social development and people's health. The removal of heavy metals is one of the hot issues of current research. Since the heavy metal itself has a small ionic radius and is easily adsorbed by the micropores of the activated carbon, it is an ideal treatment method for removing heavy metals. Heavy metal ions are divided into anions and cations. Among them, the cationic heavy metal represents Cd(II), and the anion heavy metal represents Cr(VI), which is harmful to the environment and the human body. For cadmium, the surface functional groups of activated carbon can provide attraction to the adsorbate and accelerate the adsorption process. Therefore, in order to increase the adsorption amount of Cd(II), the most common method is to load the functional group on the surface of the activated carbon. For Cr(VI), it is possible to increase the specific surface area and increase the nitrogen content to increase the quaternary nitrogen to increase the adsorption amount.

Based on the different characteristics of Cd(II) and Cr(VI), this study uses different activation methods to produce activated carbon with raw materials, thereby increasing the adsorption amount and adsorption rate. This study has been studied from the following five aspects:

(1) Isotherm, kinetic and thermodynamic studies for adsorption of Cd(II) from aqueous solutions onto mesoporous bamboo activated carbon. In this study, activated carbons were prepared from Moso bamboo by N_2 carbonization under N_2 gas

atmosphere, using H_3PO_4 as activator and oxidized by $(NH_4)_2S_2O_8$ for the removal of Cd(II). The physicochemical properties of the prepared activated carbons (BAP) and commercially available bead-shaped activated carbon (BAC) were compared. The characterization results showed that BAP had higher surface area and mesopore volume compared with BAC, and the oxidized sample BAP1 had more surface functional groups. Adsorption equilibrium data were analyzed by the Langmuir and the Freundlich models. The adsorption equilibrium data were well described by the Langmuir model and the maximum adsorption capacity of BAP1-Na was found to be 0.721 mmol/g, which was greater than that of BAC1-Na. In the adsorption thermodynamics parameters study, the adsorption was spontaneous, favorable and exothermic. The experimental kinetic data were best fitted to pseudo-second-order model, and adsorption rate of BAP1-Na was faster than that of BAC1-Na. The prepared BAC1-Na showed better adsorption capacity for Cd(II) adsorption, and pH, oxidation time, adsorbent dosage and temperature also affected adsorption capacity of Cd(II).

(2) Adsorption, reduction and regeneration behavior of high surface area activated carbon in removal of Cr(VI). Hexavalent chromium Cr(VI) pollution problem has become increasingly serious. In this study, activated carbon CGP-K3-800 was prepared from commercial Norit CGP by using KOH as activator for the removal of Cr(VI). The surface area of CGP-K3-800 was increased up to 3098 m^2/g. The adsorbent CGP-K3-800 exhibited an adsorption capacity of 4.99 mmol/g (259.5 mg/g) in the solution pH of 2 at 25℃, which was 1.64 times larger than that of the original CGP. Adsorption

equilibrium data were described and analyzed by the Langmuir models, indicating that Cr(VI) adsorption on CGP-K3-800 tended to be monolayer adsorption. The calculated thermodynamic parameters showed that the adsorption process of Cr(VI) onto CGP-K3-800 was an endothermic process. By investigating the effect of pH, the acid condition is conducive to the adsorption and reduction process of Cr(VI). CGP-K3-800 had good regeneration performance, and the reduction ability of Cr(VI) on the CGP-K3-800 would be gradually lost. CGP-K3-800 shows a higher adsorption capacity and better regeneration performance in removal of Cr(VI), can be applied as a promising adsorbent for the removal of Cr(VI) from wastewater.

(3) Adsorption behavior of Cr(VI) by N-doped biochar was derived from bamboo. In this study, N-doped biochar BZ-9.5AG-30min was prepared from bamboo by using $ZnCl_2$ as activator and heat treated at 950℃ under NH_3 gas flow for the removal of Cr(VI). The adsorbent was characterized by BET, and the amount of introduced nitrogen content and nitrogen species on BZ-9.5AG-30min was examined by CHN elemental analyzer and X-ray photoelectron spectroscopy, respectively, Herein, the obtained BZ-9.5AG-30min had a high specific surface area (1610 m^2/g) and high N content (4.52%). The pH of the solutions had a great influence on the adsorption process, indicating that the acid condition is conducive to the adsorption process of Cr(VI). Adsorption equilibrium data of Cr(VI) were analyzed by the Langmuir and the Freundlich models. The adsorption equilibrium data were well described by the Langmuir model, and BZ-9.5AG-30min had excellent adsorption capacity for Cr(VI)

(4.31 mmol/g). BZ-9.5AG-30min showed superior recyclability, and after five times regenerations, the adsorption capacity of BZ-9.5AG-30min still had 63% of the initial adsorption capacity.

(4) Preparation of bean dreg derived N-doped biochar with high adsorption for Cr(VI). In this study, N-doped biochar BDC-STM30-10.0HT was prepared from bean dreg by using steam activation and heat treated at 1000℃ under helium gas flow for the removal of Cr(VI). The properties of the prepared carbon catalysts are characterized by CHN elemental analyzer, SEM, N_2 adsorption and XPS techniques, and the obtained bean dreg biochar BDC-STM30-10.0HT had a high specific surface area (1004 m^2/g) and high quaternary nitrogen content (1.11%). The results of batch adsorption experiments show that the Cr(VI) adsorption capacity of biochar was positively correlated with the specific surface area, but it does not only depend on the specific surface area, but also other factors. The quaternary nitrogen content also has some influence on the adsorption capacity. The adsorption equilibrium data were well described by the Langmuir model, and BDC-STM30-10.0HT has excellent adsorption capacity for Cr(VI) (3.30 mmol/g). BDC-STM30-10.0HT showed superior recyclability, and after five times regenerations, the adsorption capacity of BDC-STM30-10.0HT still had 54% of the initial adsorption capacity.

(5) Preparation of bamboo-based oxidized biochar for simultaneous removal of Cd(II) and Cr(VI) from aqueous solutions. Cd(II) and Cr(VI) are highly toxic heavy metal ions, which commonly coexist in industrial wastewater. In this study,

simultaneous removal of Cd(II) and Cr(VI) by a bamboo-based oxidized biochar (BZ-APS24h) was investigated. The biochar was modified by $ZnCl_2$ and oxidized with $(NH_4)_2S_2O_8$, and its structures as characterized by SEM, BET, elemental composition and XPS. Batch adsorption experiments for Cd(II) and Cr(VI) were carried out to explore the effects of oxidation time, pH, contact time, temperature and coexistence on its adsorption process. The results showed that the BZ-APS24h exhibited excellent adsorption performance for the removal of Cd(II) (0.27 mmol/g) and Cr(VI) (0.65 mmol/g). The adsorption data were fitted well with pseudo-second-order model and Langmuir isotherm. The pH of the solutions had a great influence on the adsorption process. The coexistence of Cd(II) and Cr(VI) affected the equilibrium pH after adsorption, and synergistic adsorption was observed.

List of contents

Chapter 1 General introduction

1.1 Source and harm of heavy metal wastewater

The world economy is now experiencing rapid development, but at the same time, the environmental problems caused by the development are also becoming more and more serious. Due to the acceleration of industrialization, electroplating, fuel, metallurgy, mining, and other industries are also rapidly expanding, and these industries are prone to heavy metal pollution during the production process, such as lead, cadmium, chromium, copper, nickel pollution, etc. in the production process [1]. Because heavy metal ions can not decompose on their own, easy to aggregate, and difficult to transform in the environment [2], heavy metal ions in the natural environment will eventually enter the human body through various channels, which will cause serious harm to human health. Therefore, heavy metal pollution control has become a research hotspot for environmental workers [3].

Unlike other organic pollutants, heavy metals tend to accumulate in living organisms, and the natural circulation system can not decompose heavy metals by itself. Therefore, heavy metal pollution is widely distributed in atmosphere, water, soil, and organisms [4]. In the water environment, heavy metals accumulate in aquatic organisms such as algae and fish through water bodies, and then enter the human body through the food chain and enrich in the body to enrich in the body [5]. When heavy metal is excessive, it will inhibit the activity of biological enzymes in the human body. When the heavy metals in the human body exceed the tolerance limit of the human body, they may cause poisoning and pose a threat to human life and health [6]. Heavy metal ions

are divided into anions and cations, Cd(II) is a cation and Cr(VI) is an anion.

1.1.1 Cadmium

Cadmium is a well-known, highly toxic metal found water. According to the guidelines of the World Health Organization, the allowable limit of cadmium in water is 0.003 mg/L [7, 8]. Once absorbed by the body, cadmium quickly binds to proteins and accumulates in the liver and kidneys [9]. Cadmium is also easily enriched in other organs of the human body, such as the spleen, pancreas, thyroid, and hair [10]. The damage caused by cadmium to the human body is mainly caused by diabetes and leading to bone metabolism and causing osteoporosis [11]. In water, cadmium mainly exists as the form of Cd(II) (Cd^{2+}).

1.1.2 Chromium

Chromium is a highly toxic heavy metal. Chromium salt is an important inorganic chemical product. It usually exists in the form of Cr(III) and Cr(VI) in the natural environment [12]. The chromium-containing wastewater is mainly derived from the chrome-plating of metal parts, inferior cosmetic raw materials, leather preparations, ceramic raw materials, industrial pigments, tanned leather, rubber, etc.; breathing through to stimulate and corrode the respiratory tract, can cause pharyngitis, bronchitis and other diseases; eating can cause abdominal discomfort and diarrhea, allergic dermatitis or eczema. Frequent exposure to or excessive intake of chromium, susceptible to rhinitis, tuberculosis, diarrhea, bronchitis, dermatitis, etc [13, 14].

Cr(VI) is mainly combined with oxygen to form chromate or dichromate. Chromium has a high oxidation state and solubility in the state of hexavalent chromium, resulting in its strong migration ability and toxicity. As with cadmium, chromium toxicity can accumulate through the food chain, causing people were poisoned [15]. Cr(VI) is generally considered to be 100 times more toxic than Cr(III) [16]. Cr(III) is easy to form oxides or hydroxides separated from water, thus reducing its toxicity. The common method of treating Cr(VI) in the industry is to reduce Cr(VI) to Cr(III). Excessive Cr(VI) not only causes serious harm to the human body but also inhibits the growth of plants and crops [17]. It interferes with the absorption of nutrients in the soil by plants, affecting the physiological activities and photosynthesis of plants and crops. Moreover, chromium (VI) can also flow into the food chain through polluted water sources, which poses a great threat to human health [18].

The main forms of Cr(VI) in the natural water environment are H_2CrO_4, $HCrO_4^-$, CrO_4^{2-}, and $Cr_2O_7^{2-}$. The following balance exists between various forms [19]:

$$H_2CrO_4 \leftrightarrow H^+ + HCrO_4^- \quad (1\text{-}1)$$

$$HCrO_4^- \leftrightarrow H^+ + CrO_4^{2-} \quad (1\text{-}2)$$

$$2HCrO_4^- \leftrightarrow Cr_2O_7 + H_2O \quad (1\text{-}3)$$

1.2 Heavy metal removal technology in water

Common methods for treating heavy metals in water are mainly divided into chemical methods, biological methods, physical-chemical methods [20].

1.2.1 Chemical methods

Chemical treatment methods include precipitation, flocculation, redox, and electrolysis. The precipitation method mainly produces insoluble matter precipitated by adjusting the pH of the whole solution, so that Cu(II), Zn(II), Cr(III), Cd(II) and Ag(II) are converted into precipitates for removal [21]. For Cr(VI), reducing agents such as SO_2, $NaHSO_4$, Na_2SO_4, Fe, $FeSO_4$, etc. are used [22]. Under the acidic condition of pH 2-4, Cr(VI) is first reduced to Cr(III), and Cr(III) is precipitated from $Cr(OH)_3$ by using $Ca(OH)_2$, NaOH, etc. under alkaline conditions of pH 8-9 [23]. The advantages of chemical precipitation methods are a simple process, easy operation, and suitable for water with high concentration of heavy metals. However, it is difficult to recover heavy metals after precipitation and easy to cause secondary pollution [24].

1.2.2 Biological methods

Biological treatment methods usually use microorganisms, biofilm, and activated sludge to treat wastewater. Due to the strong metabolic functions of microorganisms, algae, and aquatic plants, heavy metal ions in water can be removed through these metabolic functions, thus reducing the concentration of heavy metals in water [25]. Among them, the remediation of microorganisms and algae method is to use microorganisms and algae in natural water to absorb or reduce heavy metal ions in water [26]. Another common method is the bacterial method. Bacteria can be used as biosorption materials because of their small size, ubiquitous presence in the environment and good adaptability to the natural environment. Algae can also adsorb

heavy metal ions very well. However, the disadvantage of biomass-based adsorbents is that they require higher culture conditions [27]. Meanwhile, due to the limited tolerance of microorganisms to heavy metal ions, biological methods are still only suitable for treating low-concentration wastewater, and at the same time, there are disadvantages such as slow metabolism of microorganisms [28].

1.2.3 Physical-chemical methods

Common physical-chemical treatment methods include ion exchange method, membrane separation method, and adsorption method.

(1) Ion exchange method

Ion exchange is a method of removing heavy metal ions from water by using functional groups on the surface of ion exchange resin. Exchange ions on functional groups can be exchanged with heavy metal ions, thus removing heavy metals. Common ion exchange resins are cation exchange resins, anion exchange resins, chelating resins, and humic acid resins [29]. Usually, OH^- and other exchangeable anions on the anion ion exchange resins can be exchanged with CrO_4^{2-} or $Cr_2O_7^{2-}$ in wastewater to replace Cr(VI); for cation exchange resins, Na^+ and H^+ ions can be exchanged with Cd^{2+}, Ag^+, Pb^{2+} or other heavy metal cations in wastewater [30].

Ion exchange is one of the most ideal methods for the treatment of heavy metal ions. Its advantages are large processing capacity, good effluent quality, high selectivity, selective recovery of precious metals from wastewater containing various metal ions, and removal. However, the price of ion exchange resins is relatively high. Therefore,

the ion exchange method is less used in larger-scale wastewater treatment projects [31].

(2) Membrane separation method

As a new and efficient water treatment technology, membrane separation technology has attracted wide attention. [32]. The membrane separation process for wastewater treatment includes electrodialysis and reverse osmosis membranes [33]. Electrodialysis refers to the process of separating the heavy metal ions in the solution from the water by the selective permeability of the anion and cation exchange membranes in the solution under the action of a direct current electric field [34]. Electrodialysis treatment of wastewater requires sufficient conductance to increase the permeation efficiency, so the concentration of electrolyte in the treated water should not be too low. [35]. And the reverse osmosis membrane is a process in which pressure is applied to one side, and only water can penetrate so that other substances are trapped on the surface of the membrane. Reverse osmosis has the advantages of simple design and operation and has the advantages of high purification efficiency, short construction period, and environmental friendliness. However, during the operation, the membrane module has a complicated process, a short life span, and is easily contaminated [36].

(3) Adsorption method

The adsorption method is a method of treating wastewater using a porous solid adsorbent [37]. The adsorption force between the adsorbent and the adsorbate is divided into three categories: physical adsorption (adsorption by intermolecular forces), chemical adsorption (adsorption by chemical bond force), and exchange adsorption (heavy metal ions accumulate on the charged points on the surface of the adsorbent due

to electrostatic attraction and replace other ions) [38]. At present, these three adsorptions coexist in the process of wastewater adsorption. With the changes of adsorbents, adsorbates, and other factors, the dominant adsorption effect will change. There are many kinds of adsorbents. At present, the most commonly used adsorbent in industrial wastewater treatment is activated carbon, in addition to polymers, zeolites, bentonite, fly ash, natural minerals, agricultural and forestry wastes, and other carbonaceous adsorbents [39]. Among the methods of heavy metal wastewater treatment, the adsorption method has the advantages of high processing efficiency, simple operation, and low process cost and is one of the most widely used heavy metal sewage treatment technologies [40]. Many studies have proved that the activated carbon adsorption method is an effective technical method for the treatment of heavy metal pollution. Whether it is for single heavy metal ions or mixed pollution wastewater, activated carbon adsorption method has a good treatment effect [41].

1.3 Adsorption of heavy metals by activated carbon

Activated carbon has excellent adsorption capacity, mainly because of its well-developed pore structure and abundant surface functional groups [42]. Carbon pores are produced during the activation process. When heated at high temperatures, the organic matter in the raw material is removed, and many pores with different shapes and sizes are formed between the basic lattices. The main parameters of activated carbon are specific surface area, pore-volume, and pore size distribution. Generally, the larger the specific surface area and pore volume, the greater the adsorption capacity of

activated carbon [43]. International Union of Pure and Applied Chemistry (IUPAC) classifies pores into three categories according to their size: macropore with a pore diameter greater than 50 nm, mesopore with a pore diameter between 2 and 50 nm, and micropore with a pore diameter less than 2 nm. The micropores are the main contribution of activated carbon with a large specific surface area so that the biomass charcoal can absorb the molecules of the small molecules [44]. In the process of pyrolysis of biomass feedstock, as the pyrolysis temperature increases, the loss of H_2O, H_2, CO, CO_2, hydrocarbons, tar vapor, etc., volume decreases, but the formed carbon skeleton substantially retains the original pore structure characteristics of the raw material [45]. The macroporous structure of activated carbon is mainly composed of the honeycomb structure of the raw material, while the micropores are formed by the loss of carbon during the pyrolysis process and the shrinkage of the carbon framework. The micropore content determines the specific surface area of the activated carbon [46].

Conventional activated carbon activation methods are divided into physical activation method and chemical activation method. The physical activation method generally first carbonizes the raw materials, and then activates the materials at a high temperature with a gas such as water vapor or carbon dioxide. In the physical activation, the activated gas reacts with the carbon atom on the "active point" inside the carbon material, and forms a large number of pore structures by opening, expanding, and creating new pores [47]. The chemical activation method is a preparation process in which raw material and an activator are mixed according to a certain impregnation ratio, and carbonization is activated under anaerobic conditions, in which an activator is

embedded in raw material or a carbon particle, and then subjected to a high temperature. The series of cross-linking, dehydration and polycondensation reactions produce abundant pores and functional groups. Commonly used activators are $ZnCl_2$, H_3PO_4 and KOH [48].

In order to further improve the physical and chemical properties of the active carbon and the adsorption amount of heavy metals, some physical or chemical modification methods can be used to change the pore size of the active carbon and the pore structure such as the pore diameter distribution, or to change and increase the acidic functional group content of the activated carbon surface [49]. Commonly used modification methods are mainly oxidation, reduction, and load-bearing metal methods. Oxidation modification refers to the use of an oxidizing agent to oxidize the surface of the active carbon material, increase the content of oxygen-containing functional groups on the surface, and enhance the surface polarity. Commonly used oxidizing agents are mainly HNO_3, O_3, H_2O_2, $(NH_4)_2S_2O_8$, and so on [50]. The reduction method is to treat and modify the surface of the activated carbon by a reducing agent, thereby increasing the ratio of the alkali group, enhancing the non-polarity of the surface, and improving the adsorption effect on the non-polar substance [51]. It is also possible to increase the adsorption capacity of activated carbon for heavy metals by loading some metal ions with catalytic activity [52].

In the above modification method, the most common and effective modification method for adsorbing heavy metal cations is to introduce an oxygen-containing functional group on the surface of the activated carbon. The oxygen-containing

functional groups on the surface of the activated carbon can lower the surface pH_{pzc} (Point of zero charge) value to improve the hydrophilicity, adsorption selectivity, ion exchange capacity, and affinity for heavy metal ions of the activated carbon [53].

1.4 Adsorption models

1.4.1 Adsorption isotherms

The theoretical equilibrium adsorption capacity of activated carbon for heavy metal ions is an important indicator to measure its adsorption capacity. In isothermal conditions, to characterize the adsorption phenomenon occurring on the solid surface in solution, the commonly used fitting models are the Langmuir isotherm model and the Freundlich isotherm model [54]. Langmuir isotherm model is a theoretical formula, which is based on three assumptions: (1) the adsorbent surface is uniform, and the adsorption energy is the same everywhere; (2) the adsorption is a monolayer, and when the adsorbent surface is saturated with the adsorbate, its adsorption capacity reaches the maximum; (3) there is no interaction between the adsorbed molecules [55]. The equation is as follows [56]:

$$\frac{C_e}{Q_e} = \frac{1}{X_m K_L} + \frac{1}{X_m} C_e, \qquad (1\text{-}4)$$

where, X_m (mmol/g) represents the theoretical maximum adsorbed amount of Cr, and K_L (L/mmol) Langmuir constant related to adsorption energy.

Freundlich isothermal model is an empirical formula, which shows that the adsorption occurs on heterogeneous surfaces and is multiphase adsorption. The

expression is as follows [57].

$$\ln Q_e = \ln K_F + \frac{1}{n}\ln C_e, \qquad (1\text{-}5)$$

where K_F is the Freundlich constant, and $1/n$ is the heterogeneity factor. The greater the value of n, the better the adsorption performance.

1.4.2 Adsorption kinetics

Adsorption kinetics are usually used to describe the amount of adsorbent adsorbed in the liquid phase per unit time and to reveal the adsorption mechanism. The commonly used adsorption kinetics models are pseudo-first-order kinetics model and pseudo-second-order kinetic model [58]. The linearized forms of the models are shown as follows [59]:

$$\ln(Q_e - Q_t) = lnQ_e - k_1 t \qquad (1\text{-}6)$$

$$\frac{t}{Q_t} = \frac{1}{k_2 Q_e^2} + \frac{t}{Q_e}, \qquad (1\text{-}7)$$

where Q_e is the amount of Cr(VI) adsorbed at equilibrium (mmol/g), Q_t is the adsorbed amount of Cr(VI) (mmol/g) at time t (min). k_1 and k_2 are the rates constant of the pseudo-first-order model (L/min) and the pseudo-second-order model (g/mmol•min).

1.5 The organization of this thesis

This research mainly aimed at the problems of the high production cost of activated carbon, low adsorption performance to heavy metals, slow adsorption rate, and inability to adsorb anions and cations at the same time. By developing a new preparation method of activated carbon, the physical and chemical properties of the prepared activated carbon are improved. And explores the adsorption mechanism of activated carbon on

heavy metal ions to improve its adsorption performance.

In chapter 2, to increase the adsorption rate of heavy metal Cd(II), activated carbon BAP having a high mesopore volume was prepared using bamboo as raw material and using phosphoric acid as an activator. The high mesoporous volume of activated carbon has a faster adsorption rate, but because the surface does not have an oxygen-containing functional group, the surface of BAP was oxidized and Na ion-exchanged using ammonium persulfate, thereby producing a high adsorption rate for Cd(II).

In chapter 3, the commercial activated carbon NORIT CGP SUPER (CGP) was further activated by KOH, and the specific surface area of CGP was increased to 3098 m^2/g, thereby greatly increasing the adsorption amount of Cr(VI). Moreover, the adsorption and reduction cycles were studied in the experiment, and the regeneration performance of activated carbon was evaluated.

In chapter 4, the N-doped biochar was prepared by using activators $ZnCl_2$ and NH_3. By increasing the nitrogen content of biochar, it was found that increasing the nitrogen content can effectively increase the adsorption of Cr(VI) by biochar. The adsorption properties and adsorption behavior of NH_3 activated biochar on heavy metal Cr(VI) were investigated to explain the adsorption contribution of quaternary nitrogen to heavy metal Cr(VI).

In chapter 5, based on the research in chapters 5, a high nitrogen content biochar was prepared using the bean dregs, and a steam activation method without secondary pollution was used. By preparing samples with different specific surface areas, the relationship between specific surface area and adsorption amount, and the role of

quaternary nitrogen in adsorption were discussed. The adsorption mechanism of Cr(VI) on N-doped biochar was investigated.

In chapter 6, the possibility of bamboo-based oxidized biochar for simultaneous removal of Cd(II) and Cr(VI) was discussed. By studying the pH changes during the simultaneous adsorption process and the interaction of Cd(II) and Cr(VI) ions, the adsorption properties and adsorption mechanism of the prepared biochars for the simultaneous adsorption of heavy metals Cd(II) and Cr(VI) were investigated.

In chapter 7, the conclusions of this study are summarized, and the prospect for the future is given.

References

[1] X.L. Ma, H. Zuo, M.J. Tian, L.Y. Zhang, J. Meng, X.N. Zhou, N. Min, X.Y. Chang, Y. Liu, Assessment of heavy metals contamination in sediments from three adjacent regions of the Yellow River using metal chemical fractions and multivariate analysis techniques, Chemosphere 144 (2016) 264-272.

[2] S. Clemens, J.F. Ma, Toxic Heavy Metal and Metalloid Accumulation in Crop Plants and Foods, in S.S. Merchant (Ed.) Annu. Rev. Plant Biol 67(2016) 489-512.

[3] Y.D. Zou, X.X. Wang, A. Khan, P.Y. Wang, Y.H. Liu, A. Alsaedi, T. Hayat, X.K. Wang, Environmental Remediation and Application of Nanoscale zero-valent Iron and Its Composites for the Removal of Heavy Metal Ions: A Review, Environ. Sci. Technol. 50 (2016) 7290-7304.

[4] R. Xiao, S. Wang, R.H. Li, J.J. Wang, Z.Q. Zhang, Soil heavy metal contamination

and health risks associated with artisanal gold mining in Tongguan, Shaanxi, China, Ecotoxicol. Environ. Saf. 141 (2017) 17-24.

[5] I. Al-Saleh, N. Shinwari, A. Mashhour, G.E. Mohamed, A. Rabah, Heavy metals (lead, cadmium, and mercury) in maternal, cord blood and placenta of healthy women, Int. J. Hyg. Environ. Health 214 (2011) 79-101.

[6] D. Sud, G. Mahajan, M.P. Kaur, Agricultural waste material as potential adsorbent for sequestering heavy metal ions from aqueous solutions - A review, Bioresour. Technol. 99 (2008) 6017-6027.

[7] S.S. Li, M. Wang, Z.Q. Zhao, X.Y. Li, Y. Han, S.B. Chen, Alleviation of cadmium phytotoxicity to wheat is associated with Cd re-distribution in soil aggregates as affected by amendments, RSC Adv. 8 (2018) 17426-17434.

[8] Ihsanullah, F.A. Al-Khaldi, B. Abusharkh, M. Khaled, M.A. Atieh, M.S. Nasser, T. Iaoui, T.A. Saleh, S. Agarwal, I. Tyagi, V.K. Gupta, Adsorptive removal of cadmium(II) ions from liquid phase using acid-modified carbon-based adsorbents, J. Mol. Liq. 204 (2015) 255-263.

[9] T. Zeinali, F. Salmani, K. Naseri, Dietary Intake of Cadmium, Chromium, Copper, Nickel, and Lead through the Consumption of Meat, Liver, and Kidney and Assessment of Human Health Risk in Birjand, Southeast of Iran, Biol. Trace Elem. Res. 191 (2019) 338-347

[10] S. Kouzbour, B. Gourich, F. Gros, C. Vial, F. Allam, Y. Scriba, Comparative analysis of industrial processes for cadmium removal from phosphoric acid: A review, Hydrometallurgy 188 (2019) 222-247.

[11] M. Valcke, N. Ouellet, M. Dube, E.A.L. Sidi, A. LeBlanc, L. Normandin, C. Balion, P. Ayotte, Biomarkers of cadmium, lead and mercury exposure in relation with early biomarkers of renal dysfunction and diabetes: Results from a pilot study among aging Canadian (vol 312, pg 148, 2019), Toxicol. Lett. 313 (2019) 207-207.

[12] H.N. Tran, D.T. Nguyen, G.T. Le, F. Tomul, E.C. Lima, S.H. Woo, A.K. Sarmah, H.Q. Nguyen, P.T. Nguyen, D.D. Nguyen, T.V. Nguyen, S. Vigneswaran, D.V.N. Vo, H.P. Chao, Adsorption mechanism of hexavalent chromium onto layered double hydroxides-based adsorbents: A systematic in-depth review, J. Hazard. Mater. 373 (2019) 258-270.

[13] S. Ye, M. Yan, X. Tan, J. Liang, G. Zeng, H. Wu, B. Song, C. Zhou, Y. Yang, H. Wang, Facile assembled biochar-based nanocomposite with improved graphitization for efficient photocatalytic activity driven by visible light, Appl. Catal., B 250 (2019) 78-88.

[14] K. Selvi, S. Pattabhi, K. Kadirvelu, Removal of Cr (VI) from aqueous solution by adsorption onto activated carbon, Bioresour. Technol. 80 (2001) 87-89.

[15] Y.Y. Deng, X.F. Xiao, D. Wang, B. Han, Y. Gao, J.L. Xue, Adsorption of Cr(VI) from Aqueous Solution by Ethylenediaminetetraacetic Acid-Chitosan-Modified Metal-Organic Framework, J. Nanosci. Nanotechnol. 20 (2020) 1660-1669.

[16] Y.L. Liu, Y.T. Li, J.F. Huang, Y.L. Zhang, Z.H. Ruan, T. Hu, J.J. Wang, W.Y. Li, H.J. Hu, G.B. Jiang, An advanced sot-gel strategy for enhancing interfacial reactivity of iron oxide nanoparticles on rosin biochar substrate to remove Cr(VI), Sci. Total Environ. 690 (2019) 438-446.

[17] N. Granizo, J.M. Vega, D. de la Fuente, B. Chico, M. Morcillo, Ion-exchange pigments in primer paints for anticorrosive protection of steel in atmospheric service: Anion-exchange pigments, Prog. Org. Coat. 76 (2013) 411-424.

[18] W. Jin, K. Yan, Recent advances in electrochemical detection of toxic Cr(VI), Rsc Advances 5 (2015) 37440-37450

[19] X.F. Shi, S.Y. Quan, L.M. Yang, C. Liu, F.N. Shi, Anchoring Co_3O_4 on $BiFeO_3$: achieving high photocatalytic reduction in Cr(VI) and low cobalt leaching, J. Mater. Sci. 54 (2019) 12424-12436.

[20] B. Jiang, Y.F. Gong, J.N. Gao, T. Sun, Y.J. Liu, N. Oturan, M.A. Oturan, The reduction of Cr(VI) to Cr(III) mediated by environmentally relevant carboxylic acids: State-of-the-art and perspectives, J. Hazard. Mater. 365 (2019) 205-226.

[21] S. Islamoglu, L. Yilmaz, H.O. Ozbelge, Development of a precipitation based separation scheme for selective removal and recovery of heavy metals from cadmium rich electroplating industry effluents, Sep. Sci. Technol. 41 (2006) 3367-3385.

[22] Y. Zhu, W.H. Fan, T.T. Zhou, X.M. Li, Removal of chelated heavy metals from aqueous solution: A review of current methods and mechanisms, Sci. Total Environ. 678 (2019) 253-266.

[23] A. Ertani, A. Mietto, M. Borin, S. Nardi, Chromium in Agricultural Soils and Crops: A Review, Water Air Soil Pollut. 228 (2017) 12.

[24] D. Kumari, X.Y. Qian, X.L. Pan, V. Achal, Q.W. Li, G.M. Gadd, Microbially-induced Carbonate Precipitation for Immobilization of Toxic Metals, in: S. Sariaslani, G.M. Gadd (Eds.), Adv. Appl. Microbiol. 94 (2016) 79-108.

[25] S. Ashraf, Q. Ali, Z.A. Zahir, S. Ashraf, H.N. Asghar, Phytoremediation: Environmentally sustainable way for reclamation of heavy metal polluted soils, Ecotoxicol. Environ. Saf. 174 (2019) 714-727.

[26] C.U. Emenike, B. Jayanthi, P. Agamuthu, S.H. Fauziah, Biotransformation and removal of heavy metals: a review of phytoremediation and microbial remediation assessment on contaminated soil, Environ. Rev. 26 (2018) 156-168.

[27] Z. Rahman, L. Thomas, V.P. Singh, Biosorption of heavy metals by a lead (Pb) resistant bacterium, Staphylococcus hominis strain AMB-2, J. Basic Microbiol. 59 (2019) 477-486.

[28] M.F. Imron, S.B. Kurniawan, A. Soegianto, Characterization of mercury-reducing potential bacteria isolated from Keputih non-active sanitary landfill leachate, Surabaya, Indonesia under different saline conditions, J. Environ. Manage. 241 (2019) 113-122.

[29] A. Bashir, L.A. Malik, S. Ahad, T. Manzoor, M.A. Bhat, G.N. Dar, A.H. Pandith, Removal of heavy metal ions from aqueous system by ion-exchange and biosorption methods, Environ. Chem. Lett. 17 (2019) 729-754.

[30] J. Placido, S. Bustamante-Lopez, K.E. Meissner, D.E. Kelly, S.L. Kelly, NanoRefinery of carbonaceous nanomaterials: Complementing dairy manure gasification and their applications in cellular imaging and heavy metal sensing, Science of the Total Environment 689 (2019) 10-20.

[31] A.B. Botelho, D.B. Dreisinger, D.C.R. Espinosa, A Review of Nickel, Copper, and Cobalt Recovery by Chelating Ion Exchange Resins from Mining Processes and Mining Tailings, Mining Metallurgy & Exploration 36 (2019) 199-213.

[32] Y.W. Qi, L.F. Zhu, X. Shen, A. Sotto, C.J. Gao, J.N. Shen, Polythyleneimine-modified original positive charged nanofiltration membrane: Removal of heavy metal ions and dyes, Sep. Purif. Technol. 222 (2019) 117-124.

[33] M. Yaqub, S.H. Lee, Heavy metals removal from aqueous solution through micellar enhanced ultrafiltration: A review, Environ. Eng. Res. 24 (2019) 363-375.

[34] C. Mahendra, S. Bera, C.A. Babu, K.K. Rajan, Separation of Cesium by Electro Dialysis Ion Exchange using AMP-PAN, Sep. Sci. Technol. 48 (2013) 2473-2478.

[35] K. Kosutic, D. Dolar, T. Strmecky, Treatment of landfill leachate by membrane processes of nanofiltration and reverse osmosis, Desalin. Water Treat. 55 (2015) 2680-2689.

[36] O. Agboola, The role of membrane technology in acid mine water treatment: a review, Korean J. Chem. Eng. 36 (2019) 1389-1400.

[37] Y.L. Niu, W. Hu, M.M. Guo, Y.L. Wang, J.P. Jia, Z.B. Hu, Preparation of cotton-based fibrous adsorbents for the removal of heavy metal ions, Carbohydr. Polym 225 (2019) 9.

[38] X.L. Liu, R. Ma, X.X. Wang, Y. Ma, Y.P. Yang, L. Zhuang, S. Zhang, R. Jehan, J.R. Chen, X.K. Wang, Graphene oxide-based materials for efficient removal of heavy metal ions from aqueous solution: A review, Environ. Pollut. 252 (2019) 62-73.

[39] S.S. Fiyadh, M.A. AlSaadi, W.Z. Jaafar, M.K. AlOmar, S.S. Fayaed, N.S. Mohd, L.S. Hin, A. El-Shafie, Review on heavy metal adsorption processes by carbon nanotubes, J. Cleaner Prod. 230 (2019) 783-793.

[40] A.I.A. Sherlala, A.A.A. Raman, M.M. Bello, A. Asghar, A review of the

applications of organo-functionalized magnetic graphene oxide nanocomposites for heavy metal adsorption, Chemosphere 193 (2018) 1004-1017.

[41] A.E. Burakov, E.V. Galunin, I.V. Burakova, A.E. Kucherova, S. Agarwal, A.G. Tkachev, V.K. Gupta, Adsorption of heavy metals on conventional and nanostructured materials for wastewater treatment purposes: A review, Ecotoxicol. Environ. Saf. 148 (2018) 702-712.

[42] H. Mahmud, A.K.O. Huq, R.B. Yahya, The removal of heavy metal ions from wastewater/aqueous solution using polypyrrole-based adsorbents: a review, RSC Adv. 6 (2016) 14778-14791.

[43] L. Wang, Y.J. Wang, F. Ma, V. Tankpa, S.S. Bai, X.M. Guo, X. Wang, Mechanisms and reutilization of modified biochar used for removal of heavy metals from wastewater: A review, Sci. Total Environ. 668 (2019) 1298-1309.

[44] W.Y. Huang, Y.M. Zhang, D. Li, Adsorptive removal of phosphate from water using mesoporous materials: A review, J. Environ. Manage. 193 (2017) 470-482.

[45] J.L. Wang, S.Z. Wang, Preparation, modification and environmental application of biochar: A review, J. Cleaner Prod. 227 (2019) 1002-1022.

[46] M.I. Inyang, B. Gao, Y. Yao, Y.W. Xue, A. Zimmerman, A. Mosa, P. Pullammanappallil, Y.S. Ok, X.D. Cao, A review of biochar as a low-cost adsorbent for aqueous heavy metal removal, Crit. Rev. Env. Sci. Technol. 46 (2016) 406-433.

[47] B. Sajjadi, W.Y. Chen, N.O. Egiebor, A comprehensive review on physical activation of biochar for energy and environmental applications, Rev. Chem. Eng. 35 (2019) 735-776.

[48] B. Sajjadi, T. Zubatiuk, D. Leszczynska, J. Leszczynski, W.Y. Chen, Chemical activation of biochar for energy and environmental applications: a comprehensive review, Rev. Chem. Eng. 35 (2019) 777-815.

[49] X.D. Yang, Y.S. Wan, Y.L. Zheng, F. He, Z.B. Yu, J. Huang, H.L. Wang, Y.S. Ok, Y.S. Jiang, B. Gao, Surface functional groups of carbon-based adsorbents and their roles in the removal of heavy metals from aqueous solutions: A critical review, Chem. Eng. J. 366 (2019) 608-621.

[50] Y.C. Chiang, R.S. Juang, Surface modifications of carbonaceous materials for carbon dioxide adsorption: A review, J. Taiwan Inst. Chem. Eng. 71 (2017) 214-234.

[51] A.A. Adelodun, K.H. Kim, J.C. Ngila, J. Szulejko, A review on the effect of amination pretreatment for the selective separation of CO_2, Appl. Energy 158 (2015) 631-642.

[52] S.S. Zhu, S.H. Ho, X.C. Huang, D.W. Wang, F. Yang, L. Wang, C.Y. Wang, X.D. Cao, F. Ma, Magnetic Nanoscale Zerovalent Iron Assisted Biochar: Interfacial Chemical Behaviors and Heavy Metals Remediation Performance, ACS Sustainable Chem. Eng. 5 (2017) 9673-9682.

[53] K. Takeuchi, Y. Amano, M. Machida, F. Imazeki, Batch and Fixed-Bed Column Adsorption of Cd(II) from Aqueous Solution onto Oxidized Bead-Shaped Activated Carbon, J. Chem. Eng. Jpn. 48 (2015) 123-126.

[54] P. Jutakridsada, C. Prajaksud, L. Kuboonya-Aruk, S. Theerakulpisut, K. Kamwilaisak, Adsorption characteristics of activated carbon prepared from spent ground coffee, Clean Technol. Environ. Policy 18 (2016) 639-645.

[55] C.H. Zhang, H.M. Wang, C. Gao, E.Q. Chen, H.Z. Wang, L.S. Hong, Equilibrium and kinetics studies of Cu(II) ions adsorption on polyamidoamine dendrimer starch, Res. Chem. Intermed. 38 (2012) 2411-2425.

[56] T.S. Malarvizhi, T. Santhi, Lignite fired fly ash modified by chemical treatment for adsorption of zinc from aqueous solution, Res. Chem. Intermed. 39 (2013) 2473-2494.

[57] Y. Liu, Y. Liu, Biosorption isotherms, kinetics and thermodynamics, Separation And Purification Technology 61 (2008) 229-242.

[58] M. Abbas, S. Kaddour, M. Trari, Kinetic and equilibrium studies of cobalt adsorption on apricot stone activated carbon, Sep. Purif. Technol. 20 (2014) 745-751.

[59] J. Febrianto, A.N. Kosasih, J. Sunarso, Y.H. Ju, N. Indraswati, S. Ismadji, Equilibrium and kinetic studies in adsorption of heavy metals using biosorbent: A summary of recent studies, J. Hazard. Mater. 162 (2009) 616-645.

Chapter 2 Isotherm, kinetic and thermodynamic studies for adsorption of Cd(II) from aqueous solution onto mesoporous bamboo activated carbon

2.1 Introduction

Cadmium is a common toxic metal and can cause several diseases, including lung dysfunction, renal dysfunction, cancer, disease, and high blood pressure [1]. According to WHO regulations, the maximum allowable concentration of cadmium in drinking water is 0.003 mg/L [2]. Therefore, the removal and elimination of cadmium from contaminated water and wastewater are necessary to protect the environment and human health.

Activated carbon is a black porous material that has been activated by physical or chemical methods [3]. It has the characteristics of internal porosity development, large specific surface area, and high adsorption capacity [4]. Activated carbon is stable nature, high acid, and alkali resistance and heat tolerance, insoluble in water or organic solvents, and easy to regenerate, so it is widely used as an environment-friendly adsorbent [5].

Bamboo is abundant, especially in Asia, and possesses the rapid growth ability compared to other plants because it can be matured at only 3-5 years of age so that bamboo could be regarded as cheaply available material [6, 7]. Surface physical structure modification for activated carbon refers to the process by physical or chemical activation methods to increase the specific surface area [8], to change the pore volume and structure, and to adjust the pore size distribution, thus changing the physical adsorption properties of activated carbon. In the chemical activation method, raw

material is crushed first, and the activator and the crushed raw materials are mixed with the desired percentage. According to the different activators, raw materials were selectively heated under inert atmosphere, to complete carbonization and activation of the materials. The main activator used is $ZnCl_2$ [9-11], H_3PO_4 [12-14], alkali such as KOH [15] and NaOH [16, 17].

The H_3PO_4 activation method is relatively mature. After the dephosphorylation process, wide pore distribution can be obtained in the activated carbon. Comparing with the alkali activation method, the H_3PO_4 activation method has relatively low requirements for the equipment. The activated carbon products of the H_3PO_4 activation method are stable. Thereby, H_3PO_4 activation method can be used as an excellent liquid adsorption material.

Under the appropriate conditions, the use of oxidants for the activated carbon surface oxidation can improve the amount of oxygen-containing functional groups such as carboxy, lactone and hydroxy on the carbon surface, enhancing the hydrophilicity of activated carbon surface and improving its adsorption capacity of toxic metal ion [18, 19].

This study aimed to perform the adsorption of Cd(II) in aqueous solution onto activated carbon prepared from bamboo comparing with the commercially available bead-shaped activated carbon (BAC), and kinetic, and equilibrium adsorption characteristics were discussed.

2.2 Materials and methods

2.2.1 Preparation of activated carbons

Moso bamboo obtained in Aichi prefecture, Japan, was cut into chips of 8 mm width, 10 mm length and 5 mm thickness and used as a precursor for preparation of adsorbent. The bamboo chips were dried in an oven at 110°C for one hour, followed by immersion in 3 M NaOH solution for three hours at 90°C. Then, the sample was washed with 0.1 M HCl and hot distilled water and dried again in an oven at 110°C overnight. About 15 g of the base-treatment bamboo chips were impregnated with 300 mL of H_3PO_4 solution with impregnation ratio of 3 g/g for eighth. Impregnation was carried out at 70°C to ensure proper penetration of H_3PO_4 in the raw material and the mixture was dried in an oven at 110°C overnight. The resulting mixture was transferred to a steel tube reactor and heated up to 500°C under N_2 gas atmosphere and hold for one hour. The N_2 gas flow rate was 200 mL/min. After carbonization, the reactor was cooled to room temperature under N_2 gas atmosphere. The prepared activated carbon was placed in 1 M HCl solution, stirred for one hour, rinsed in a Soxhlet extractor for 24 hours, and dried overnight at 110°C. The final product was referred to as BAP.

The activated carbons were oxidized to load the functional groups. $(NH_4)_2S_2O_8$ solution was used as an oxidant. It was dissolved in 1 M H_2SO_4, and the ratio of $(NH_4)_2S_2O_8$ to sulfuric acid was 60 g: 100 mL (w/v). The prepared BAP was added into in the $(NH_4)_2S_2O_8$ solution and oxidized at 30°C for 1-3 days. The obtained sample was named as BAP*x*, where *x* was the number of days for oxidation. For comparison, commercially available bead-shaped activated carbon (BAC) was also subjected to the

same oxidation treatment for one day and referred to as BAC1.

In the adsorption isotherm and kinetic experiments, the activated carbon was subjected to Na^+ treatment in order to keep the solution pH constant during the adsorption. Na-intercalated activated carbons were prepared by adding 2 g of BAP*x* and BAC1 into 500 mL of 0.5 mol/L sodium chloride solution. The solution pH during ion loading was adjusted to 4.0. The mixtures were stirred continuously for 6 hours, and then filtered and washed in a Soxhlet extractor for 24 hours to remove chloride anions and other impurities, and the samples were referred to as BAPx-Na (x=1,2,3) and BAC1-Na, respectively.

2.2.2 Characterization of activated carbon

Specific surface area (S_{BET}), mesopore volume (V_{meso}) and micropore volume (V_{micro}) for the prepared activated carbons were analyzed by N_2 adsorption-desorption at −196°C with a surface area and pore size analyzer. The α_s-plot with subtracting pore effect (SPE) method was applied to estimate the micropore volume (V_{micro}). The mesopore volume (V_{meso}) was obtained from the difference between V_{total} and V_{micro}. The amounts of acidic surface functional groups and basic sites for the prepared activated carbon were quantified by Boehm titration method. About 0.05 g of the prepared activated carbon were added into 25 mL of 0.05 M Na_2CO_3, 0.1 M NaOH, 0.1 M HCl or 0.1 M $NaHCO_3$ solution in flasks. The flasks were shaken at 100 rpm for 48 hours at 25°C. $NaHCO_3$ neutralizes only the carboxy group on the surface of the carbon, and Na_2CO_3 neutralizes the carboxy and lactone groups, while NaOH neutralizes the

carboxy, lactone and phenolic hydroxyl groups. The amount of the corresponding functional group can be calculated from the difference in alkali consumption.

2.3 Results and discussion

2.3.1 Characterization of activated carbon

The nitrogen adsorption-desorption isotherm curve of the BAP is shown in **Fig. 2-1**. From **Fig. 2-1**, a type IV isotherm was observed, which indicates the mainly mesoporous structure existence. The textural and surface properties of the prepared activated carbons are shown in **Table 2-1**. The data showed that the highest surface area and the highest mesopore volume were obtained for BAP. In the oxidized samples, the amount of acidic functional groups was larger than that for the non-oxidized sample, and the surface area and pore volume were significantly decreased. BAP was introduced with more acidic functional groups than BAC under the same period of oxidation**.**

Table 2-1 Textural and surface properties of each prepared activated carbon

Sample	S_{BET} [m^2/g]	V_{micro} [cm^3/g]	V_{meso} [cm^3/g]	Surface functional groups of each sample [meq/g]			
				Carboxy	Lactone	Hydroxy	Basic
BAC	1380	0.57	0.03	0.00	0.16	0.10	0.60
BAP	1470	0.32	1.64	0.00	0.00	0.19	0.06
BAC1	940	0.34	0.12	2.40	0.23	1.48	0.00
BAP1	580	0.14	0.24	3.71	0.26	3.65	0.00

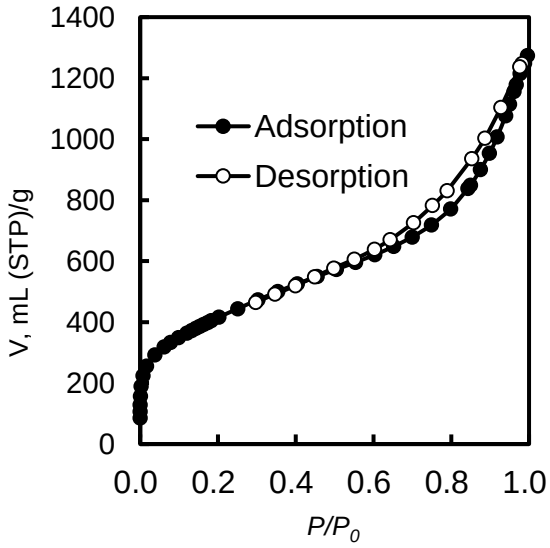

Fig. 2-1 Nitrogen sorption isotherm of BAP

2.3.2 Effect of equilibrium pH

Equilibrium solution pH plays a significant role in the removal efficiency of Cd(II) from aqueous solution. The amount of Cd(II) adsorbed at equilibrium increased gradually in the equilibrium pH range from 1.5 to 5.5.

In the process of Cd(II) adsorption on activated carbon, Cd(II) ions were exchanged with hydrogen ions on the surface carboxy group or other functional groups of the oxidized activated carbon, causing the decrease in the solution pH. It is also obvious from **Fig. 2-2** that the decrease in the pH would reduce the adsorption capacity. In the experiments of adsorption isotherms and adsorption kinetics, Na-intercalated activated carbons were used.

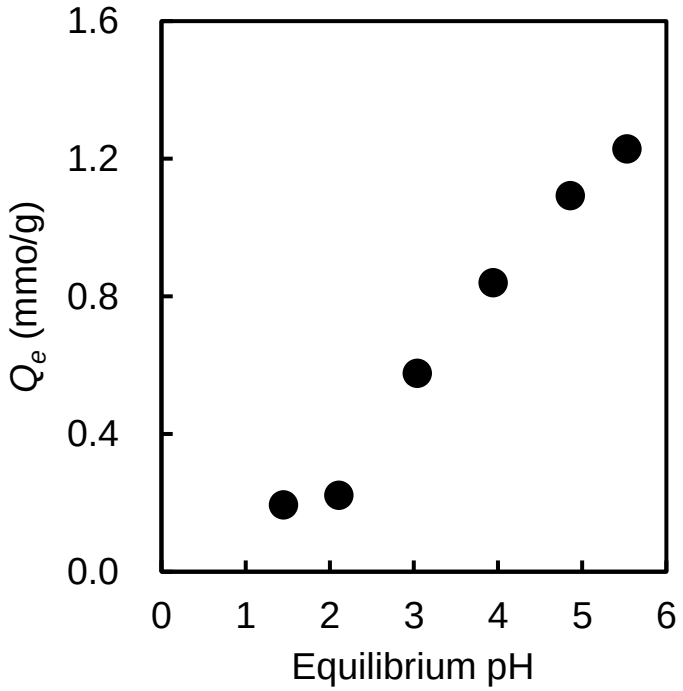

Fig. 2-2 The Cd(II) adsorption capacity of BAP1 under different equilibrium pH values (Amount of adsorbent: 50 mg. Solution volume: 25 mL).

2.3.3 Adsorption equilibrium experiments

(1) Adsorption isotherms for different adsorbents

Adsorption isotherms of Cd(II) for BAC1-Na and BAP1-Na are shown in **Fig.2-3.** Adsorption isotherms using Langmuir and Freundlich models were applied to

investigate the adsorption process of Cd(II) at 25°C and the different isotherm constants determined were presented in **Table 2-2.**

Through the Langmuir and Freundlich data fitting of adsorption isotherms of Cd(II) for BAP1-Na, the R^2 values were greater than 0.999, indicating that the two models can be a good description of Cd(II) adsorption behavior. In the Langmuir isothermal adsorption model, R_L was 0.008 ($0 \leq R_L \leq 1$), indicating favorable adsorption of Cd(II) on the AC samples.

In the Freundlich isothermal adsorption model, n = 12.804 also draw the same conclusion. Fitting of experiment data to Langmuir model is slightly better than Freundlich model, indicating that Cd(II) adsorption onto modified activated carbon tended to be monolayer adsorption. Similar trends could be drawn from the adsorption isotherms experiments data of BAC1-Na. Comparison of the maximum adsorption capacity (X_m) of two adsorbents in adsorption isotherm experiment, the X_m value for BAP1-Na was larger than that for BAC-APS-Na, implying that the adsorption capacity of BAP1-Na was better than that of BAC1-Na. This may be because BAP has a greater specific surface area than BAC, as shown in **Table 2-1**. And adsorption capacity of Cd(II) was higher than that reported by Mohan et al. [20] (0.34 mmol/L), Lu et al. [21] (0.11 mmol/L) and Moreno-Tovar et al. [22] (0.39 mmol/L).

Table 2-2 Langmuir and Freundlich parameters of Cd(II) at 25°C in aqueous solutions

	Langmuir model				Freundlich model		
Sample	X_m [mmol/g]	K_L [L/mmol]	R_L	R^2	n	K_F [(mmol/g)(mmol/L)^n]	R^2
BAP1-Na	0.721	16.4	0.008	0.999	12.8	0.634	0.930
BAC1-Na	0.494	7.44	0.166	0.995	14.3	0.421	0.923

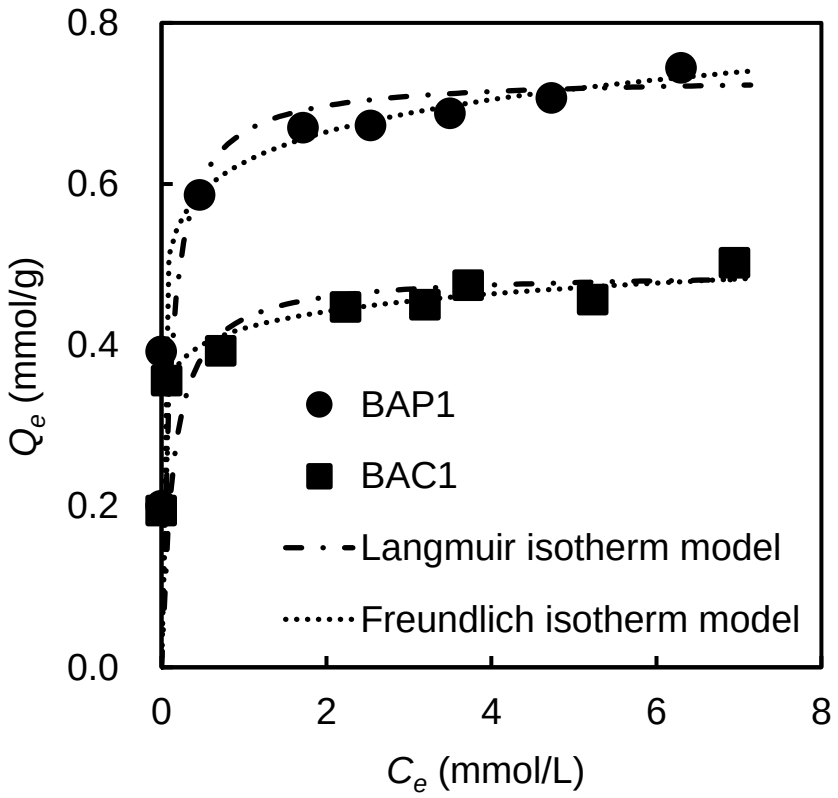

Fig. 2-3 Adsorption isotherms of Cd(II) for 48 h at 25°C (Amount of adsorbent: 50 mg. Solution volume: 25 mL).

(2) Adsorption thermodynamics parameters

Adsorption isotherms of Cd(II) for BAP1-Na at the temperature of 298, 308, 318K are shown in **Fig. 2-4**. The thermodynamic parameters, Gibbs free energy change $\Delta G°$ (kJ mol^{-1}), enthalpy change $\Delta H°$ (, kJ mol^{-1}) and $\Delta S°$ (entropy change, J $mol^{-1}K^{-1}$) are calculated by Eqs.(2-1) , (2-2) and (2-3).

$$\Delta G° = -RT\ln K_d \qquad (2\text{-}1)$$

$$\Delta G° = \Delta H° - T\Delta S° \qquad (2\text{-}2)$$

$$\ln K_d = -\frac{\Delta H°}{RT} + \frac{\Delta S°}{R} \ , \qquad (2\text{-}3)$$

where R (8.314 J mol^{-1} K^{-1}) is a general gas constant, T (K) is the thermodynamic temperature, and K_d (L mg^{-1}) is the standard thermodynamic equilibrium constant defined by q_e/C_e, which is from the Langmuir equation (K_L) or Freundlich equation k_f. The correlation coefficients (R^2) are given in **Table 2-3**. Because Cd(II) adsorption data on the BAP1-Na fitted better with the Langmuir adsorption isothermal equation in this study, the Langmuir adsorption isothermal constant was used. The slopes and intercepts of the plots of ln K_d vs. 1/T were shown in **Fig. 2-5**. The values of $\Delta H°$, $\Delta S°$, and $\Delta G°$ for Cd(II) adsorption on BAP1-Na are given in **Table 2-4**. The negative values of $\Delta H°$ indicated an exothermic process of adsorption, and the negative values of $\Delta S°$ showed that the system of Cd(II) adsorption disorder decreased at the solid/solution interface during adsorption. The negative value of $\Delta G°$ indicates that all adsorption process were viable and spontaneous, similar to that reported by Mohan et al. [20] for the adsorption of Cd(II).

Table 2-3 Langmuir and Freundlich parameters of Cd(II) at different temperature

		Langmuir model				Freundlich model		
Sample	Temperature [K]	X_m [mmol/g]	K_L [L/mmol]	R_L	R^2	n	K_F [(mmol/g)(mmol/L)^n]	R^2
BAP1-Na	298	0.721	16.4	0.008	0.999	12.8	0.634	0.930
	308	0.670	13.6	0.009	0.998	17.4	0.597	0.899
	318	0.610	12.4	0.010	0.996	28.8	0.563	0.584

Table 2-4 Adsorption thermodynamic parameters for Cd(II) adsorbed on BAP1-Na

ΔS° [J/mol K]	*ΔH°* [kJ/mol]	*ΔG° (298K)* [KJ/mol]	*ΔG° (308K)* [KJ/mol]	*ΔG° (318K)* [KJ/mol]
-14.1	-11.1	-6.89	-6.74	-6.60

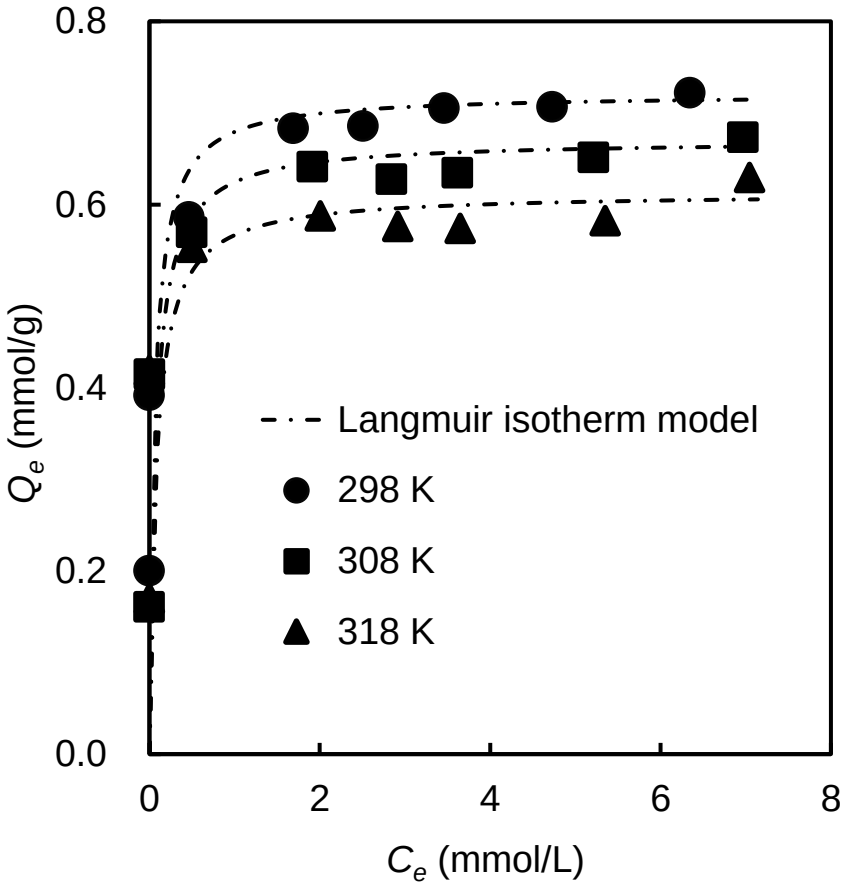

Fig. 2-4 Adsorption isotherms of Cd(II) for 48 h at 298K, 308K and 318K

(Amount of adsorbent: 50 mg. Solution volume: 25 mL).

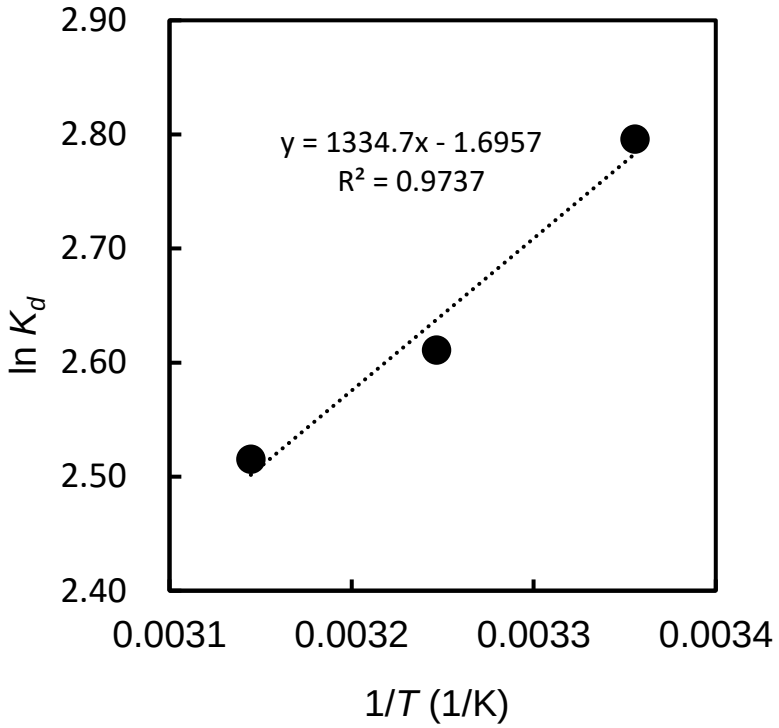

Fig. 2-5 Plot of ln K_d vs. 1/T for Cd(II) adsorption on BAP1

2.3.4 Cd(II) adsorption kinetics of the prepared AC

In the adsorption experiment, 0.1 g of the prepared activated carbons were mixed with 100 mL of 500 mg/L Cd(II) solution and agitated at 100 rpm at 25°C and the solution pH was not adjusted.

(1) Effect of adsorbent type

The effects of adsorbent type on Cd(II) adsorption were compared. The amount of Cd(II) adsorbed on the AC was studied as a function of shaking time at different adsorbent types (BAP1-Na and BAC1-Na). The relationship between adsorption time and adsorption capacity is shown in **Fig. 2-6**.

It is evident from these figures that the adsorptivity of Cd(II) was enhanced with the increase in contact time from 0 to 20 min, and was almost saturated after 20 min BAC1-Na. The adsorption rate of BAP1-Na was significantly faster than BAC1-Na, and was almost saturated after 10 min. Under the same experimental conditions, the adsorption capacity of Cd(II) for BAP1-Na was higher than that of BAC1-Na.

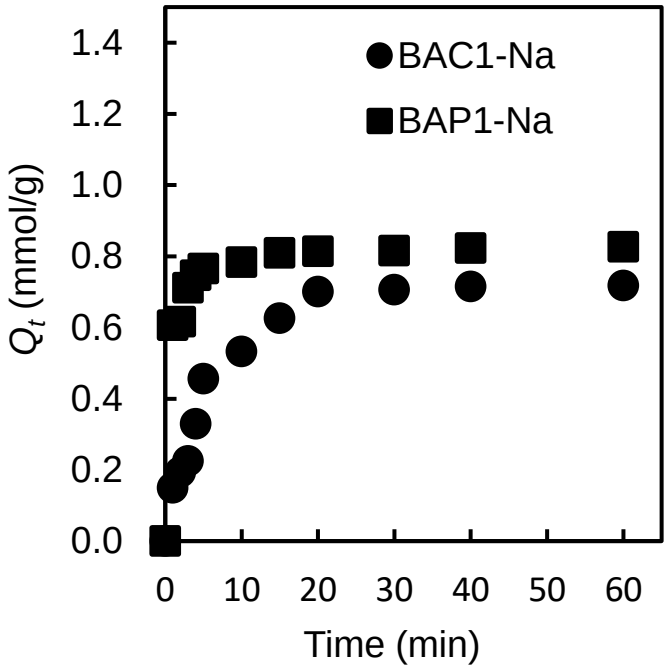

Fig. 2-6 Effect of adsorbent type on Cd(II) adsorption rate (Amount of adsorbent: 100 mg. Solution volume: 100 mL).

(2) Effect of oxidation time

Fig. 2-7 shows the relationship between the amount of Cd(II) adsorbed and oxidation time of activated carbon (1 d, 2 d or 3 d).

With increasing the oxidation time, the adsorption capacity of Cd(II) was also increased. This trend would be due to the increased oxidation time after the activated carbon was loaded with more acidic functional groups. Mena Aguilar et al. had the same conclusion in studying the Pb(II) adsorption onto oxidized activated carbon fiber [23].

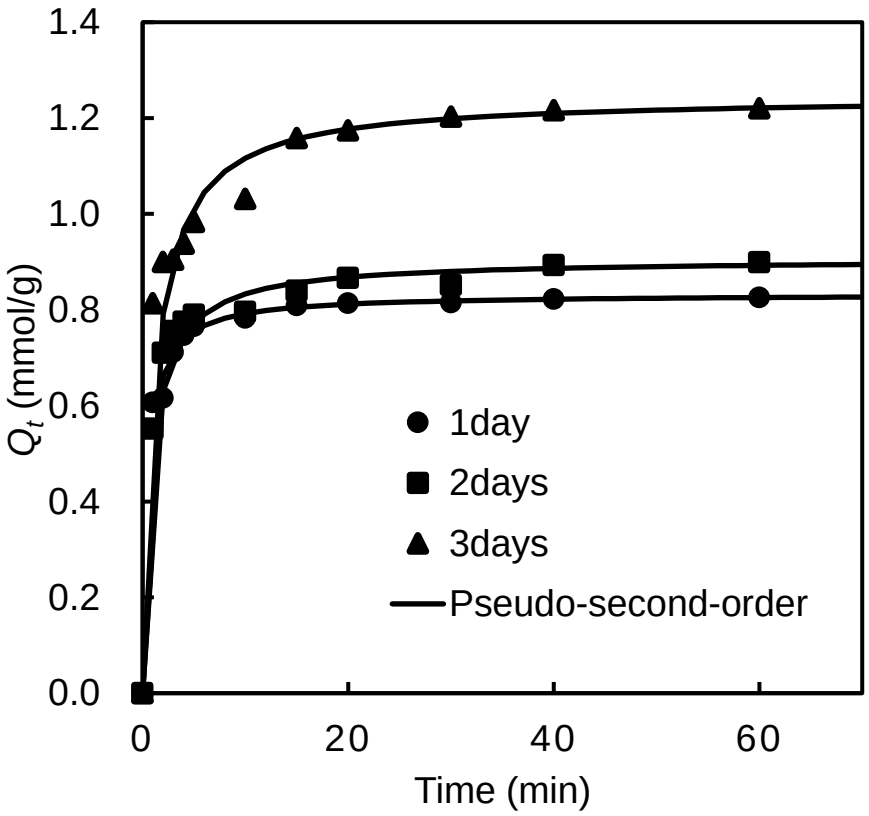

Fig. 2-7 Effect of Oxidation time on Cd(II) adsorption rate (Amount of adsorbent: 100 mg. Solution volume: 100 mL).

(3) Effect of adsorbent dosage

The influence of adsorbent dosage on Cd(II) adsorption was studied by varying the amount of adsorbent (BAP1-Na) from 1.0 to 3.0 g/L. **Fig. 2-8** depicts the adsorption

capacity of Cd(II) with different adsorbent dosages. With the increase in the amount of adsorbent dosage, the accumulation of particles causes the aggregation and overlap of the adsorption sites, resulting in a decrease in the available surface area of the adsorbents and an increase in the length of the diffusion path.

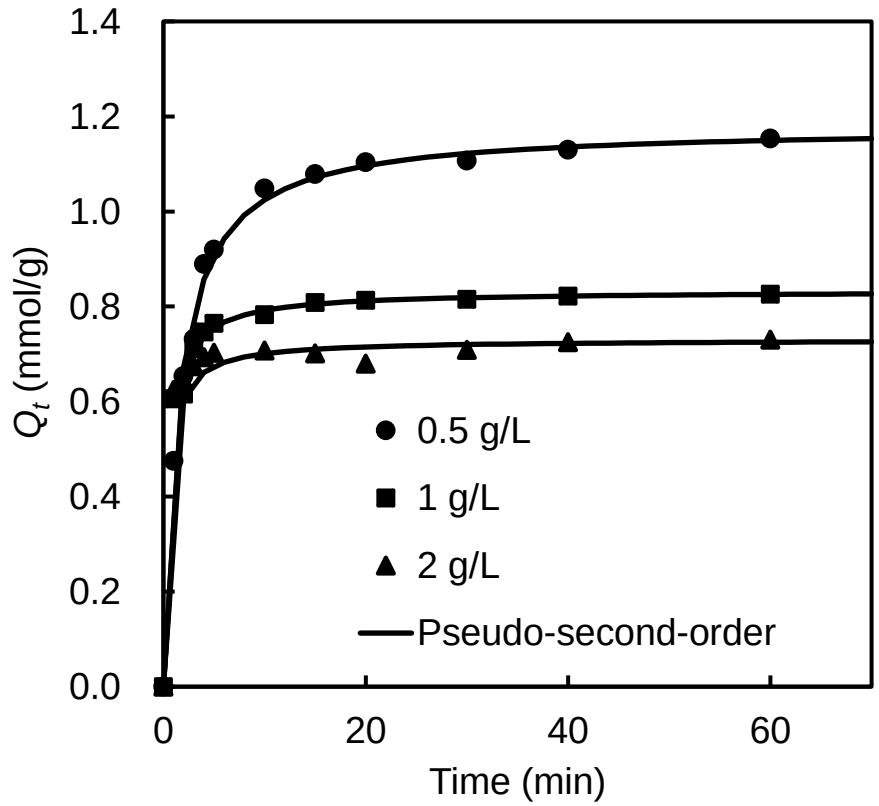

Fig. 2-8 Effect of adsorbent dosage on Cd(II) adsorption rate (Amount of adsorbent: 100 mg. Solution volume: 100 mL).

2.3.5 Kinetic analysis

The experimental data in **Figs. 2-6 - 2-8** are fitted with pseudo-first-order model and pseudo-second-order model when BAP1-Na was used. The results of the kinetic

analysis are shown in **Tables 2-5 - 2-7**.

The pseudo-first-order model has lower correlation coefficient (R^2) when compared to the pseudo-second-order models, and all R^2 values are greater than 0.99 for pseudo-second-order models. The prepared BAP1-Na displayed higher adsorption rate than BAC1-Na. This may be due to the higher surface area and larger mesopore volumes for BAP than BAC, which cause higher adsorption rate.

The adsorption rate for Cd(II) decreased with the increase in oxidation time. With the increase of the oxidation time, and the number of acidic functional groups on the activated carbon surface, the adsorption capacity was also increased, and the adsorption rate was decreased. With the increase of the activated carbon dosage, the time for adsorption equilibrium was decreased. It may be due to the enhanced number of active sites for adsorption.

Table 2-5 Kinetic parameters obtained for Cd(II) adsorption using different adsorbents

Sample	Pseudo-first-order model			Pseudo-second-order model		
	k_1 [1/h]	Q_{e1} [mmol/g]	R^2	k_2 [g/mmol h]	Q_{e2} [mmol/g]	R^2
BAC1-Na	0.107	1.10	0.977	0.253	0.797	0.994
BAP1-Na	0.110	4.43	0.832	2.343	0.833	0.999

Table 2-6 Effect of oxidation time on kinetic parameters obtained for Cd(II) adsorption

Sample	Pseudo-first-order model			Pseudo-second-order model		
	k_1 [1/h]	Q_{e1} [mmol/g]	R^2	k_2 [g/mmol h]	Q_{e2} [mmol/g]	R^2
BAP1-Na	0.110	4.43	0.832	2.34	0.833	0.999
BAP2-Na	0.414	0.088	0.811	1.27	0.906	0.999
BAP3-Na	0.119	0.887	0.959	0.703	1.244	0.999

Table 2-7 Effect of adsorbent dosage on kinetic parameters obtained for Cd(II) adsorption

Sample	Adsorbent dosage [g/L]	Pseudo-first-order model			Pseudo-second-order model		
		k_1 [1/h]	Q_{e1} [mmol/g]	R^2	k_2 [g/mmol h]	Q_{e2} [mmol/g]	R^2
BAP1-Na	0.5	0.088	2.34	0.332	0.596	1.16	0.999
	1.0	0.110	4.43	0.832	2.34	0.833	0.999
	2.0	0.069	7.25	0.544	3.30	0.730	0.999

2.4 Conclusions

Moso bamboo was used as a precursor for the production of mesoporous activated carbon by H_3PO_4 activation, and it was indicated that the prepared activated carbon BAP had high surface area (1470 m^2/g) and mesopore volume (1.64 cm^3/g). The initial solution pH played an important role in the removal of Cd(II) from aqueous phase, and the decrease in pH resulted in the decrease in the amount of cadmium adsorbed by activated carbon. The oxidized activated carbon BAP1-Na could keep the pH of the solution constant during the adsorption process, and it was very effective for the removal of Cd(II). The adsorption equilibrium was well explained by the Langmuir isotherm and the pseudo-second order kinetics. BAP1-Na showed higher adsorption capacity and adsorption rate than those of BAC1-Na. According to the adsorption thermodynamics parameters study, the $\Delta H°$ value was negative, suggesting an exothermic process and the negative value of $\Delta S°$ showed that the system of Cd(II) adsorption disorder decreased at the solid/solution interface during adsorption.

Oxidation time, adsorbent dosage and temperature could affect the adsorption capacity and kinetics of Cd(II).

References

[1] R. Karthik, S. Meenakshi, Removal of Pb(II) and Cd(II) ions from aqueous solution using polyaniline grafted chitosan, Chem. Eng. J. 263 (2015) 168-177.

[2] Y. Huang, S.X. Li, H.B. Lin, J.H. Chen, Fabrication and characterization of mesoporous activated carbon from Lemna minor using one-step H3PO4 activation for Pb(II) removal, Appl. Surf. Sci. 317 (2014) 422-431.

[3] I. Kula, M. Ugurlu, M.H. Karaoglu, A. Celik, Adsorption of Cd(II) ions from aqueous solutions using activated carbon prepared from olive stone by ZnCl2 activation, Bioresour. Technol. 99 (2008) 492-501.

[4] A.A. Wasim, M.N. Khan, Physicochemical effect of activation temperature on the sorption properties of pine shell activated carbon, Water Sci. Technol. 75 (2017) 1158-1168.

[5] J. Guo, Y.P. Luo, F. Ge, Y.L. Ding, J.J. Fei, Voltammetric determination of cadmium (II) based on a composite film of a thiol-functionalized mesoporous molecular sieve and an ionic liquid, Microchim. Acta 172 (2011) 387-393.

[6] B.H. Hameed, A.T.M. Din, A.L. Ahmad, Adsorption of methylene blue onto bamboo-based activated carbon: Kinetics and equilibrium studies, J. Hazard. Mater. 141 (2007) 819-825.

[7] Q.S. Liu, T. Zheng, P. Wang, L. Guo, Preparation and characterization of activated

carbon from bamboo by microwave-induced phosphoric acid activation, nd. Crops Prod. 31 (2010) 233-238.

[8] R. Gottipati, S. Mishra, Preparation of microporous activated carbon from Aegle Marmelos fruit shell and its application in removal of chromium(VI) from aqueous phase, J. Ind. Eng. Chem. 36 (2016) 355-363.

[9] E.B. Simsek, I. Novak, O. Sausa, D. Berek, Microporous carbon fibers prepared from cellulose as efficient sorbents for removal of chlorinated phenols, Res. Chem. Intermed. Res. Chem. Intermed. 43 (2017) 503-522.

[10] D.L. Vu, J.S. Seo, H.Y. Lee, J.W. Lee, Activated carbon with hierarchical micro-mesoporous structure obtained from rice husk and its application for lithium-sulfur batteries, RSC Adv. 7 (2017) 4144-4151.

[11] A. Kumar, H.M. Jena, Removal of methylene blue and phenol onto prepared activated carbon from Fox nutshell by chemical activation in batch and fixed-bed column, J. Cleaner Prod. 137 (2016) 1246-1259.

[12] C.Y. Li, L.B. Zhang, H.Y. Xia, J.H. Peng, S.Z. Zhang, S. Cheng, J.H. Shu, Kinetics and isotherms studies for congo red adsorption on mesoporous Eupatorium adenophorum-based activated carbon via microwave-induced H3PO4 activation, J. Mol. Liq. 224 (2016) 737-744.

[13] Y.Y. Sun, H. Li, G.C. Li, B.Y. Gao, Q.Y. Yue, X.B. Li, Characterization and ciprofloxacin adsorption properties of activated carbons prepared from biomass wastes by H_3PO_4 activation, Bioresour. Technol. 217 (2016) 239-244.

[14] Suhas, V.K. Gupta, P.J.M. Carrott, R. Singh, M. Chaudhary, S. Kushwaha,

Cellulose: A review as natural, modified and activated carbon adsorbent, Bioresour. Technol. 216 (2016) 1066-1076.

[15] T.M. Darweesh, M.J. Ahmed, Batch and fixed bed adsorption of levofloxacin on granular activated carbon from date (Phoenix dactylifera L.) stones by KOH chemical activation, Environ. Toxicol. Pharmacol. 50 (2017) 159-166.

[16] M.A. Islam, M.J. Ahmed, W.A. Khanday, M. Asif, B.H. Hameed, Mesoporous activated carbon prepared from NaOH activation of rattan (Lacosperma secundiflorum) hydrochar for methylene blue removal, Ecotoxicol. Environ. Saf. 138 (2017) 279-285.

[17] R. Zhao, Y. Wang, X. Li, B.L. Sun, Y.M. Li, H. Ji, J. Qiu, C. Wang, Surface Activated Hydrothermal Carbon-Coated Electrospun PAN Fiber Membrane with Enhanced Adsorption Properties for Herbicide, ACS Sustainable Chem. Eng. 4 (2016) 2584-2592.

[18] A.N.A. El-Hendawy, Influence of HNO_3 oxidation on the structure and adsorptive properties of corncob-based activated carbon, Carbon 41 (2003) 713-722.

[19] T. Qiu, Y. Zeng, C.S. Ye, H. Tian, Adsorption Thermodynamics and Kinetics of p-Xylene on Activated Carbon, J. Chem. Eng. Data 57 (2012) 1551-1556.

[20] D. Mohan, K.P. Singh, Single- and multi-component adsorption of cadmium and zinc using activated carbon derived from bagasse - an agricultural waste, WWater Res. 36 (2002) 2304-2318.

[21] L.H. Lu, H.B. Zhao, L. Yan, G.W. Wang, Y.L. Mao, X. Wang, K. Liu, X.F. Liu, Q. Zhao, T.S. Jiang, Removal characteristics of Cd(II) ions from aqueous solution on ordered mesoporous carbon, Korean J. Chem. Eng. 32 (2015) 2161-2167.

[22] R. Moreno-Tovar, E. Terres, J.R. Rangel-Mendez, Oxidation and EDX elemental mapping characterization of an ordered mesoporous carbon: Pb(II) and Cd(II) removal, Appl. Surf. Sci. 303 (2014) 373-380.

[23] K.M.M. Aguilar, Y. Amano, M. Machida, Ammonium persulfate oxidized activated carbon fiber as a high capacity adsorbent for aqueous Pb(II), J. Environ. Chem. Eng. 4 (2016) 4644-4652.

Chapter 3 Adsorption, reduction and regeneration behavior of high surface area activated carbon in removal of Cr(VI)

3.1. Introduction

With the development of global industrialization, environmental pollution has become increasingly serious. In view of the harm of heavy metals to human beings, heavy metal pollution in water has become one of the hot research issues in environmental research [1]. Chromium is a recognized carcinogen which is widely found in environmental media [2]. The chromium pollution mainly comes from wastewater in industries such as leather tannins, electroplating, metallurgy, printing and dyeing. In addition, some natural activities (volcanic activity and rock weathering) also produce chromium pollution [3]. These chromium elements can accumulate in body through the food chain, and excessive chromium content in human body will lead to upper respiratory tract stimulation, causing liver and kidney failure and even cancer [4, 5].

Chromium mainly presents as Cr(III) and Cr(VI) in the environment. Cr(III) is approximately 500 times less toxic than Cr(VI) [6], while Cr(VI) has good water solubility and stronger toxicity. Cr(VI) can be easily absorbed and accumulated by human body, especially by kidneys, stomach and liver [7]. The permissible limit for Cr(VI) in drinking water in Japan is 0.05 mg/L, which is identical to the drinking water guideline value recommended by World Health Organization [8].

In the past, the adsorption amount of anion was mainly increased by making nitrogen-doped activated carbon. For example, the activated carbon was heated by NH_3 gas at high temperature to enhance the adsorption capacity of nitrate [9]. Heat treatment of urea and melamine were applied to enhance the adsorption capacity of Cr(VI) [10]. However, nitrogen-doped activated carbon may have complex reaction and produce carbon, and nitrogen functional groups tend to degrade during the nitrogen removal process, which leads to non-recyclability of activated carbon [11]. Therefore, it is still a challenge to prepare activated carbon with high adsorption capacity and recyclable carbon.

Surface structural modification for activated carbon refers to the process of increasing the specific surface area by physical or chemical activation methods. The carbonization and activation of the materials were realized by selectively heating raw materials under inert atmosphere using different activators. The main activators used include $ZnCl_2$ [12, 13], H_3PO_4 [14], alkali such as KOH [15] and NaOH [16]. It is worth noting that KOH activation method can significantly increase the specific surface area of activated carbon.

Previous studies showed that the adsorption amount of Cr(VI) on activated carbon was relatively higher under acidic conditions [17]. However, under acidic conditions, Cr(VI) has strong oxidation and redox reaction may occur on the surface of activated carbon [18]. Therefore, it is necessary to separate the reduction process from the adsorption process for the study of adsorption of Cr(VI) onto activated carbon.

Based on these considerations, the commercial activated carbon NORIT CGP

SUPER (CGP) was further activated by KOH in this study, in order to increase the adsorption capacity for Cr(VI) in aqueous solution. Moreover, the adsorption and reduction cycles were studied in the experiment, and the regeneration performance of activated carbon was evaluated.

3.2. Materials and methods

3.2.1. Preparation of activated carbon

The activated carbon NORIT CGP SUPER (CGP) was purchased from CABOT Company (Japan). The CGP was dried in an oven at 110°C for 1 h. In activation step, the samples were mixed with solid KOH by different impregnation ratios (KOH/CGP mass ratio of 1:1, 2:1 and 3:1). Then, the mixtures were transferred to a stainless steel tube reactor and heated up to temperature range from 500°C to 800°C in N_2 gas atmosphere and held for 1 hour. The N_2 gas flow rate was 400 mL/min. After cooling to room temperature, the carbons were placed in 1 M HCl solution, stirred for 1 hour, then washed with hot distilled water until the pH in a Soxhlet was unchanged. Finally, the activated carbon was dried in an oven at 100°C overnight to remove the moisture, then cooled down in desiccators to room temperature. The obtained samples were referred to as CGP-K*x*-*y*, where *x* is the impregnation ratio (g KOH/g CGP) and *y* is the activation temperature in degree centigrade.

3.2.2. Characterization of activated carbon

The specific surface area (S_{BET}), mesopore volume (V_{meso}) and micropore volume (V_{micro}) of the prepared activated carbon were calculated based on N_2 adsorption/desorption isotherms at −196°C using Bellsorp-mini II (MicrotracBEL, Co., Ltd., Japan) surface area analyzer. The surface morphology of the activated carbon was observed by Hitachi S-4800 SEM instrument (Hitachi, Japan). The elemental composition of C, H and N for the adsorbents was determined with Perkin Elmer 2400 II (Perkin Elmer Japan, Co., Ltd., Japan), and O content was obtained by difference. X-ray photoelectron spectroscopy (XPS) analysis was performed using an ULVAC-PHI Model-1800 spectrometer.

3.2.3. Batch adsorption

Batch experiments for Cr(VI) adsorption were conducted to examine the adsorption and reduction performance of the prepared activated carbons as adsorbents. All batch experiments were carried out in Erlenmeyer flask. CGP, CGP-K3-800 and ion exchange resin HP555 were mainly compared in the experiment. The effects of the adsorbent dosage, contact time, initial pH, initial concentration of Cr(VI) and temperature were investigated in the batch experiments. The solution pH was adjusted with 0.1 M HCl and 0.1 M NaOH. The flasks were agitated in a thermostatic shaker at 100 rpm for 24 h. The concentration of Cr(VI) in the aqueous solution was determined by 1, 5-diphenylcarbohydrazide using UV-spectrophotometer (UV-2550, SHIMADZU, Japan) at 540 nm. The concentration of total chromium was measured by atomic

absorption spectrometer novAA300 (Analytik Jena AG, Germany), based on which the adsorption amount of Cr(VI) on activated carbons at the equilibrium was calculated by the following equation:

$$Q_e = (C_0 - C_{e1}) \times V/m, \qquad (3\text{-}1)$$

The removal percentage (R%) of Cr(VI) was calculated by the following equation:

$$R(\%) = (C_0 - C_{e2}) \times 100\%, \qquad (3\text{-}2)$$

where C_0 (mmol/L) represents the initial concentration of Cr(VI), C_{e1} (mmol/L) is the final adsorption equilibrium concentration of total chromium, C_{e2} (mmol/L) is the final adsorption equilibrium concentration of Cr(VI) as shown in Fig. 3-1. The m is the mass of sample (mg), V is the volume of solvent (mL).

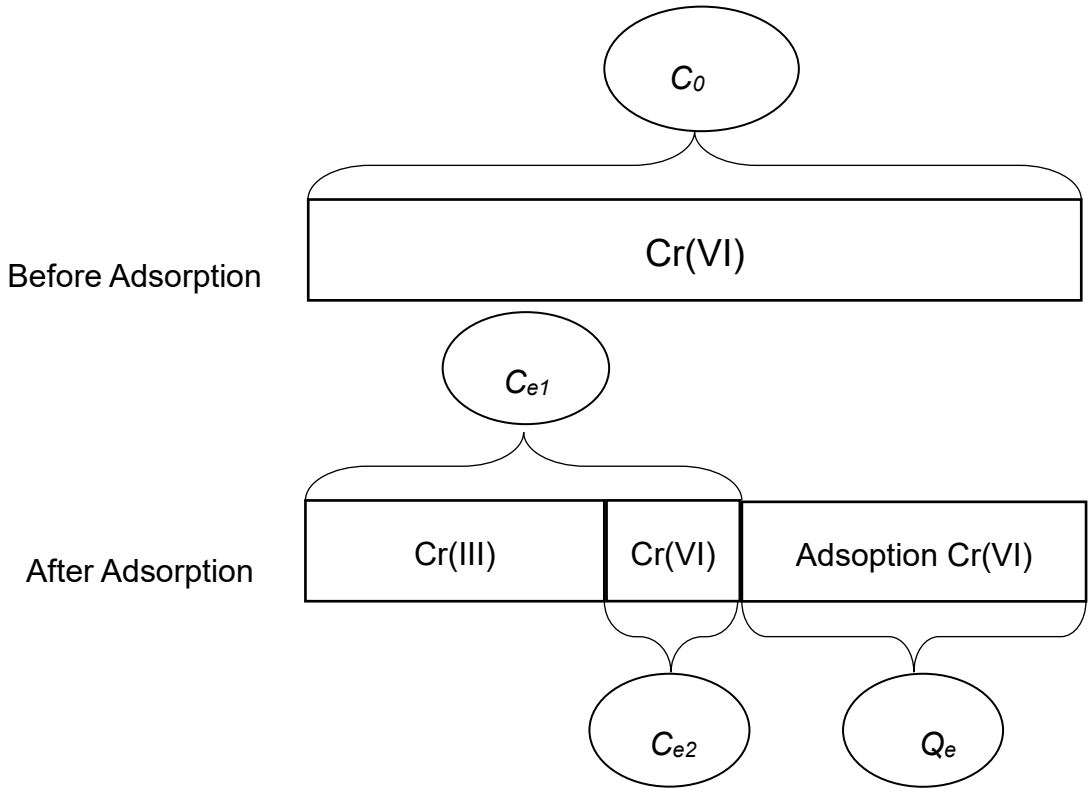

Fig. 3-1. State diagram of Cr(VI) before and after adsorption

3.2.4 Regeneration experiment

In regeneration experiment, 100 mg of adsorbents were added in a Erlenmeyer flask (500 mg/L) containing 100 mL of Cr(VI) solution with initial pH of 2. Then, the Erlenmeyer flask was placed in a reciprocal shaker and agitated at 100 rpm at 25°C. Meanwhile, 1 mol/L NaOH solution was used as the desorption agent. In the desorption agent, the solution was heated to 90℃ and kept for 1 h before filtering out the adsorbents. This process was repeatedly performed until the filtered solution was clear. The regeneration experiment was repeated in the successive adsorption-desorption cycles that were conducted for five times.

3.3. Results and discussion

3.3.1 Physicochemical characterization

The specific surface area (BET) and micro-/mesoporous structure parameters of the adsorbent were calculated and shown in Table 3-1. It can be seen that when the activation ratio is 3:1 and the activation temperature was 800℃, the adsorbent had maximum specific surface area and microporous volume. Moreover, the BET of CGP-K3-800 (3098 m^2/g) nearly doubles that of CGP (1634 m^2/g). Fig. 3-2 shows SEM images of the CGP and CGP-K3-800, where the surface of the samples can be clearly observed. The surface of the CGP-K3-800 is rougher than that of the original CGP. It has been reported that the high surface area and high pore volume can facilitate the transfer of heavy metal ions. Therefore, CGP-K3-800 is expected to have higher removal efficiency of Cr(VI). The elemental composition of CGP and CGP-K3-800 is showed in Table 3-2. It can be seen from Table 3-2 that the nitrogen contents in CGP and CGP-K3-800 were very low, indicating that there are a very limited number of nitrogen functional groups in the two adsorbents.

Table 3-1 Textural and surface properties of each prepared activated carbon.

Sample	S_{BET} (m^2/g)	V_{total} (cm^3/g)	V_{micro} (cm^3/g)	V_{meso} (cm^3/g)	D_{ave} (nm)
CGP	1634	1.36	1.2	0.13	0.95
CGP-K1-500	1532	1.25	1.1	0.11	0.92
CGP-K1-600	1610	1.10	1.0	0.10	0.84
CGP-K1-700	1897	1.27	1.2	0.10	0.86
CGP-K1-800	1858	1.07	1.0	0.10	0.90
CGP-K2-800	1918	1.36	1.3	0.10	1.02
CGP-K3-800	3098	2.23	2.1	0.14	1.30

Table 3-2 Elemental composition of CGP and CGP-K3-800.

Sample	C	H	N	O*
CGP	79.6	2.0	0.4	18.1
CGP-K3-800	91.4	0.1	0.3	8.2

* Calculated by difference

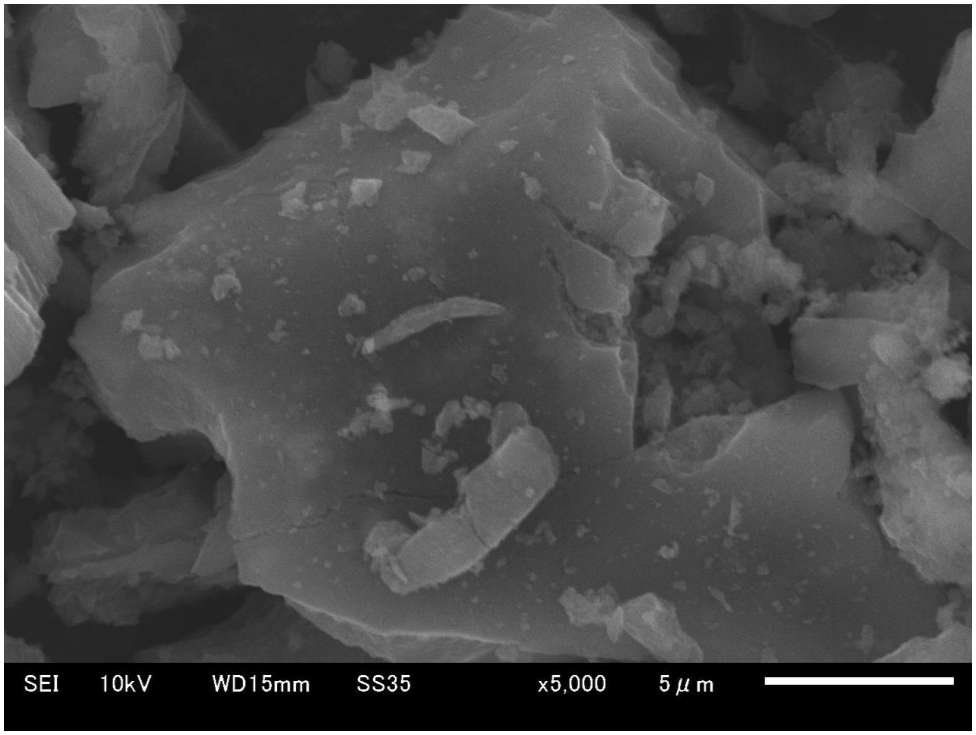

(a) CGP

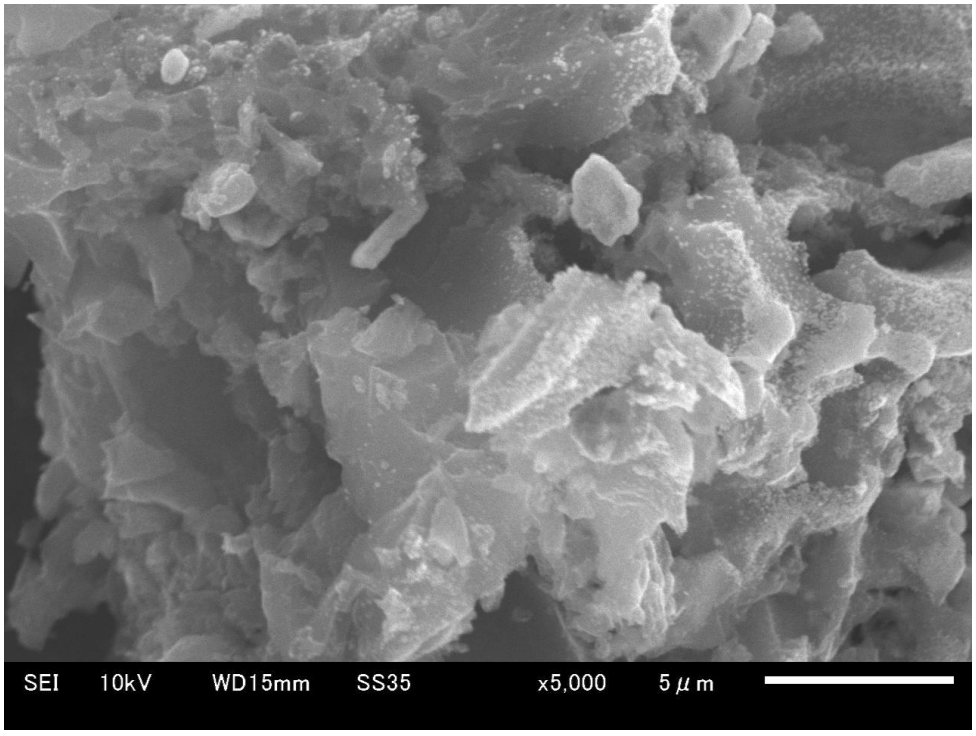

(b) CGP-K3-800

Fig. 3-2. SEM images of CGP (a) and CGP-K3-800 (b).

3.3.2 Removal efficiency of Cr(VI) for each prepared adsorbent

The experiment was carried out with the Cr(VI) concentration of 500 mg/L at pH 2.0 for 24 h. The Cr(VI) removal efficiency by different prepared adsorbents are shown in **Fig. 3-3**. It showed that the removal efficiency of the CGP modified by KOH activation (51.6% - 87.8%) was higher than that of the original CGP (42.3%). When the impregnation ratio (KOH/ CGP mass ratio) was 3:1 and the activation temperature was 800°C, the removal efficiency can reach 87.8%. Compared with the results of **Fig. 3-3**, it can be seen that the relatively larger specific surface area of CGP-K3-800 would be conductive to the removal of Cr(VI) on the activated carbons modified by CGP.

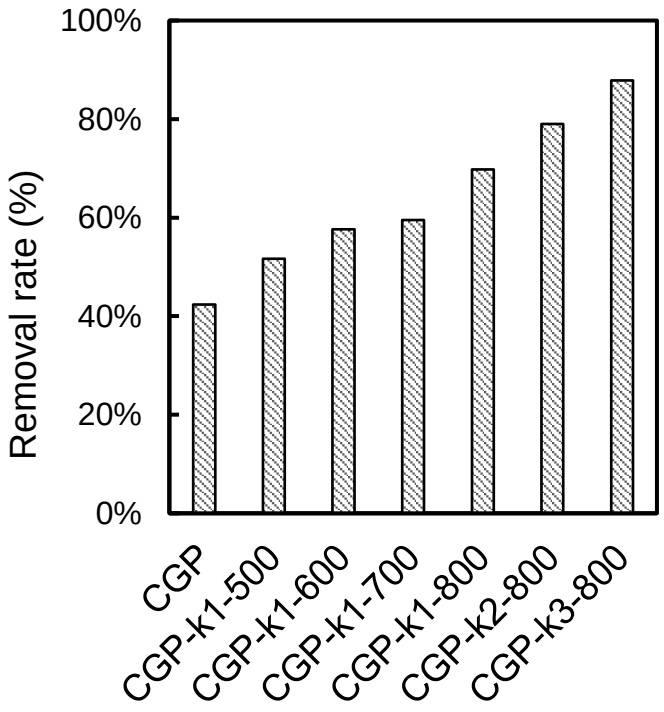

Fig. 3-3. Removal rate of Cr(VI) for each adsorbent,

(conditions: pH 2; initial concentrations of Cr(VI) : 500 mg/L; contact time : 24 h; concentration of adsorbent : 1 g/L; temperature : 298K).

3.3.3 Effect of initial solution pH

Initial solution pH has an significant impact on the removal efficiency of Cr(VI) in aqueous solution. Different solution pH values will cause different surface charges of the activated carbon and different anionic forms of the Cr(VI) . The Cr(VI) presents as different ionic forms in aqueous solution, when solution pH > 6, it presents as CrO_4^{2-}; when pH is within 1.0 – 6.0, the species are $Cr_2O_7^{2-}$ and $HCrO_4^-$, H_2CrO_4 will be dominant in case of pH < 1.0 [19]. In this experiment, the solution pH was adjusted from 2.0 to 12.0 with 0.1 M HCl and 0.1 M NaOH. The adsorption amount and the reduction amount were investigated within pH range from 2.0 to 12.0. The results are given in **Fig. 3-4.** It can be seen that the lower the solution pH value was, the larger the adsorption capacity for Cr(VI). This is because the solution pH value significantly affected the structure of the adsorbents and the surface charges of the adsorbent and the surface-reactive functional groups in the solution. When the solution pH was less than 6, Cr(VI) was reduced to Cr(III) to some extent on CGP-K3-800, so it can be known that the acid condition was conducive to the reduction process of Cr(VI).

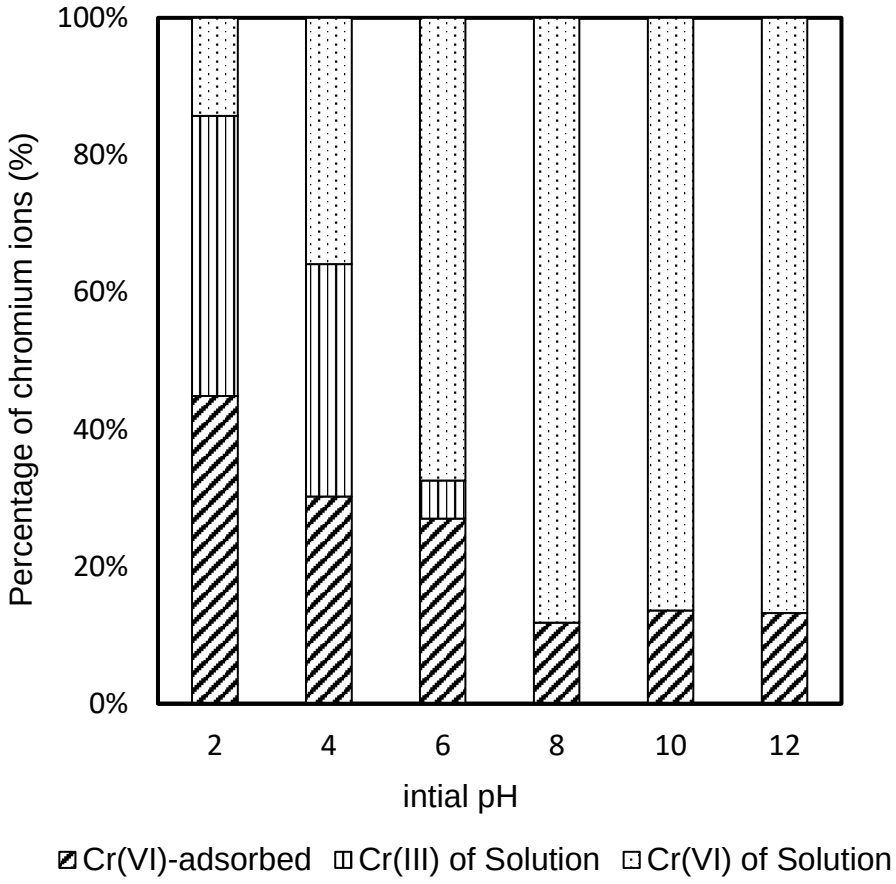

Fig. 3-4. Effect of pH of Cr(VI) adsorption onto CGP-K3-800.

(conditions: pH 2-12; initial concentrations of Cr(VI) : 500 mg/L; contact time : 24 h; concentration of adsorbent : 1 g/L; temperature : 298K).

3.3.4 Effect of adsorbents dosage

Adsorbents dosage can change the adsorbent–adsorbate equilibrium of the system. The effect of adsorbents dosage on Cr(VI) removal rate was investigated with the Cr(VI) concentration of 500 mg/L at pH 2.0 for 24 h in this work. As shown in **Fig. 3-5.**, the removal rate of Cr(VI) increased with the adsorbent dosage, which reached nearly 100% at the adsorbent dosage of 4 g/L. However, the adsorption capacity decreases with the increase of the adsorbents dosage, this may be due to the adsorption competition for adsorbents. Therefore, it is necessary to determine the dosage of adsorbents in actual water treatment. In this work, the adsorbent dosage set to 1 g/L for experiments.

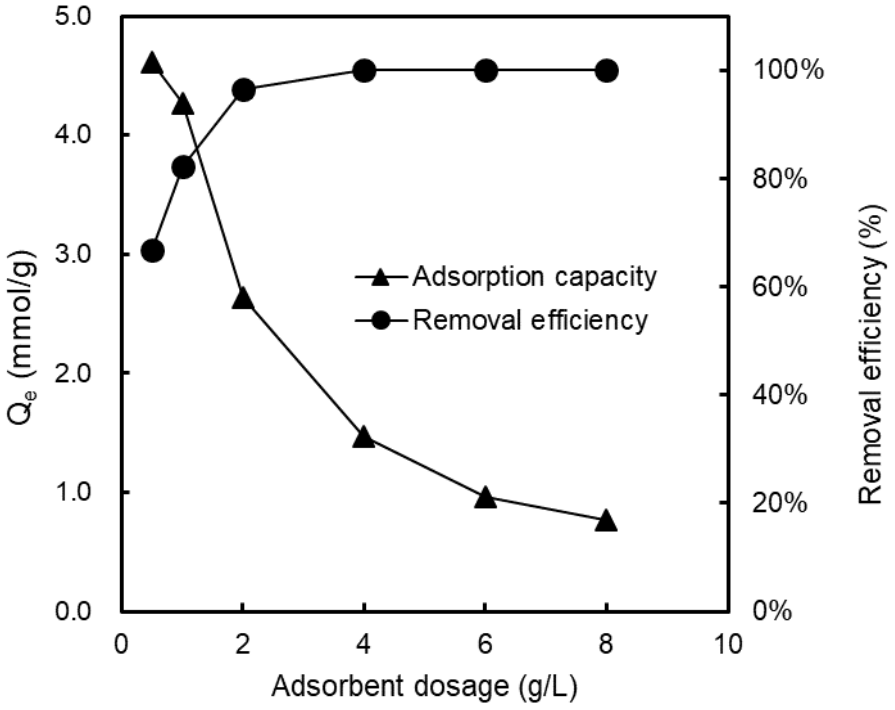

Fig. 3-5. The effect of adsorbent dosage on the CGP-K3-800 of Cr(VI) (conditions: pH 2; initial concentrations of Cr(VI) : 500 mg/L; contact time : 24 h; concentration of adsorbent : 0.5-8 g/L; temperature : 298K).

3.3.5 Adsorption isotherms

The adsorption isotherms of Cr(VI) on CGP, CGP-K3-800 and exchange resin HP555 under different initial concentrations (from 100 to 1000 mg/L) of Cr(VI) solution are shown in **Fig. 3-6**. Langmuir and Freundlich models were applied to investigate the adsorption process of Cr(VI) at 25°C.The different isotherm constants determined are shown in **Table 3-3**. Through the Langmuir and Freundlich data fitting of adsorption isotherms of Cr(VI), the R^2 values were greater than 0.99, indicating that the two models could well describe Cr(VI) adsorption behavior. In the Langmuir isothermal adsorption model, $R_L = 0.006$ ($0 < R_L < 1$), indicating favorable adsorption of Cr(VI) on the adsorbents. Langmuir model-based fitting data were slightly better than Freundlich adsorption model-based fitting data, indicating that Cr(VI) adsorption on CGP-K3-800 tended to be monolayer adsorption. Similar trends could be drawn from the adsorption isotherm data of CGP-K3-800**.** In comparison with the maximum adsorption capacity (X_m) of three adsorbents in adsorption isotherm experiment, the X_m value for CGP-K3-800 was larger than that for CGP and exchange resin HP555, implying that the adsorption capacity of CGP-K3-800 was better than that of CGP and exchange resin HP555. This may be because CGP-K3-800 has a greater specific surface area as shown in **Table 1**. Moreover, the adsorption capacity of CGP-K3-800 for Cr(VI) was higher than that reported in existing literature, as shown in **Table 3-4** [2, 10, 20, 21].

Table 3-3 Langmuir and Freundlich adsorption isotherm parameters of Cr(VI) at 298 K in aqueous solutions.

Sample	Langmuir model				Freundlich		
	X_m (mmol/g)	K_L (L/mmol)	R_L	R^2	n	K_F [(mmol/g)(mmol/L)^n]	R^2
CGP	3.09	1.97	0.031	0.981	3.55	1.68	0.916
CGP-K3-800	4.99	11.0	0.006	0.996	4.41	3.82	0.673
HP555	3.69	7.48	0.008	0.997	24.0	3.29	0.693

Table 3-4 Comparison with other similar adsorbents for Cr(VI) removal.

Adsorbent	Q_{max} (mmol/g)	Reference
bamboo	1.83	[10]
Auricularia auricula	0.23	[21]
hyacinth	0.84	[20]
longan seed	3.26	[2]
HP555*	3.69	This work
CGP*	3.09	This work
CGP-K3-800	4.99	This work

* Commercially available

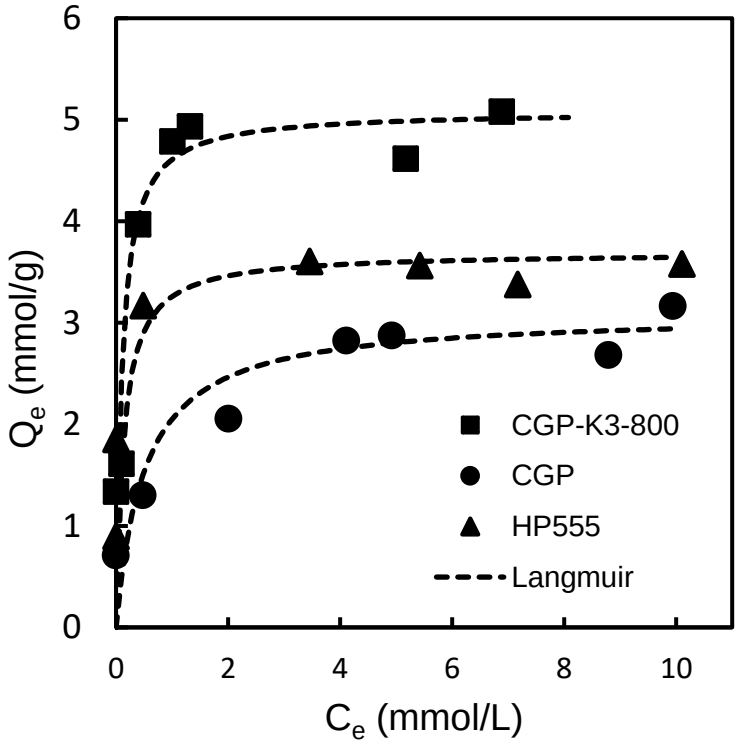

Fig. 3-6. Adsorption isotherms of Cr(VI) onto HP555, CGP and CGP-K3-800. (Conditions: initial concentrations of Cr(VI) : 100 to 1000 mg/L; contact time : 24 h; adsorbent : 1 g/L, respectively; temperature : 298 K).

3.3.6 Adsorption thermodynamics parameters

The correlation coefficients (R^2) are given in **Table 3-5**. Since Cr(VI) adsorption data on the CGP-K3-800 fitted better to the Langmuir adsorption isothermal equation in the study, there by the Langmuir adsorption isothermal constant K_L was adopted. The slopes and intercepts of the plots of ln K_L against 1/T are shown in **Fig. 3-7**. The values of $\Delta H°$, $\Delta S°$ and $\Delta G°$ for Cr(VI) adsorption on CGP-K3-800 are given in **Table 3-6.**

The positive values of $\Delta H°$ indicate that the adsorption process was an endothermic process. The negative value of $\Delta G°$ indicates that all adsorption processes were viable and spontaneous.

Table 3-5 The Langmuir and Freudlich adsorption isotherm parameters of Cr(VI) at different temperature onto CGP-K3-800

Temperature	Langmuir model			Freundlich model		
(K)	X_m (mmol/g)	K_L (L/mmol)	R_2	n	K_F [(mmol/g)(mmol/L)^n]	R_2
298	4.99	11.0	0.996	4.41	3.82	0.673
308	5.78	15.6	0.998	5.38	4.78	0.855
318	6.79	18.9	0.999	8.89	5.93	0.824

Table 3-6 Thermodynamic parameters of CGP-K3-800 for the adsorption of Cr(VI).

$\Delta S°$	$\Delta H°$	$\Delta G_1°$ (298 K)	$\Delta G_2°$ (308 K)	$\Delta G_3°$ (318 K)
(KJ/mol K)	(KJ/mol)	(KJ/mol)	(KJ/mol)	(KJ/mol)
0.0921	21.5	-5.99	-6.91	-7.83

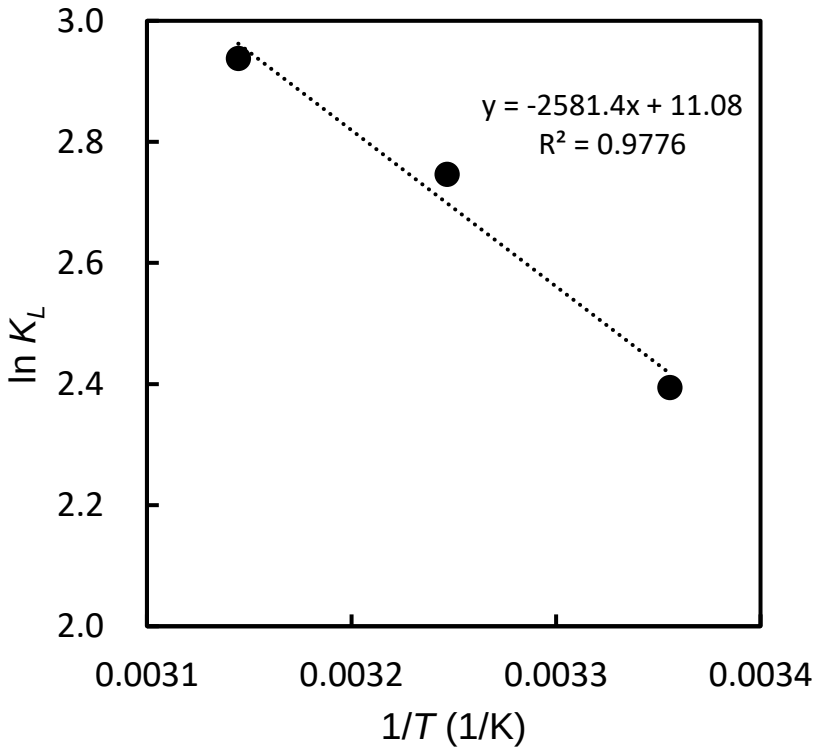

Fig.3-7. Plot of ln K_L vs. 1/T for Cr(VI) adsorption on CGP-K3-800

3.3.7 Adsorption kinetics

The experimental data in **Fig. 3-8** were fitted with pseudo-first-order model and pseudo-second-order model when CGP-K3-800, CGP and HP555 were used. The results of the kinetic analysis are shown in **Table 3-7**.

The pseudo-first-order model had lower correlation coefficient (R^2) compared to that of the pseudo-second-order models, and all R^2 values are greater than 0.99 for pseudo-second-order models. It can be seen from **Fig. 3-8** that both CGP and CGP-K3-800 had very high adsorption rates. The adsorption equilibrium can be reached within 30 min for CGP and CGP-K3-800, and their adsorption rates are appreciably higher than that of HP555.

Table 3-7 Kinetic parameters for Cr(VI) adsorption onto prepared adsorbents

Sample	Pseudo-first-order			Pseudo-second-order		
	Q_e (mmol/g)	k_1 (min^{-1})	R_2	Q_e (mmol/g)	k_2 (g/mmol min)	R_2
HP555	1.48	0.016	0.916	4.06	0.022	0.999
CGP	7.87	0.013	0.242	3.42	0.155	0.998
CGP-K3-800	7.45	0.021	0.366	4.69	0.099	0.999

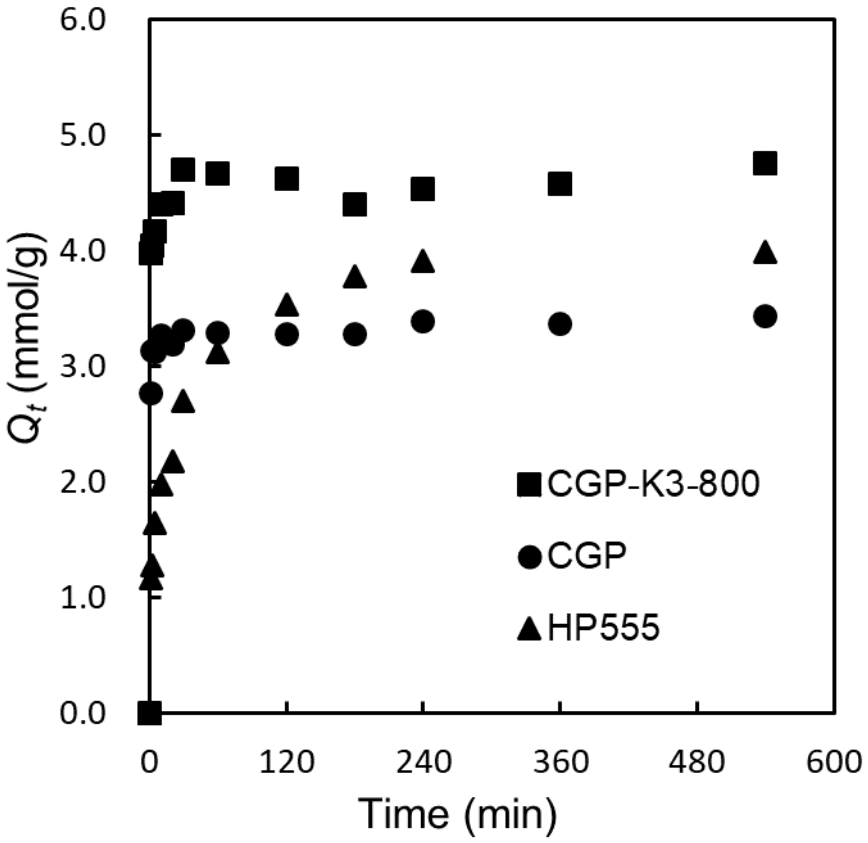

Fig. 3-8. Effect of contact time on the adsorption capacity of HP555, CGP and CGP-K3-800 (conditions: pH 2; initial concentrations of Cr(VI) : 500 mg/L; adsorbent : 1 g/L, respectively; temperature : 298 K)

3.3.8 XPS Analysis

Detailed XPS survey of the regions for Cr 2p of Cr(VI)-loaded CGP-K3-800 was shown in **Fig. 3-9**. Chromium element was detected which indicated the successful adsorption of chromium on the carbon surface. The peak at 576.5 eV in the Cr2p of CGP-K3-800 after adsorption in **Fig. 3-9** can be assigned to Cr(III), and the the binding energy of Cr(VI) in the Cr2p was generally higher than that of Cr(III), so the peaks at

578.1 eV in the Cr2p can be assigned to Cr(VI) [22]. According to the Cr2p peak areas, the ratio of adsorbed Cr(III) to Cr(VI) onto the CGP and CGP-K3-800 surface were all about 1.5:1, it was indicated that about 3/5 of the Cr(VI) was reduced to Cr(III) inside the CGP-K3-800.

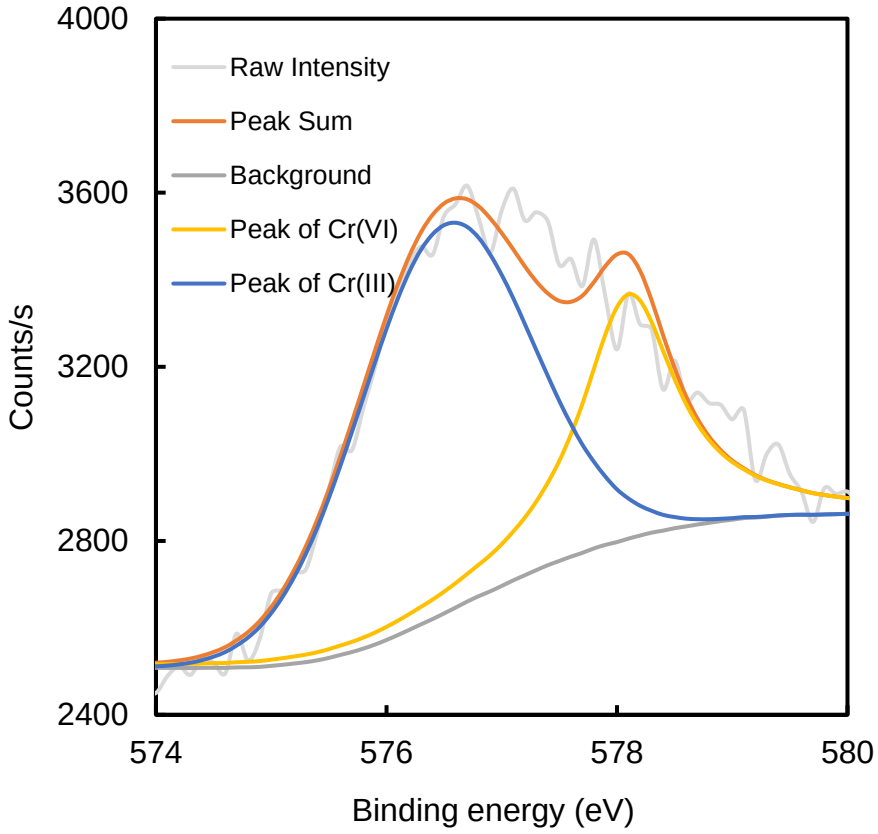

Fig. 3-9 Detailed XPS survey of the region Cr 2p

3.3.9 Regeneration experiment

In order to ascertain the reusability of the Cr(VI) on the adsorbents, this study evaluated the reproducible properties of CGP and analyzed the adsorption and reduction of Cr(VI) in the regeneration process. Fig. 3-10 shows that the adsorption capacity and

reduction efficiency decrease with the increase of cycle times. CGP-K3-800 had a higher regeneration rate than CGP, and kept high adsorption capacity until the 5th cycle. The decrease in percentage of adsorption was about 5% for each regeneration experiment. Moreover, it can be seen that the reduction performance gradually decreased, which was contributed to the decline of the percentage of removal. The decrease in reducing properties may be due to the continuous oxidation of the surface of the activated carbon.

3.4. Conclusions

In conclusion, the adsorbent CGP-K3-800 activated by KOH activation has a larger specific-surface-area and better effect on the removal of Cr(VI). The adsorbent CGP-K3-800 exhibits an adsorption capacity of 4.99 mmol/g at 25℃, which is 1.64 times larger than that of the CGP. The Cr(VI) adsorption capacity and capacity amount of CGP-K3-800 decrease with increase of solution pH value. The adsorption reaction conforms to the Langmuir model, and the increase of temperature can enhance the adsorption capacity of CGP. The CGP-K3-800 also shows a higher adsorption rate, and its adsorption equilibrium can be reached within 30 minutes. With respect to regenerative performance, CGP-K3-800 has better regeneration performance than CGP. With the increase of reutilization times, the surface of activated carbon is step wisely oxidized, which leads to gradual decrease of the reducing capacity.

References

[1] P. Miretzky, A.F. Cirelli, Cr(VI) and Cr(III) removal from aqueous solution by raw

and modified lignocellulosic materials: a review, J. Hazard. Mater. 180 (2010) 1-19.

[2] J.B. Yang, M.Q. Yu, W.T. Chen, Adsorption of hexavalent chromium from aqueous solution by activated carbon prepared from longan seed: Kinetics, equilibrium and thermodynamics, J. Ind. Eng. Chem. 21 (2015) 414-422.

[3] T.D. Çiftçi, E. Henden, Nickel/nickel boride nanoparticles coated resin: A novel adsorbent for arsenic(III) and arsenic(V) removal, Powder Technol. 269 (2015) 470-480.

[4] J.B. Dima, C. Sequeiros, N.E. Zaritzky, Hexavalent chromium removal in contaminated water using reticulated chitosan micro/nanoparticles from seafood processing wastes, Chemosphere 141 (2015) 100-111.

[5] W. Liu, J. Zhang, C. Zhang, L. Ren, Preparation and evaluation of activated carbon-based iron-containing adsorbents for enhanced Cr(VI) removal: mechanism study, Chem. Eng. J. 189 (2012) 295-302.

[6] P.K. Ghosh, Hexavalent chromium [Cr(VI)] removal by acid modified waste activated carbons, J. Hazard. Mater. 171 (2009) 116-122.

[7] M. Cieślak-Golonka, Toxic and mutagenic effects of chromium(VI). A review, Polyhedron 15 (1996) 3667-3689.

[8] M. Bansal, D. Singh, V. Garg, A comparative study for the removal of hexavalent chromium from aqueous solution by agriculture wastes' carbons, J. Hazard. Mater. 171 (2009) 83-92.

[9] M. Machida, T. Goto, Y. Amano, T. Iida, Adsorptive Removal of Nitrate from Aqueous Solution Using Nitrogen Doped Activated Carbon, Chem. Pharm. Bull. 64

(2016) 1555-1559.

[10] T.X. Shang, J. Zhang, X.J. Jin, J.M. Gao, Study of Cr (VI) adsorption onto nitrogen-containing activated carbon preparation from bamboo processing residues, J. Wood Sci. 60 (2014) 215-224.

[11] J. Sun, Z. Zhang, J. Ji, M. Dou, F. Wang, Removal of Cr6+ from wastewater via adsorption with high-specific-surface-area nitrogen-doped hierarchical porous carbon derived from silkworm cocoon, Appl. Surf. Sci. 405 (2017) 372-379.

[12] A. Kumar, H.M. Jena, Adsorption of Cr (VI) from aqueous phase by high surface area activated carbon prepared by chemical activation with $ZnCl_2$, Process Saf. Environ. Prot. 109 (2017) 63-71.

[13] C. Chen, P. Zhao, Z. Li, Z. Tong, Adsorption behavior of chromium(VI) on activated carbon from eucalyptus sawdust prepared by microwave-assisted activation with $ZnCl_2$, Desalin. Water Treat. 57 (2016) 12572-12584.

[14] N. Zhao, C. Zhao, Y. Lv, W. Zhang, Y. Du, Z. Hao, J. Zhang, Adsorption and coadsorption mechanisms of Cr(VI) and organic contaminants on H_3PO_4 treated biochar, Chemosphere 186 (2017) 422-429.

[15] B. Feng, W. Shen, L. Shi, S. Qu, Adsorption of hexavalent chromium by polyacrylonitrile-based porous carbon from aqueous solution, R. Soc. Open Sci. 5 (2018) 171662.

[16] R. Zhao, Y. Wang, X. Li, B. Sun, Y. Li, H. Ji, J. Qiu, C. Wang, Surface activated hydrothermal carbon-coated electrospun PAN fiber membrane with enhanced adsorption properties for herbicide, ACS Sustainable Chem. Eng. 4 (2016) 2584-2592.

[17] S. Wei, D. Li, Z. Huang, Y. Huang, F. Wang, High-capacity adsorption of Cr (VI) from aqueous solution using a hierarchical porous carbon obtained from pig bone, Bioresour. Technol. 134 (2013) 407-411.

[18] D. Park, S.-R. Lim, Y.-S. Yun, J.M. Park, Reliable evidences that the removal mechanism of hexavalent chromium by natural biomaterials is adsorption-coupled reduction, Chemosphere 70 (2007) 298-305.

[19] D. Mohan, C.U. Pittman Jr, Activated carbons and low cost adsorbents for remediation of tri-and hexavalent chromium from water, J. Hazard. Mater. 137 (2006) 762-811.

[20] J. Yu, C. Jiang, Q. Guan, P. Ning, J. Gu, Q. Chen, J. Zhang, R. Miao, Enhanced removal of Cr (VI) from aqueous solution by supported ZnO nanoparticles on biochar derived from waste water hyacinth, Chemosphere 195 (2017) 632-640.

[21] L. Dong, Y. Jin, T. Song, J. Liang, X. Bai, S. Yu, C. Teng, X. Wang, J. Qu, X. Huang, Removal of Cr (VI) by surfactant modified Auricularia auricula spent substrate: biosorption condition and mechanism, Environ. Sci. Pollut. Res. 24 (2017) 17626-17641.

[22] D. Park, Y.-S. Yun, J.H. Jo, J.M. Park, Mechanism of hexavalent chromium removal by dead fungal biomass of Aspergillus niger, Water Res. 39 (2005) 533-540.

Chapter 4 Adsorption behavior of Cr(VI) by N-doped biochar derived from bamboo

4.1 Introduction

Heavy metal wastewater pollution triggered by organic dyes has been recognized as a global issue of concern [1]. Cr(VI) is the common toxic heavy metal, which widely exists in manufacturing and dyeing wastewater, electroplating wastewater and other industrial wastewater [2, 3]. Cr(VI) has different compounds in aqueous solution, such as $Cr_2O_7^{2-}$, CrO_4^{2-} and $HCrO_4^-$ [4], and Cr(VI) is approximately 100 times higher toxicity than Cr(III) [5, 6]. Cr(VI) causes harmful effects on the human body due to its strong oxidizing characteristic and can be easily absorbed and accumulated, especially by kidneys, stomach, and liver [7]. WHO has set the Cr(VI) lower limit of drinking water to be 0.05 mg/L or less [8]. Therefore, it is necessary to carry out effluent treatment before discharging the Cr(VI) wastewater into the environment.

At present, conventional treatment methods of Cr(VI) containing wastewater include reduction [9], ion exchange [10], biological treatment method [11] and adsorption [12]. Among these, adsorption is a better method because of its high efficiency, low cost and simplicity of design [13]. Carbon adsorbents generally include activated carbon, carbon molecular sieves and carbon-containing nanomaterials [14]. Activated carbon is the most widely used carbon adsorption material [15]. Activated carbon is mostly made from bamboo, wood and other raw materials, which are activated after carbonization at high temperature [16]. Generally, activated carbon can be divided

into granular activated carbon and powdered activated carbon according to particle size. Activated carbon has a high specific surface area of up to 1500 m^2/g, and there are many kinds of oxygen-containing functional groups on the surface.

Biochar is an activated carbon like adsorbent [17]. However, due to the lack of porous structure, the specific surface area of most biochar is relatively low. To overcome this shortcoming, the primary activator used is $ZnCl_2$, H_3PO_4, KOH and NaOH. Among them, $ZnCl_2$ activation method is relatively sophisticated method [18]. Recent studies have reported that nitrogen (N) doping can enhance the adsorption capacity of activated carbon for anions such as nitrate [19]. Since the presence of quaternary nitrogen on the surface of nitrogen-doped activated carbon, it acts as a positively charged adsorption site on carbon, surface which is beneficial to the adsorption of various anions [20].

Bamboo could be regarded as cheaply available biochar material [21]. A large number of low-value bamboo wastes will be produced in the process of bamboo exploitation, processing, and utilization. The effective utilization rate of bamboo wastes is only about 35-40%. Bamboo waste, if discarded, decayed, buried or burned at will, not only will cause environmental pollution, but also a waste of bamboo resources. Bamboo contains a lot of cellulose and lignin, and its resource utilization is extensive. Biochar materials can be prepared by treating bamboo forest solid wastes, which have good adsorption effect on heavy metals and organic pollutants in water.

Based on these considerations, in this work, the commercial bamboo chips was further activated by $ZnCl_2$ and heat treated at 950℃ under NH_3 gas flow, in order to

increase the adsorption capacity for Cr(VI) in aqueous solution.

4.2 Material and methods

The feedstock for the production of biochar was willow residues pruned from moso bamboo. Moso bamboo obtained in Aichi prefecture, Japan, was cut into chips and used as a precursor for preparation of adsorbent.

The bamboo chips were dried in an oven at 110°C for 1 h. In this study, using the $ZnCl_2$ as an activator, the prepared bamboo chips were impregnated with $ZnCl_2$ solution at a ratio of 3 g-$ZnCl_2$/g-bamboo, and then the mixture was dried in an oven at 110°C overnight. The resulting mixture was pyrolyzed for 1 h at 400°C under N_2 atmosphere in a tubular furnace. The prepared biochar was placed in 1 M HCl solution and stirred for 1 h, rinsed in a Soxhlet extractor for 24 h, and dried at 110°C overnight. The obtained samples were referred to as BZ.

N-doped biochars were prepared from BZ. The prepared BZ was heated from room temperature to 600℃ under a helium atmosphere in a tubular furnace, then, the helium gas was directly replaced by NH_3 gas, then heated up to 950°C and kept it for 0, 15, 30 and 45 minutes. Finally, the NH_3 gas was changed to helium and cooled the samples were cooled to room temperature. The obtained samples were referred to as BZ-9.5AG-*x*min, where *x* is the heating retention time.

4.3 Biochar characterization

The specific surface area (S_{BET}), mesopore volume (V_{meso}) and micropore volume

(V_{micro}) of the prepared biochar were calculated based on N_2 adsorption/desorption isotherms at −196°C using Bellsorp-mini II (MicrotracBEL, Co., Ltd., Japan) surface area analyzer. The elemental composition of C, H and N of the adsorbents was determined with Perkin Elmer 2400 II (Perkin Elmer Japan, Co., Ltd., Japan) and O content was obtained by difference. X-ray photoelectron spectroscopy (XPS) analysis was performed using a JEOL JPS-9030 spectrometer. The concentrations of Cr(VI) solution after batch experiments were determined with atomic adsorption spectrometer novAA300 (Analytik Jena AG, Germany).

4.4 Batch adsorption

The removal of Cr(VI) by the biochar was examined by measuring the concentrations of Cr(VI) in a batch system. All batch experiments were carried out in Erlenmeyer flasks. Batch experiments were conducted in 30 mL Erlenmeyer flasks, with 0.02 g of the sample was put into a flask containing 20 mL of Cr(VI) solution with various initial concentrations. The flasks were agitated in a water bath shaker at 25°C by the speed of 100 rpm.

The effect of solution pH on Cr(VI) adsorption was examined by mixing 20 mg of adsorbent with 20 mL of 9 mmol/L Cr(VI) solution. The mixed solution had different pH values, ranging from 2 to 9. The initial pH of Cr(VI) solution was adjusted by 0.1 M HCl and 0.1 M NaOH.

The adsorption kinetics of Cr(VI) on biochar samples were studied by mixing 0.2 g of adsorbent with 200 ml of 9 mmol/L Cr(VI) solution, and the concentration was

analyzed at disparate time intervals (1, 2, 3, 4, 5, 10, 15, 20, 25, 30, 60, 120, 180, 240, 300, 480, 1500, and 1920 min). The data were analyzed using both the pseudo-first-order and the pseudo-second-order models.

In order to test the regeneration capacity of the biochar, added 300 mg of adsorbent to an Erlenmeyer flask containing 300 mL of Cr(VI) solution with an initial pH of 2 and an initial concentration of 9 mmol/L. The flasks were shaken at 100 rpm at 25℃ for 24 h to reach apparent equilibrium. Then the mixture was filtered with 0.45 μm filter paper, in the desorption agent, the filtered biochar was washed with distilled water and placed in 300 mL of 1 mol/L NaOH solution at 90℃ for 2 h. The regeneration experiment was repeated in the successive adsorption-desorption cycles that were conducted for five times.

4.5 Results and discussion

4.5.1 Characterization of biochar

The elemental composition of oxidized biochar with different NH_3 retention time is shown in **Table 4-1**. It can be seen from **Table 4-1** that the N content of BZ was only 0.4%, by contrast, the N content of biochar after NH_3 treatment increased. As the NH_3 retention time increased from 0 min to 30 min, the N content increased from 3.06% to 4.52%. And as the NH_3 retention time increased to 45 min, the N content of biochar decreased to 2.83%. This shows that the N content of biochar reaches the maximum when the NH_3 retention time was 30 min. Therefore, BZ-9.5AG-30min is expected to

have higher removal efficiency of Cr(VI).

The nitrogen adsorption-desorption isotherm curve of the BZ-9.5AG-*x*min is shown in **Fig. 4-1**. From **Fig. 4-1**, a type I isotherm was observed, which indicates the mainly microporous structure existence. The specific surface area (BET) and micro-/mesoporous structure parameters of the adsorbent were calculated and shown in **Table 4-2**. It can be seen that the specific surface area (S_{BET}) of biochar decreased after the beginning of NH_3 gas introduction, but the specific surface area of biochar increases with the increased of NH_3 retention time. This may be due to the formation of N-containing functional groups on the surface of biochar at the beginning of NH_3 introduction, thus reducing the surface area. With the increased of NH_3 retention time at high temperature, the microporous structure was developed continuously and the specific surface area of biochar increased.

Table 4-1 Elemental composition of BZ-9.5AG-30min

Sample	C [wt%]	H [wt%]	N [wt%]	O* [wt%]
BZ	90.4	1.41	0.20	7.92
BZ-9.5AG-0min	91.3	0.49	3.06	5.16
BZ-9.5AG-15min	90.7	0.44	3.50	5.36
BZ-9.5AG-30min	88.7	0.39	4.52	6.43
BZ-9.5AG-45min	90.6	0.41	2.83	6.18

* Calculated by difference

Table 4-2 Textural and surface properties of each prepared biochar

Sample	S_{BET} [m^2/g]	V_{total} [cm^3/g]	V_{micro} [cm^3/g]	V_{meso} [cm^3/g]
BZ	1400	0.75	0.74	0.01
BZ-9.5AG-0min	1120	0.55	0.55	0.01
BZ-9.5AG-15min	1280	0.63	0.63	0.01
BZ-9.5AG-30min	1610	0.85	0.85	0.01
BZ-9.5AG-45min	1870	1.00	0.99	0.01

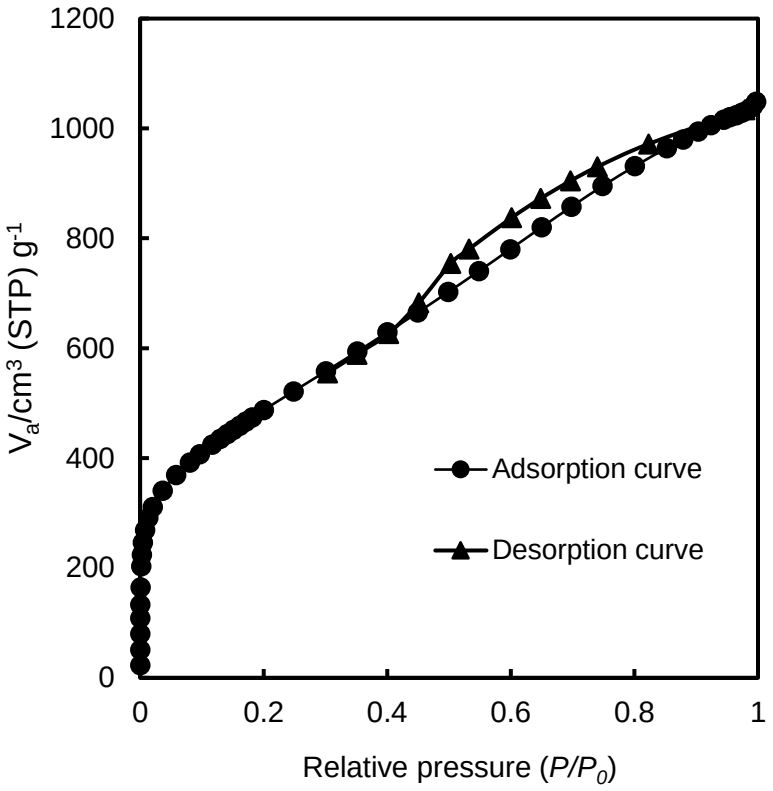

Fig. 4-1 Nitrogen adsorption isotherm of BZ-9.5AG-30min

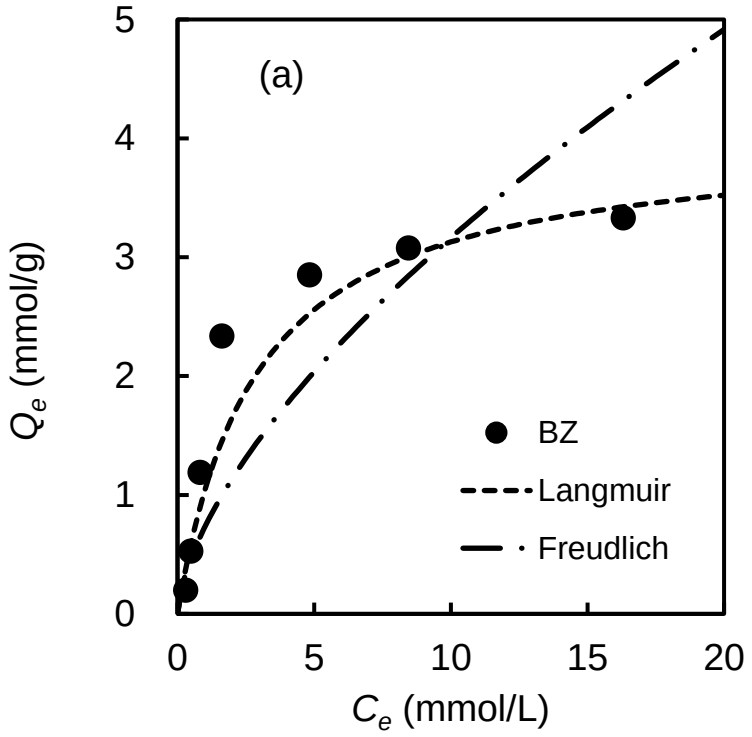

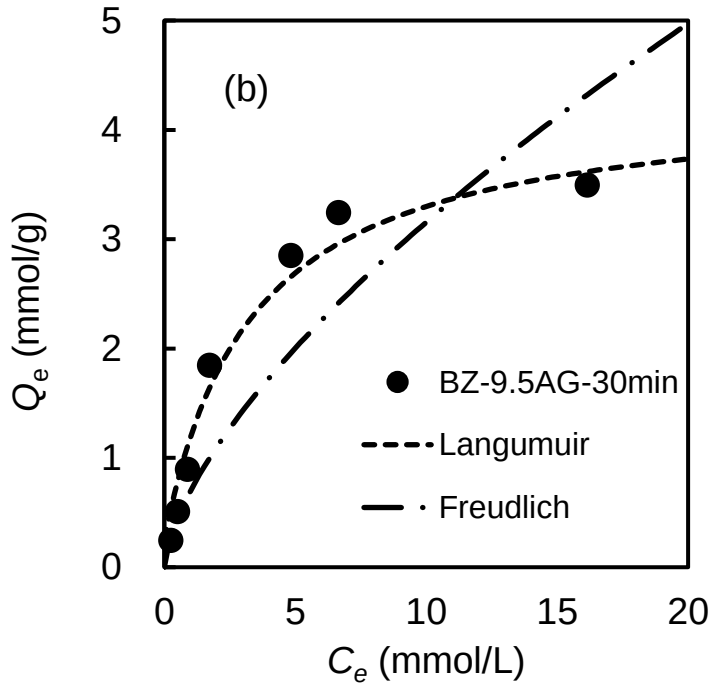

Fig. 4-2 Adsorption isotherms of BZ (a) and BZ-9.5AG-30min (b) for Cr(VI)

4.5.2 Adsorption isotherms and adsorption capacity

Adsorption isotherms of Cr(VI) on the BZ and BZ-9.5AG-30min are shown in **Fig 4-2**. Both Langmuir and Freundlich models were used to fit the adsorption data. The adsorption process of Cr(VI) at 25°C and the different isotherm constants determined were presented in **Table 4-3**. The R^2 values of the Langmuir model were larger than those of the Freundlich model, indicating that the Langmuir models can be a good description of Cr(VI) adsorption behavior. The Langmuir isotherm is usually used to describe the monolayer adsorption on a homogenous surface, indicating that Cr(VI) adsorption onto BZ and BZ-9.5AG-30min tended to be monolayer adsorption. BZ and BZ-9.5AG-30min all did exhibit high adsorption capacity for Cr(VI). Comparatively, the maximum adsorbed amount (X_m) of Cr(VI) onto BZ-9.5AG-30min was large than the X_m of BZ, which indicated that N-doped biochar has better adsorption capacity for Cr(VI). The increase of adsorbed amount can be explained by the increase of specific surface area and nitrogen content. Compared with BZ, BZ-9.5AG-30min had a larger specific surface area and total pore volume, so it can provide more adsorption sites. With the increase of nitrogen content, more quaternary nitrogen (N-Q) can be formed on the surface of biochar. Positive charges on quaternary nitrogen can provide more adsorption sites for anions, thus increasing the adsorption of Cr(VI).

Comparison with values in the literature (**Table 4-4**) shows that BZ-9.5AG-30min is among the highest carbon adsorbents for Cr(VI) [22-27], so it have great potential in practical water treatment applications.

Table 4-3 Langmuir and Freundlich adsorption isotherm parameters of Cr(VI) at 298K in aqueous solutions

	Langmuir model			Freudlich model		
Sample	X_m (mmol/g)	K_L (L/mmol)	R^2	1/n	K_F	R^2
BZ	3.81	0.38	0.95	0.64	0.73	0.80
BZ-9.5AG-30min	4.31	0.32	0.98	0.66	0.69	0.92

Table 4-4 Comparison with other similar adsorbents for Cr(VI) removal

Adsorbent	Q_e (mmol/g)	Reference
Swietenia mahagoni shell	1.13	[22]
Hevea brasilinesis saw dust AC	0.85	[23]
Biochar derived from waste water hyacinth	0.46	[24]
Bismuth modified biochar	0.23	[25]
Biochar derived from *Melia azedarach* wood	0.49	[28]
Ion exchange resin HP555	3.69	[27]
N-doped biochar BZ-9.5AG-30min	4.31	This work

4.5.3 Effect of pH

The initial pH of the solution usually has a great influence on the adsorption capacity of biochar. The effect of initial pH on the adsorption of Cr(VI) by BZ-9.5AG-30min is shown in **Fig. 4-3**. For adsorption of Cr(VI), the adsorbed amount of Cr(VI) on BZ-9.5AG-30min decreased as pH increased from 2 to 9. The effect of initial pH on

adsorption can be explained by the surface charge of biochar and the ionic forms of Cr(VI). Cr(VI) exists primarily as an oxyanion, and it exists in different ionic forms in aqueous solution. When solution pH is greater than 6, it presents as CrO_4^{2-}; when pH is ranging between 1.0 - 6.0, it exists as $Cr_2O_7^{2-}$ and $HCrO_4^-$. Therefore, when the solution pH has changed the form of the Cr(VI) ions will influence the Cr(VI) uptake capacity of the biochar. Moreover, amino groups exist on the surface of N-doped biochar. Under acidic conditions, amino groups present as $-NH_3^+$, with positive sites, which are also beneficial to the adsorption of Cr(VI) [28]. With the increase of pH, the amount of OH^- ions in the solution increases, and the competition between OH^- ions and Cr(VI) ions resulted in the decrease of the adsorption capacity of biochar to Cr(VI) [29].

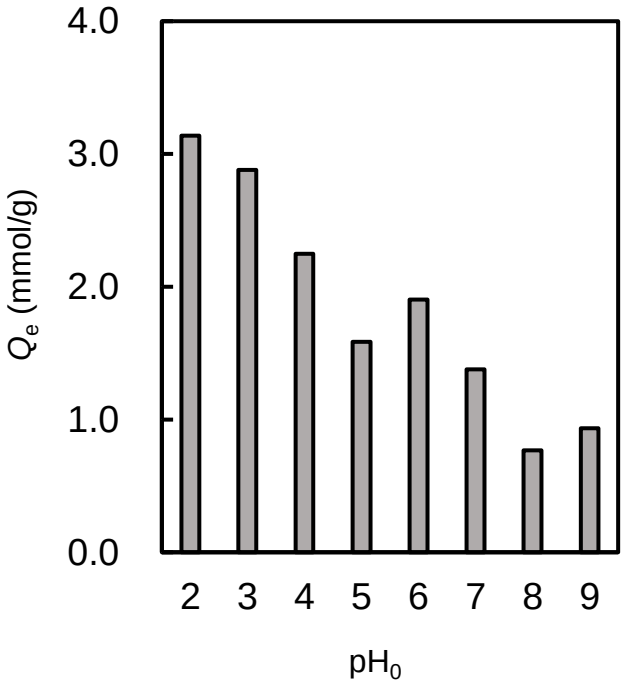

Fig. 4-3 Effect of initial pH value on Cr(VI) removal.

4.5.4 Effect of contact time and adsorption kinetics

The effects of contact time on the adsorption capacity of BZ-9.5AG-30min for

Cr(VI) were also investigated. As shown in **Fig. 4-4**, determination of the relationship between the amount of adsorption of Cr(VI) and time in the range of 0-2000 min. The adsorption rate of Cr(VI) was initially higher, reaching 86% of the maximum adsorption capacity at 480 minutes, and the adsorption capacity (Q_t) would not change after 1000 minutes. So the optimum adsorption time of BZ-9.5AG-30min for Cr(VI) was about 1000 min. The experimental data in **Fig. 4-4** were fitted with pseudo-first-order model and pseudo-second-order model, and the results of the kinetic analysis are shown in **Tables 4-5**. As shown in **Table 4-5**, the R^2 values of the pseudo-first-order model and the pseudo-second-order model are both higher than 0.95, however, the R^2 value of the pseudo-second-order model was larger than that of the pseudo-first-order model and larger than 0.99, which indicates that the pseudo-second-order model can better describe the adsorption of BZ on Cr(VI). These facts suggest that the adsorption behavior is mainly governed by diffusion control mechanism in Cr(VI) solution.

Table 4-5 Kinetic parameters for Cr(VI) adsorption onto BZ-9.5AG-30min

Pseudo-first-order			Pseudo-second-order		
Q_e (mmol/g)	k_1 (min^{-1})	R^2	Q_e (mmol/g)	k_2 (g/mmol min)	R^2
2.89	0.003	0.97	2.92	0.008	0.998

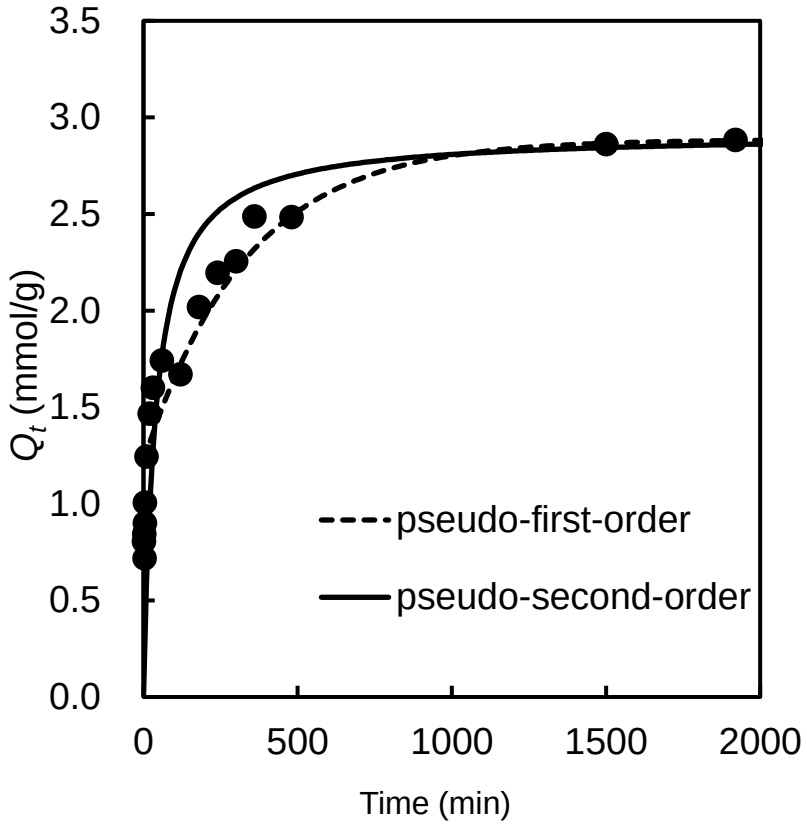

Fig. 4-4 Cr(VI) adsorption kinetic by BZ-9.5AG-30min

4.5.5 XPS analysis

The XPS spectra measurement was performed to investigate the surface chemical state and elemental changes of BZ-9.5AG-30min before and after adsorption. As shown in **Fig. 4-5(a)**, before the adsorption of Cr(VI), the XPS spectra of biochar showed three peaks, such as C 1s (284 eV), N 1s (400 eV) and O 1s (531 eV), respectively. After the experiment of Cr(VI) adsorption, a very obvious peak appeared at 578 eV, which is assigned to the Cr $2p_{3/2}$ energy level, suggesting that Cr(VI) was successfully adsorbed on the biochar. The N1s spectra of BZ-9.5AG-30min before and after the removal of Cr(VI) are shown in **Fig. 4-5(b)** and **Fig. 4-5(c)**. The N 1s spectrum was resolved into four individual peaks at 398.7 eV, 400.4 eV, 401.3eV and 403.3 eV, which are assigned

to pyridinic nitrogen (N-6), pyrrolic nitrogen (N-5), quaternary nitrogen (N-Q) and pyridine-N-oxide (N-X), respectively. Among them, because N-Q has a positive charge, the adsorption capacity of anions should be increased. Notably, as shown in **Table 4-6**, the percentage of N-Q in BZ-9.5AG-30min decreases from 22.3% to 5.5% after adsorption, and this would because the reduction process of Cr(VI) consumes the positive charge on the adsorbent surface, resulting in the decrease of N-Q.

Fig. 4-5(d) shows the Cr $2p_{3/2}$ spectrum, and the Cr $2p_{3/2}$ spectrum is divided into two peaks at 577.6 eV and 579.5 eV, which are assigned to Cr(III) and Cr(VI). The adsorbed chromium predominantly existed in Cr(III), and only a small amount was present as Cr(VI). As shown in **Fig. 4-5(d)**, 69.7% of the adsorbed chromium existed in trivalent form, and the remaining 30.3% was present as Cr(VI).

Table 4-6 Relative surface atomic ratios of different N species in BZ-9.5AG-30min before and after Cr(VI) adsorption

	N-6 (%)	N-5 (%)	N-Q (%)	N-X (%)
Before adsorption	37.1	11.4	22.3	29.2
After adsorption	25.9	50.4	5.5	18.2

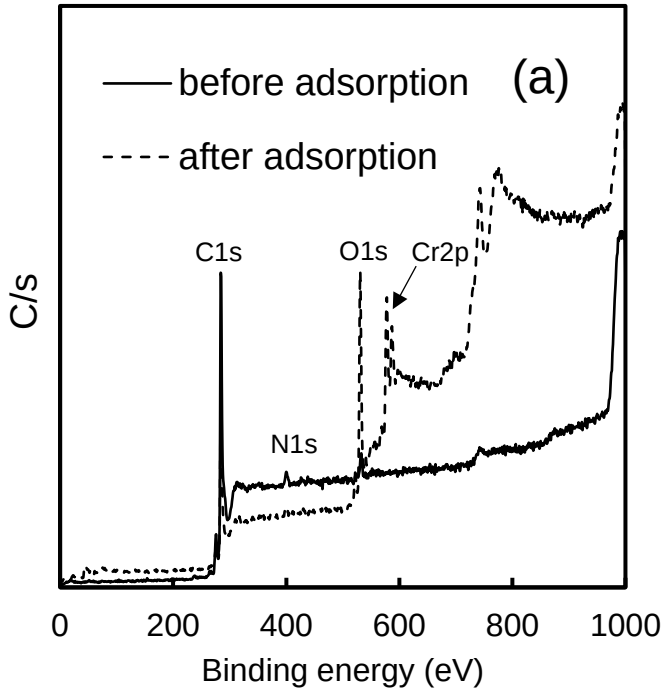
before adsorption
(a)
after adsorption
C1s
O1s
Cr2p
N1s
C/s
0
200
400
600
800
1000
Binding energy (eV)

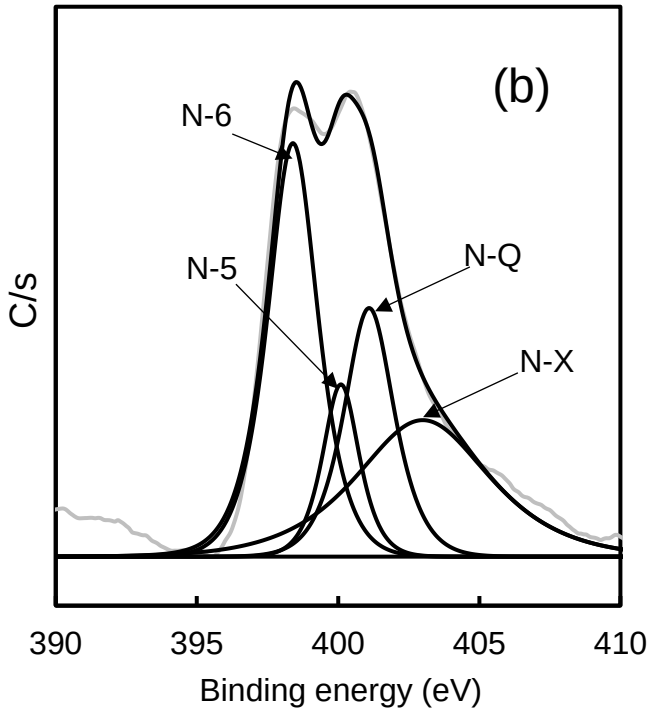
(b)
N-6
N-5
N-Q
N-X
C/s
390
395
400
405
410
Binding energy (eV)

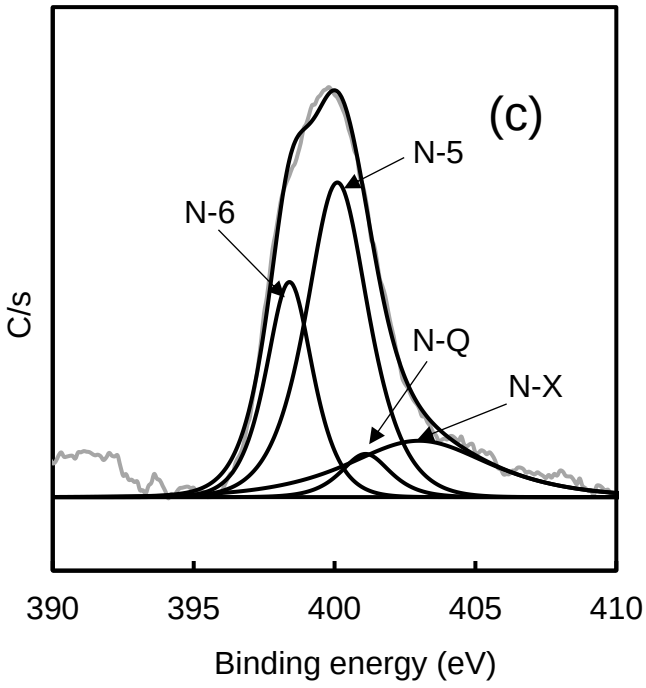

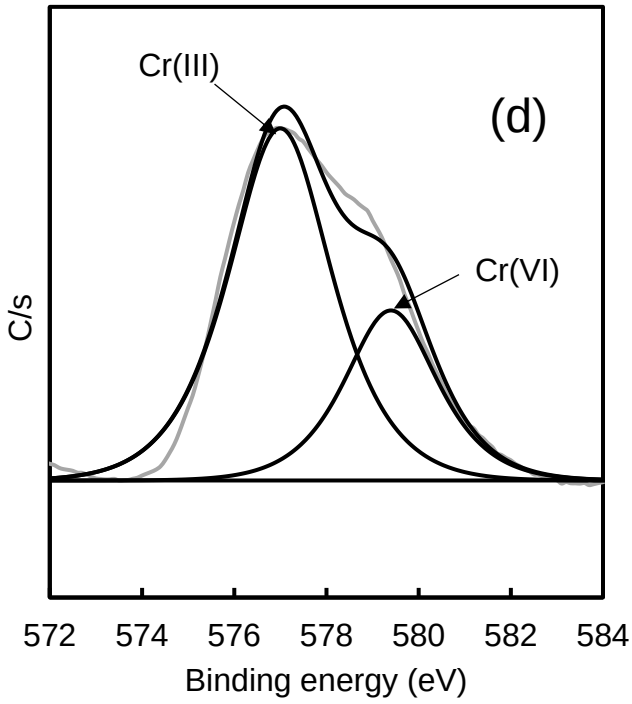

Fig. 4-6 (a) XPS survey spectra of BZ-9.5AG-30min before and after Cr(VI) adsorption; (b) N 1s spectrum of BZ-9.5AG-30min before Cr(VI) adsorption; (c) N 1s spectrum of BZ-9.5AG-30min after Cr(VI) adsorption; (d) Cr 2p spectrum of BZ-9.5AG-30min after Cr(VI) adsorption.

4.5.6 Regeneration experiment

In order to evaluate the recoverability of N-doped biochar BZ, five cycles of adsorption-desorption experiments were carried out on N-doped biochar BZ-9.5AG-30min. **Fig. 4-6** shows the adsorption capacity of BZ-9.5AG-30min for Cr(VI) in the function of the adsorption-desorption cycles. After five times regenerations, the adsorption capacity of BZ-9.5AG-30min still had 63% of the initial adsorption capacity, indicating that it had better regeneration ability for the removal of Cr(VI).

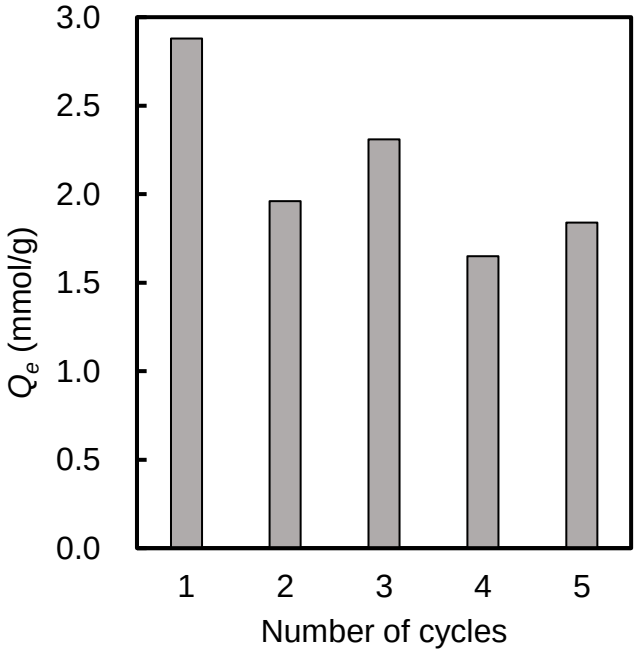

Fig. 4-6 The regeneration adsorptive performance of BZ-9.5AG-30min after five cycles.

4.6 Conclusions

In conclusion, we have successfully prepared N-doped biochar adsorbent BZ-9.5AG-30min for heavy metal Cr(VI) removal. The Cr(VI) removal experiments showed that BZ-9.5AG-30min had a high adsorption capacity (4.31 mmol/g) of Cr(VI), which was much higher than previous reports. The effect of pH has shown that the

highest adsorption capacity of Cr(VI) by BZ-9.5AG-30min was at pH 2. The adsorption reaction conformed to the Langmuir model, and the kinetic analyses indicated that the adsorption of Cr(VI) by BZ-9.5AG-30min was fitted well with the pseudo-second-order model. After 5 regeneration experiments, BZ-9.5AG-30min showed superior recyclability, and therefore, BZ-9.5AG-30min is expected to be a promising adsorbent for the efficient removal of Cr(VI) from wastewater.

References

[1] M.A. Farajzadeh, A.B. Monji, Adsorption characteristics of wheat bran towards heavy metal cations, Sep. Purif. Technol. 38 (2004) 197-207.

[2] R. Xiao, J.J. Wang, R. Li, J. Park, Y. Meng, B. Zhou, S. Pensky, Z. Zhang, Enhanced sorption of hexavalent chromium [Cr (VI)] from aqueous solutions by diluted sulfuric acid-assisted MgO-coated biochar composite, Chemosphere 208 (2018) 408-416.

[3] H. Lyu, J. Tang, Y. Huang, L. Gai, E.Y. Zeng, K. Liber, Y. Gong, Removal of hexavalent chromium from aqueous solutions by a novel biochar supported nanoscale iron sulfide composite, Chem. Eng. J. 322 (2017) 516-524.

[4] Z. Peng, C. Xiong, W. Wang, F. Tan, Y. Xu, X. Wang, X. Qiao, Facile modification of nanoscale zero-valent iron with high stability for Cr (VI) remediation, SSci. Total Environ. 596 (2017) 266-273.

[5] H. Shen, Y.-T. Wang, Simultaneous chromium reduction and phenol degradation in a coculture of Escherichia coli ATCC 33456 and Pseudomonas putida DMP-1, Appl. Environ. Microbiol. 61 (1995) 2754-2758.

[6] H. Dong, J. Deng, Y. Xie, C. Zhang, Z. Jiang, Y. Cheng, K. Hou, G. Zeng, Stabilization of nanoscale zero-valent iron (nZVI) with modified biochar for Cr (VI) removal from aqueous solution, J. Hazard. Mater. 332 (2017) 79-86.

[7] P. Miretzky, A.F. Cirelli, Cr (VI) and Cr (III) removal from aqueous solution by raw and modified lignocellulosic materials: a review, J. Hazard. Mater. 180 (2010) 1-19.

[8] M. Bansal, D. Singh, V. Garg, A comparative study for the removal of hexavalent chromium from aqueous solution by agriculture wastes' carbons, J J. Hazard. Mater. 171 (2009) 83-92.

[9] V. Pinos, A. Dafinov, F. Medina, J. Sueiras, Chromium (VI) reduction in aqueous medium by means of catalytic membrane reactors, J. Environ. Chem. Eng. 4 (2016) 1880-1889.

[10] S. Rapti, A. Pournara, D. Sarma, I.T. Papadas, G.S. Armatas, A.C. Tsipis, T. Lazarides, M.G. Kanatzidis, M.J. Manos, Selective capture of hexavalent chromium from an anion-exchange column of metal organic resin–alginic acid composite, Chem. Sci. 7 (2016) 2427-2436.

[11] Q. Zeng, Y. Hu, Y. Yang, L. Hu, H. Zhong, Z. He, Cell envelop is the key site for Cr (VI) reduction by Oceanobacillus oncorhynchi W4, a newly isolated Cr (VI) reducing bacterium, J. Hazard. Mater. 368 (2019) 149-155.

[12] B. Ramavandi, G. Asgari, J. Faradmal, S. Sahebi, B. Roshani, Abatement of Cr (VI) from wastewater using a new adsorbent, cantaloupe peel: taguchi L 16 orthogonal array optimization, Korean J. Chem. Eng. 31 (2014) 2207-2214.

[13] Y. Yan, Q. An, Z. Xiao, W. Zheng, S. Zhai, Flexible core-shell/bead-like alginate@

PEI with exceptional adsorption capacity, recycling performance toward batch and column sorption of Cr (VI), Chem. Eng. J. 313 (2017) 475-486.

[14] D. Mohan, K.P. Singh, V.K. Singh, Removal of hexavalent chromium from aqueous solution using low-cost activated carbons derived from agricultural waste materials and activated carbon fabric cloth, Ind. Eng. Chem. Res. 44 (2005) 1027-1042.

[15] S. Lalvani, T. Wiltowski, A. Hübner, A. Weston, N. Mandich, Removal of hexavalent chromium and metal cations by a selective and novel carbon adsorbent, Carbon 36 (1998) 1219-1226.

[16] B.G. Salas-Enríquez, A.M. Torres-Huerta, E. Conde-Barajas, M.A. Domínguez-Crespo, M.L. Negrete-Rodríguez, H.J. Dorantes-Rosales, A.B. López-Oyama, Stabilized landfill leachate treatment using Guadua amplexifolia bamboo as a source of activated carbon: kinetics study, Environ. Technol. 40 (2019) 768-783.

[17] X.-f. Tan, Y.-g. Liu, Y.-l. Gu, Y. Xu, G.-m. Zeng, X.-j. Hu, S.-b. Liu, X. Wang, S.-m. Liu, J. Li, Biochar-based nano-composites for the decontamination of wastewater: a review, Bioresour. Technol. 212 (2016) 318-333.

[18] Y. Su, X. Sun, X. Zhou, C. Dai, Y. Zhang, Zero-valent iron doped carbons readily developed from sewage sludge for lead removal from aqueous solution, J. Environ. Sci. 36 (2015) 1-8.

[19] T. Goto, Y. Amano, M. Machida, Preparation of Anion Exchangers Derived from Melamine Sponge and Its Adsorption Characteristics of Nitrate Ion, J. Chem. Eng. Jpn. 50 (2017) 692-695.

[20] P. Yoo, Y. Amano, M. Machida, Adsorption of nitrate onto nitrogen-doped

activated carbon fibers prepared by chemical vapor deposition, Korean J. Chem. Eng. 35 (2018) 2468-2473.

[21] R. Su, X. Dong, Preparation and Electrochemical Properties of Bamboo-based Carbon for Lithium-Ion-Battery Anode Material, Int. J. Electrochem. Sci. 14 (2019) 2452-2461.

[22] S. Rangabhashiyam, N. Selvaraju, Efficacy of unmodified and chemically modified Swietenia mahagoni shells for the removal of hexavalent chromium from simulated wastewater, J. Mol. Liq. 209 (2015) 487-497.

[23] T. Karthikeyan, S. Rajgopal, L.R. Miranda, Chromium (VI) adsorption from aqueous solution by Hevea Brasilinesis sawdust activated carbon, J. Hazard. Mater. 124 (2005) 192-199.

[24] J. Yu, C. Jiang, Q. Guan, P. Ning, J. Gu, Q. Chen, J. Zhang, R. Miao, Enhanced removal of Cr (VI) from aqueous solution by supported ZnO nanoparticles on biochar derived from waste water hyacinth, Chemosphere 195 (2018) 632-640.

[25] N. Zhu, T. Yan, J. Qiao, H. Cao, Adsorption of arsenic, phosphorus and chromium by bismuth impregnated biochar: Adsorption mechanism and depleted adsorbent utilization, Chemosphere 164 (2016) 32-40.

[26] X. Zhang, L. Lv, Y. Qin, M. Xu, X. Jia, Z. Chen, Removal of aqueous Cr (VI) by a magnetic biochar derived from Melia azedarach wood, Bioresour. Technol. 256 (2018) 1-10.

[27] B. Chu, M. Yamoto, Y. Amano, M. Machida, Adsorption, reduction and regeneration behavior of high surface area activated carbon in removal of Cr (VI),

Desalin. Water Treat. 136 (2018) 395-404.

[28] G. Zhao, J. Li, X. Ren, C. Chen, X. Wang, Few-layered graphene oxide nanosheets as superior sorbents for heavy metal ion pollution management, Environ. Sci. Technol. 45 (2011) 10454-10462.

[29] C. Liu, R.-N. Jin, X.-k. Ouyang, Y.-G. Wang, Adsorption behavior of carboxylated cellulose nanocrystal—polyethyleneimine composite for removal of Cr (VI) ions, Appl. Surf. Sci. 408 (2017) 77-87.

Chapter 5 Preparation of bean dreg derived N-doped activated carbon with high adsorption for Cr(VI)

5.1. Introduction

With the development of mining, chemical manufacturing, machinery and electronics industries, the problem of heavy metal pollution in water bodies has become increasingly serious [1]. Chromium is a heavy metal, and the major forms of existence in aqueous solution are Cr(VI) and Cr(III), respectively. Cr(VI) is approximately 100 times higher toxic than Cr(III) [2-4]. Cr(VI) is a highly toxic heavy metal ion that is carcinogenic and teratogenic to the human body [5, 6]. Generally, the concentration of Cr(VI) in drinking water should be lower than the 50 μg/L prescribed by WHO [7]. Common treatment methods of chromium containing wastewater include separation, reduction, ion exchange, and adsorption. Among them, the adsorption method is simple and the low cost, so it becomes a mainstream Cr(VI) removal method.

In the last decade, researches on agricultural-waste-based activated carbon adsorbents are in ascendant [8]. Activated carbon has been proved to be a universal adsorbent for heavy metal because of its favorable physicochemical properties and relatively low cost. Presently, many raw materials exist for activated carbon preparation [9], such as sawdust [10], wheat straw [11], camellia seed husk [12], pine tree residues [13], sludge [14], peanut hull [15], Enteromorpha prolifera [16], and other wood-based material such as bamboo [17], etc. In order to increase the specific surface area of activated carbon, the primary activator used is $ZnCl_2$, H_3PO_4, KOH, and steam. Among

them, steam activation is a low cost and environment friendly activation method [18].

Previous studies have shown that nitrogen doping is an effective method to improve the adsorption properties of carbon materials [19-22]. The increase in the content of quaternary nitrogen on the activated carbon surface enhances the adsorption capacity of nitrate ions [23]. Because of presence of quaternary nitrogen on the surface of nitrogen-doped activated carbon, it acts as a positively charged adsorption site on carbon, the surface which is beneficial to the adsorption of various anions. Recent studies have shown that nitrogen-doped activated carbon can enhance the adsorption capacity of activated carbon for Cd(II), Cu(II), and other heavy metal ions [21]. Bean dreg is an industrial waste with high protein content, and rich in nitrogen content, activated carbon made from bean dreg was used in the production of capacitors, etc [24, 25]. Meanwhile, with the high specific surface area bean dreg-derived activated carbon was also used to adsorb methyl blue [26]. However, according to our current knowledge, no attempt has been found on the use of nitrogen in bean dreg to generate quaternary nitrogen to increase the adsorption capacity of Cr(VI). Herein, in this work, bean dreg was used as a raw materials for large-scale manufacture of porous carbons by activation with steam, in order to increase the adsorption capacity for Cr(VI) in aqueous solution.

5.2. Materials and methods

5.2.1. Preparation of bean dregs derived activated carbon

Crude bean dregs were obtained from a workshop for making soya-bean milk in Chiba, Japan, and washed with distilled water, and dried in an oven at 110°C. The bean

dregs biomass was then placed into a porcelain crucible and capped, heating in a muffle furnace at 400℃ to eliminate volatiles, and then the sample was placed in 1 M HCl solution, stirred for 1 h, then washed with hot distilled water until the pH in extracted water was unchanged. The obtained samples were referred to as BDC. Thereafter, the prepared BDC was activated under a nitrogen atmosphere in a tubular furnace. The activation process was divided into two parts, steam activation, and heat treatment, respectively. Two grams of the BDC was inserted in the quartz pipe and heated from room temperature to 800℃ in 30 minutes, then, 30 mL of water was introduced for 30 minutes under a nitrogen atmosphere flow, and the steam activated samples were referred to as BDC-STM30. Finally heat the BDC-STM30 to 950℃, 1000℃ and 1050℃, and keep it for 30 minutes, after that, the samples were cooled to room temperature under N_2 gas flow. The obtained samples were referred to as BDC-STM30-9.5HT, BDC-STM30-10.0HT, and BDC-STM30-10.5HT, respectively. For comparison, the heat treatment process and the steam activation process were reversed in sequence, and the obtained samples were referred to as BDC-9.5HT-STM30, BDC-10.0HT-STM30, and BDC-10.5HT-STM30. For comparison, BDC was heated to 1000℃ for 30 minutes under N_2 gas flow, referred to as BDC-10.0OG.

5.2.2. Activated carbon characterization

The specific surface area (S_{BET}), mesopore volume (V_{meso}) and micropore volume (V_{micro}) of the prepared activated carbons were calculated based on N_2 adsorption/desorption isotherms at −196°C using Bellsorp-mini II (MicrotracBEL, Co.,

Ltd., Japan) surface area analyzer. The surface morphology of the activated carbon was observed by Hitachi S-4800 SEM (Hitachi, Japan). The elemental composition of C, H and N of the adsorbents was determined with Perkin Elmer 2400 II elemental analyzer (Perkin Elmer Japan, Co., Ltd., Japan), and O content was obtained by difference. X-ray photoelectron spectroscopy (XPS) analysis was performed using a ULVAC-PHI Model-1800 spectrometer. The concentrations of Cr(VI) solution after batch experiments were determined with atomic adsorption spectrometer novAA300 (Analytik Jena AG, Germany). FTIR spectrophotometer (IRAffinity-1, SHI-MADZU, Japan) was used to analyze surface functional groups of adsorbents.

5.2.3. Batch adsorption test

Potassium chromate (K_2CrO_4) was used to prepare Cr(VI) solution. A 10 mmol/L Cr(VI) stock solution was produced via dissolving 1.94 g of K_2CrO_4 in 1000 mL of distilled water. The adsorption experiments were conducted using a batch equilibrium method in 30 mL Erlenmeyer flasks at room temperature (25°C). The dosage of the experiments was 1g/L, and the initial Cr(VI) concentrations were 0.5-8 mmol/L. The calculation of adsorption capacity of Cr(VI) is based on the decrease of solute concentration in aqueous solution, as shown in Eq(5-1).

$$Q_e = (C_0 - C_e) \times V/m \qquad (5\text{-}1)$$

where Q_e (mmol/g) is the equilibrium adsorption capacity for Cr(VI) of activated carbon, m (g) is the mass of the activated carbon, V (L) is the volume of the Cr(VI) solution, C_0 (mmol/L) represents the initial concentration of Cr(VI), C_e (mmol/L) is the

adsorption equilibrium concentration of Cr(VI).

To determine the best adsorption capacity of Cr(VI) by each activated carbon. The activated carbons were added to 30 mL flasks of an 8 mmol/L Cr(VI) solution. The initial pH of the Cr(VI) was 2. The adsorption capacities of each activated carbon were compared.

In order to explore the effect of pH on the adsorption of Cr(VI), the pH of Cr(VI) solution with the initial concentration of 8 mmol/L was adjusted to 2-9 with 0.1 M HCl or NaOH solution. The pH of the Cr(VI) solutions was measured using a pH meter (HORIBA, SS054, JAPAN). After 24 h of shaking, the equilibrium Cr(VI) concentration was measured.

The adsorption kinetics of Cr(VI) on activated carbon samples were studied by mixing 0.2 g of adsorbent with 200 mL of 4 mmol/L Cr(VI) solution, and the concentration was analyzed at disparate time intervals (1, 2, 3, 4, 5, 10, 15, 20, 25, 30, 60, 120, 180, 240, 300, and 480 min). The data were analyzed using both the pseudo-first-order and the pseudo-second-order models. The linearized forms of the models are shown as follows:

$$\ln(Q_e - Q_t) = lnQ_e - k_1 t, \quad (5\text{-}2)$$

$$\frac{t}{Q_t} = \frac{1}{k_2 Q_e^2} + \frac{t}{Q_e}, \quad (5\text{-}3)$$

where Q_e is the amount of Cr(VI) adsorbed at equilibrium (mmol/g), Q_t is the adsorbed amount of Cr(VI) (mmol/g) at time t (min). k_1 and k_2 are the rates constant of the pseudo-first-order model (min^{-1}) and the pseudo-second-order model (g/mmol•min).

By fitting and analyzing the adsorption isothermal model of Cr(VI) by activated

carbon, the information of the interaction between activated carbon and Cr(VI) ions and the surface properties of activated carbon can be obtained. Two isotherm models (Langmuir and Freundlich) were utilized to describe the adsorption isotherm data.

The Langmuir isothermal adsorption model is a theoretical model assuming that the adsorbents were adsorbed in monolayer on the uniform surface of the adsorbent. The Langmuir adsorption isotherm is applicable to both physical and chemical adsorption. It describes the monolayer adsorption on the solid surface. Generally, the Langmuir model can be used to determine the maximum adsorption capacity of adsorbents with monolayer adsorption as the main adsorbent. The linear form of Langmuir equation can be given as follow:

$$\frac{C_e}{Q_e} = \frac{1}{X_m K_L} + \frac{1}{X_m} C_e, \qquad (5\text{-}4)$$

where Q_e (mmol/g) is the adsorbed amount of Cr(VI) at equilibrium, C_e (mmol/L) is the equilibrium concentration of Cr(VI) in the solution, X_m (mmol/g) is the monolayer maximum adsorption capacity, and K_L (L/mmol) is the Langmuir constant related to adsorption energy.

The Freundlich adsorption model is another widely used model to simulate the adsorption behavior on the surface of heterogeneous adsorbents. It considers that the adsorption sites have different adsorption energies or are not independent of each other during the adsorption process. The linear form of the Freundlich equation is:

$$\ln Q_e = \ln K_F + \frac{1}{n} \ln C_e, \qquad (5\text{-}5)$$

where K_F is the Freundlich constant and $1/n$ is the heterogeneity factor. The greater the value of n is, the better the adsorption performance will be.

In order to test the regeneration capacity of the activated carbon, 300 mg of adsorbent was added to an Erlenmeyer flask containing 300 mL of Cr(VI) solution with an initial pH of 2 and an initial Cr(VI) concentration of 4 mmol/L. The flasks were shaken at 100 rpm at 25℃ for 24 h to reach apparent equilibrium. Then the mixture was filtered with 0.45 μm filter paper. Meanwhile, 1 mol/L NaOH solution was used as the desorption agent. filtered activated carbon was washed with distilled water and placed in the desorption agent. Then, the NaOH solution was heated to 90 ℃ and kept for 2 h before filtering out the adsorbents. The regeneration experiment was repeated in the successive adsorption-desorption cycles that was conducted five times.

5.3. Results and discussion

5.3.1. Physicochemical characteristics of activated carbons

The C, H, N, and O contents and BET surface area of the activated carbons are shown in **Table 5-1**. It can be seen from Table 1 that the specific surface area of BDC samples before steam activation was very small, only 31 m^2/g. After steam activation and high temperature heating, the specific surface area of activated carbon increased in varying degrees. The specific surface area of activated carbon decreases with the increase of heating temperature when heating above 950℃ and then steam activation. This is because with the increase of heating temperature, the texture of activated carbon hardens, and then steam activation becomes difficult. When steam activation was carried out before high treatment temperature, the specific surface area of activated carbon reaches a maximum at 1000°C as the heating temperature increases. It can be

seen from the results of the elemental analysis that the nitrogen content in the raw material of the bean dregs was relatively high, reaching 4.62%, higher than known N-doped adsorbent materials [23]. After steam activation and high temperature treatment, the nitrogen content decreased to varying degrees, and the nitrogen content decreased with increasing heating temperature.

The XPS spectra measurement was performed to investigate the surface chemical state and elemental changes of BDC-STM30 before and after 1000℃ heating. Detailed XPS survey of the regions for C1s and N1s of BDC-STM30 and BDC-STM30-10.0HT are shown in **Fig. 5-1**. As shown in **Fig. 5-1**, there were differences between the main functional groups on the BDC-STM30 and BDC-STM30-10.0HT. For the C1s XPS spectrum of the BDC-STM30 and BDC-STM30-10.0HT, a strong peak appeared at 285.4 eV, which is attributed to C-C, and the other peaks located at 286.7 and 288.4 eV are assigned to the C-O and C=O, respectively [27]. The N1s spectrum was resolved into four individual peaks at 398.7 eV, 400.4 eV, 401.3eV and 403.3 eV, which are assigned to pyridinic nitrogen (N-6), pyrrolic nitrogen (N-5), quaternary nitrogen (N-Q) and pyridine-N-oxide (N-X), respectively [28]. Among them, because N-Q has a positive charge, the adsorption capacity of anions should be increased [29]. As shown in **Table 5-2**, after 1000℃ heating, the mass ratio of the carboxyl groups (–COOH) decreased from 8.31% to 4.83%, and the percentage of N-Q increased from 0.06% to 1.11%. This indicates that 1000℃ heating reduces the oxygen-containing functional groups on the surface of the activated carbon and greatly increases the proportion of the quaternary nitrogen.

Table 5-1 Porosity structures and elemental analysis results of various BD-derived carbon materials.

Sample	C (wt%)	H (wt%)	N (wt%)	O (wt%)	S_{BET} (m^2/g)	V_{total} (cm^3/g)	V_{micro} (cm^3/g)	V_{meso} (cm^3/g)	Q_e (mmol/g)
Bean Dregs	48.2	6.76	4.62	40.5					
BDC	71.5	3.80	6.30	18.4	31	0	0	0	0.01
BDC-9.5HT-STM30	81.7	0.42	3.16	14.8	583	0.33	0.3	0.03	1.57
BDC-10.0HT-STM30	83.5	0.35	2.88	13.3	551	0.31	0.29	0.02	1.51
BDC-10.5HT-STM30	85.7	0.22	2.26	12.4	308	0.21	0.19	0.02	0.66
BDC-10.0OG	87.3	0.38	4.17	8.15	133	0.08	0.07	0.01	0.02
BDC-STM30	87.0	0.96	4.53	7.53	673	0.32	0.30	0.02	0.78
BDC-STM30-9.5HT	87.7	0.56	3.27	8.51	794	0.38	0.36	0.02	1.58
BDC-STM30-10.0HT	89.4	0.40	2.42	7.81	1004	0.50	0.47	0.03	3.30
BDC-STM30-10.5HT	81.6	0.38	2.09	15.9	547	0.33	0.31	0.02	0.98

Table 5-2 Relative surface atomic ratios BDC-STM30 and BDC-STM30-10.0HT

	-COOH (wt%)	N-6 (wt%)	N-5 (wt%)	N-Q (wt%)	N-X (wt%)
BDC-STM30	8.31	2.04	1.46	0.06	0.96
BDC-STM30-10.0HT	4.83	0.74	0.18	1.11	0.39

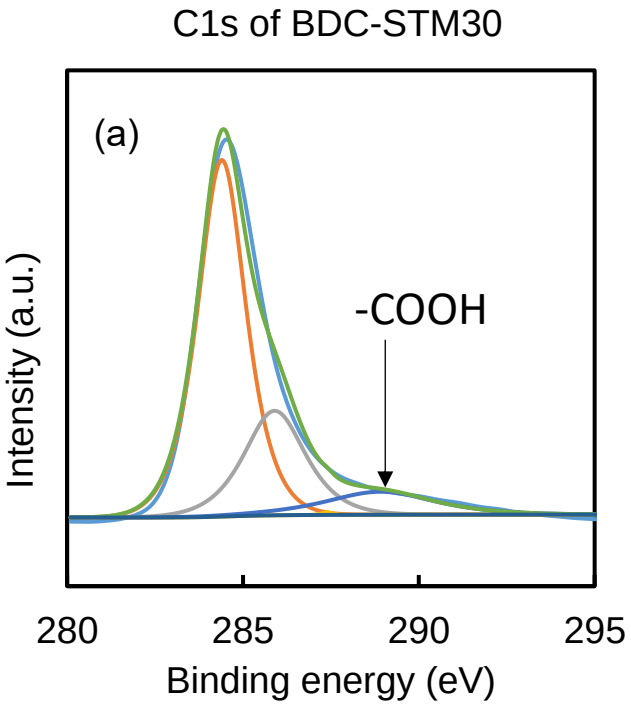
C1s of BDC-STM30
(a)
-COOH
Intensity (a.u.)
280
285
290
295
Binding energy (eV)

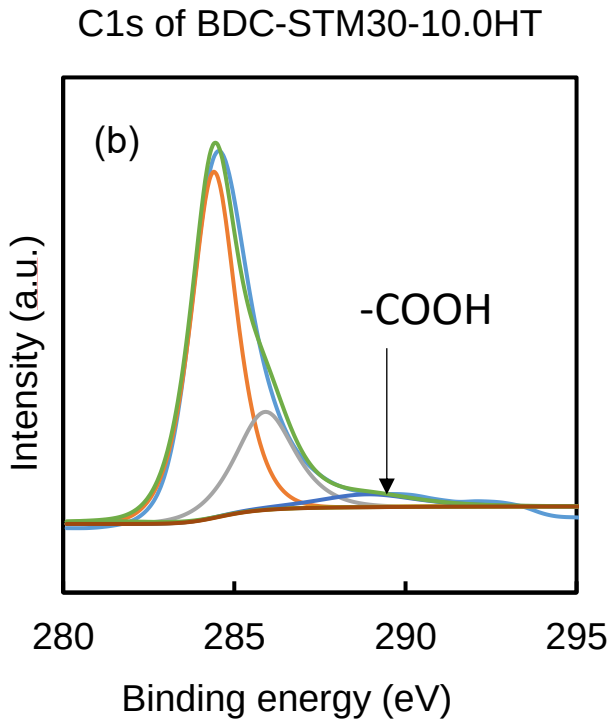
C1s of BDC-STM30-10.0HT
(b)
-COOH
Intensity (a.u.)
280
285
290
295
Binding energy (eV)

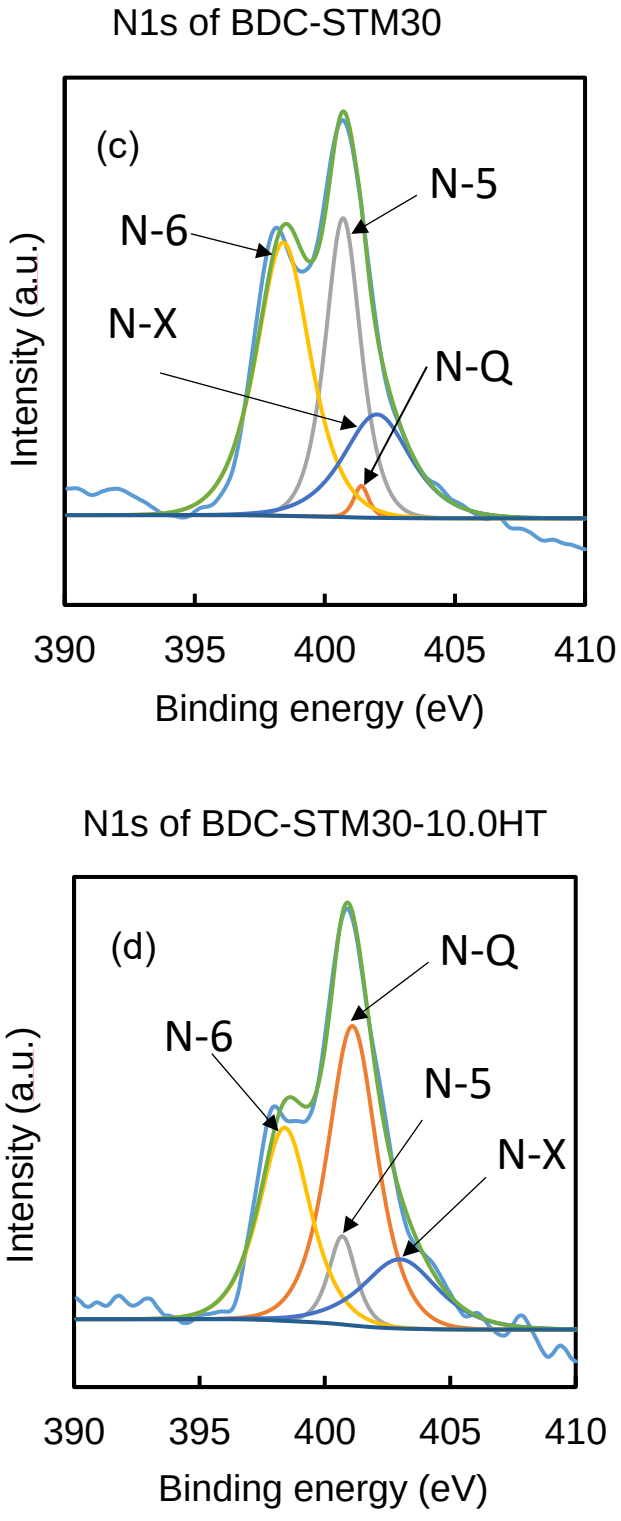

Fig. 5-1. XPS survey spectra of BDC-STM30 and BDC-STM30-10.0HT

5.3.2 Adsorption experiments

Cr(VI) adsorption onto bean dregs derived activated carbon materials is compared

in **Fig. 5-2(a)**. The activated carbons without steam activation, such as BDC and BDC-10.0OG, had almost no adsorption effect on Cr(VI) ($Q_e \leq 0.02$ mmol/g), and the adsorption capacity of Cr(VI) by steam activated bean dregs carbon BDC-STM30 was high, this indicates that steam activation is an important step to increase the amount of adsorption. The adsorption capacity of Cr(VI) decrease in BDC-9.5HT-STM30, BDC-10.0HT-STM30, and BDC-10.5HT-STM30, and increase in BDC-STM30, BDC-STM30-9.5HT, and BDC-STM30-10.0HT. Therefore, the sequence of steam activation and heating, and heating temperature are pivotal factors to obtain the best adsorption capacity. Furthermore, linear relationship between of Q_e and the surface area of bean dregs derived activated carbon materials ($R_2 = 0.799$) are observed in **Fig. 5-2(b)**. It conforms that the adsorption amount of Cr(VI) by activated carbon has a certain positive correlation with the specific surface area, but it was not completely determined by the specific surface area.

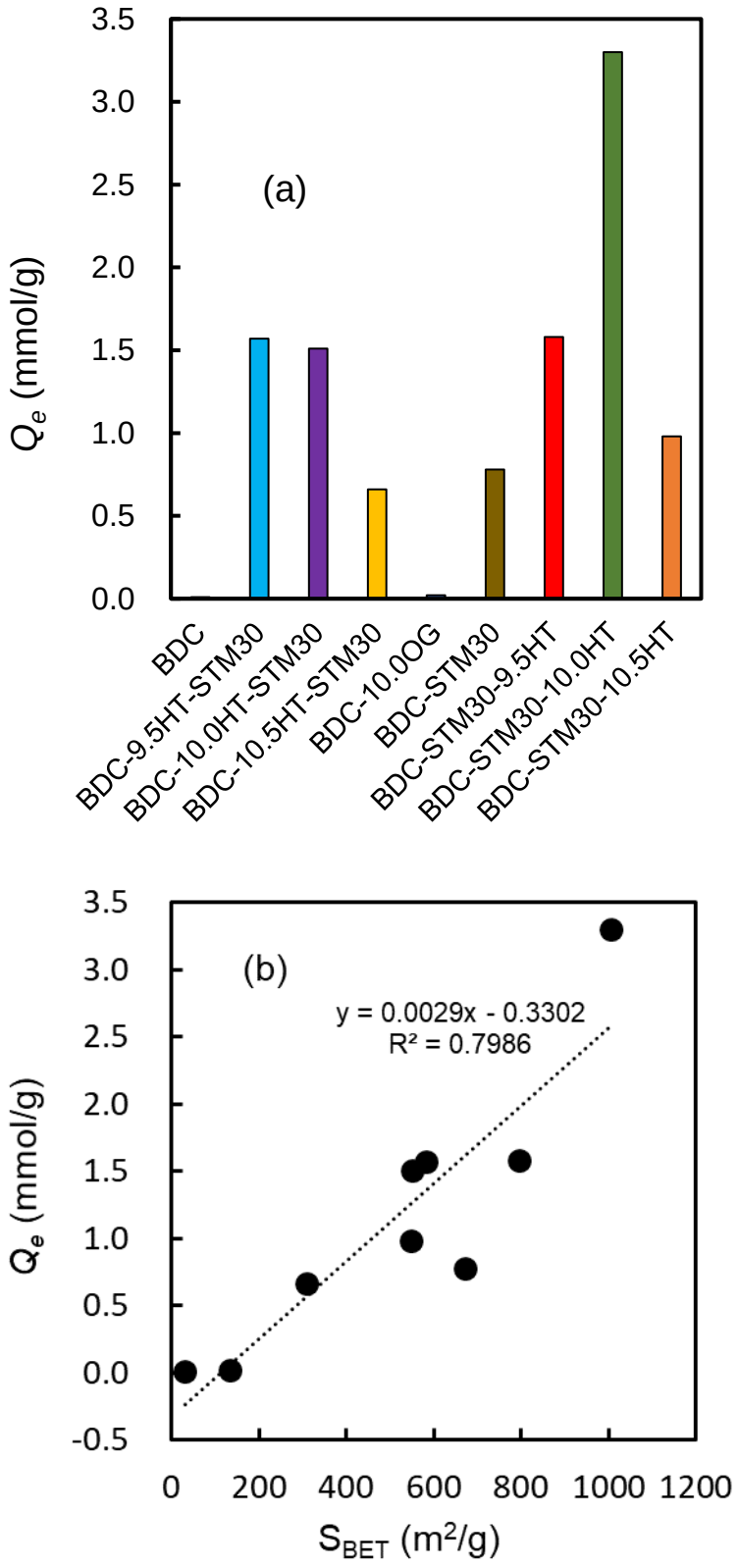

Fig. 5-2. (a) Comparison of adsorption capacity of Cr(VI) by different adsorbents; (b) Linear relationships of Q_e with the surface area of Bean dreg carbon materials.

5.3.3 Effect of solution pH

In order to further explore the adsorption mechanism of activated carbon on Cr(VI), the effects of different pH on the adsorption of Cr(VI) by BDC-STM30 and BDC-STM30-10.0HT were compared. The effect of initial pH on the adsorption of Cr(VI) by BDC-STM30 and BDC-STM30-10.0HT is shown in **Fig. 5-3**. Overall, at pH 2-9, BDC-STM30-10.0HT adsorbed more Cr(VI) than BDC-STM30. For BDC-STM30 and BDC-STM30-10.0HT, the adsorption capacity of Cr(VI) decreased sharply in the pH range 2-7, and then decreased slowly. The effect of initial pH on adsorption can be explained by the surface charge of activated carbon and the ionic forms of Cr(VI). Cr(VI) exists primarily as an oxyanion, and it exists in different ionic forms in aqueous solution. When solution pH is greater than 6.0, it presents as CrO_4^{2-}; when pH is ranged between 1.0 - 6.0, it exists as $Cr_2O_7^{2-}$ and $HCrO_4^-$ [30]. At high pH as well as at low pH, chromium ions having the negative charge. Therefore, when the solution pH has changed the form of the Cr(VI) ions will influence the Cr(VI) uptake capacity of the activated carbon. Moreover, amino groups exist on the surface of the N-doped activated carbon. Under acidic conditions, amino groups present as $-NH_3^+$, with positive sites, which are also beneficial to the adsorption of Cr(VI). Under acidic conditions, Cr(VI) has stronger oxidizing properties, which also affects the adsorption capacity of activated carbon.

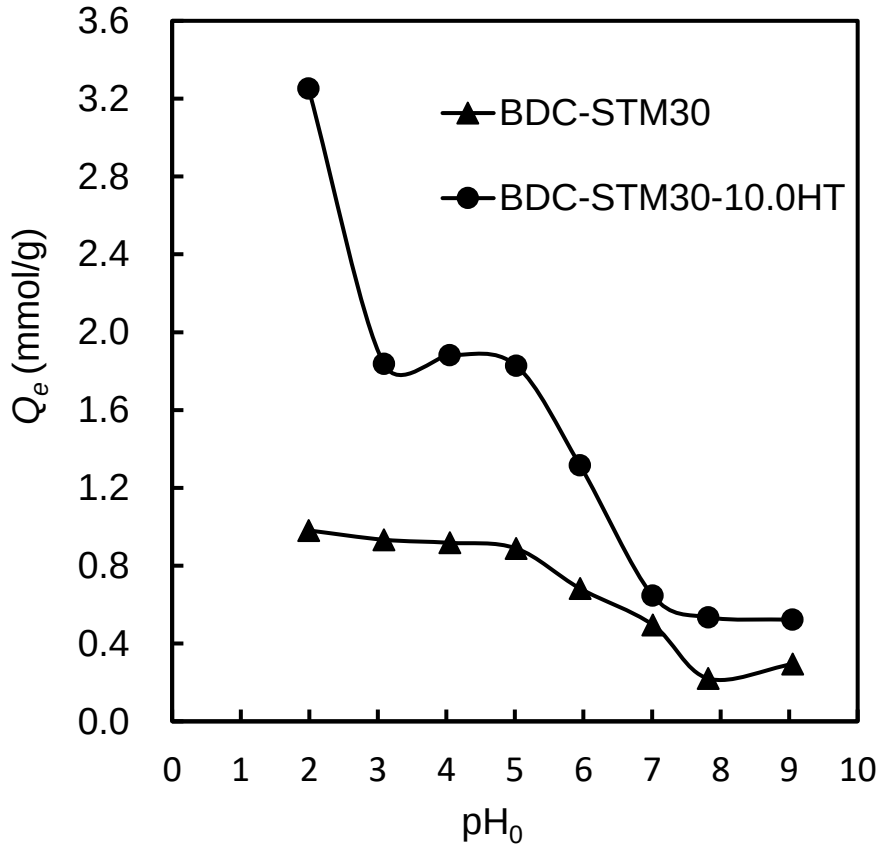

Fig. 5-3. Effect of initial pH value on Cr(VI) removal.

5.3.4 Adsorption isotherms

The adsorption isotherm data and its fitting Langmuir and Freundlich isotherm models are shown in **Fig. 5-4** and **Table 5-3**. It can be seen from **Fig. 5-4** that the amount of adsorption increases gradually with the increase of the initial concentration of Cr(VI), which indicates that there are a large number of adsorption sites of BDC-STM30 and BDC-STM30-10.0HT, which were not fully utilized at low concentrations. As shown in Table 3, The R^2 values of the Langmuir model were larger than those of the Freundlich model, indicating that the Langmuir models can be a good description of

Cr(VI) adsorption behavior. The Langmuir isotherm is usually used to describe the monolayer adsorption on a homogenous surface, indicating that Cr(VI) adsorption onto BDC-STM30 and BDC-STM30-10.0HT tended to be monolayer adsorption [31]. As can be seen from **Table 5-3**, the maximum adsorbed amount (X_m) of Cr(VI) onto BDC-STM30-10.0HT was 3.30 mmol/g, which was more than four times the X_m of BDC-STM30. The increase of adsorption capacity can be explained by the increase of specific surface area and quaternary nitrogen (N-Q) content. Compared with BDC-STM30, the specific surface area of BDC-STM30-10.0HT increased from 673 to 1004 m^2/g, and the total pore volume increased from 0.08 to 0.50 cm^3/g, so BDC-STM30-10.0HT can provide more adsorption sites. Positive charges of quaternary nitrogen can provide more adsorption sites for anions, thus increasing the adsorption of Cr(VI). Moreover, the adsorption capacity of BDC-STM30-10.0HT for Cr(VI) was higher than that reported in the literature [32-36].

The Langmuir isothermal adsorption model defines R_L as the separation factor, which is represented as Eq. (6):

$$R_L = \frac{1}{1+K_L C_0}, \quad (6)$$

In the Langmuir isothermal adsorption models, $0 < R_L < 1$, indicating favorable adsorption of Cr(VI) on the adsorbents.

Table 5-3 Langmuir and Freundlich adsorption isotherm parameters of Cr(VI) at 298K in aqueous solutions

	Langmuir model				Freudlich model		
	X_m (mmol/g)	K_1 (L/mmol)	R_L	R^2	1/n	K_F	R^2
BDC-STM30	0.78	1.35	0.08	0.993	0.43	0.11	0.909
BDC-STM30-10.0HT	3.30	2.40	0.05	0.992	0.40	4.87	0.843

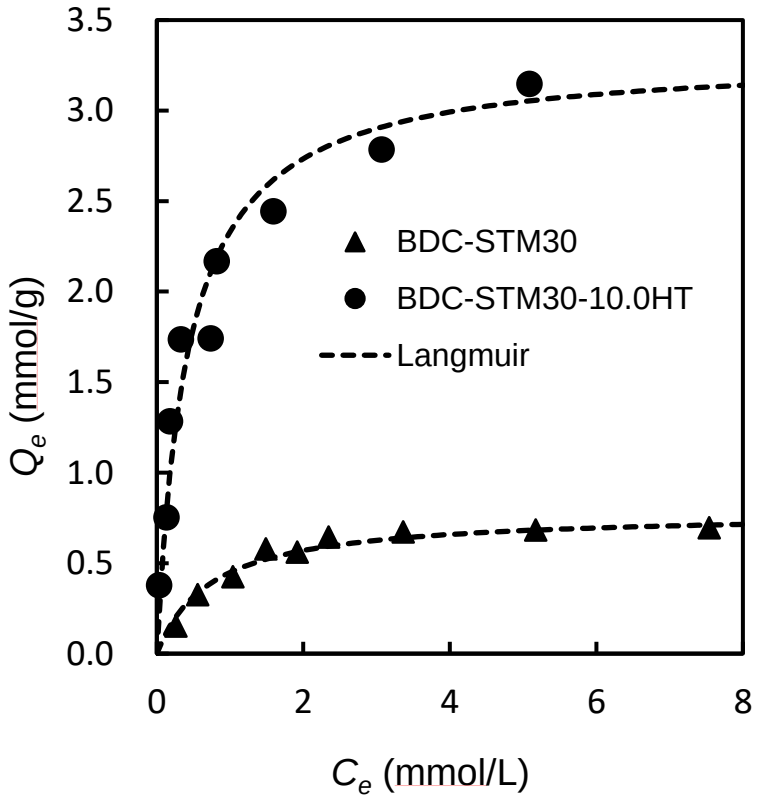

Fig. 5-4. Adsorption isotherms of Cr(VI) onto BDC-STM30 and BDC-STM30-10.0HT.

5.3.5 Adsorption kinetics

Fig. 5-5 shows the influence of the contact time of the activated carbon adsorbent with the heavy metal Cr(VI) on the adsorption amount. BDC-STM30 and BDC-STM30-10.0HT have the same trend except for the adsorption amount of Cr(VI). In the first 30 minutes of contact time, the adsorption amount of activated carbons on Cr(VI) increased rapidly, and then gradually becomes slower with time. Finally, a stable adsorption saturation state was reached. This is because the pore structure and the adsorption sites in the activated carbon were gradually occupied by the adsorbed Cr(VI), and finally reach a saturated state. In order to more accurately describe the effect of contact time on adsorption behavior, pseudo-first-order and pseudo-secondary dynamics models were used to fit the adsorption data, and the results of the kinetic analysis are shown in **Tables 5-4**. As shown in **Table 5-4**, the R^2 value of the pseudo-second-order model was larger than that of the pseudo-first-order model and larger than 0.99, which indicates that the pseudo-second-order model can better describe the adsorption of BDC-STM30 and BDC-STM30-10.0HT on Cr(VI). These facts suggest that the adsorption behavior is mainly governed by a chemisorption [37].

Table 5-4 Kinetic parameters for Cr(VI) adsorption onto BDC-STM30 and BDC-SM30-10.0HT

	Pseudo-first-order			Pseudo-second-order		
	Q_e (mmol/g)	k_1 (min^{-1})	R^2	Q_e (mmol/g)	k_2 (g/mmol min)	R^2
BDC-STM30	0.77	0.06	0.815	0.74	0.37	0.993
BDC-SM30-10.0HT	2.31	0.01	0.867	2.20	0.06	0.998

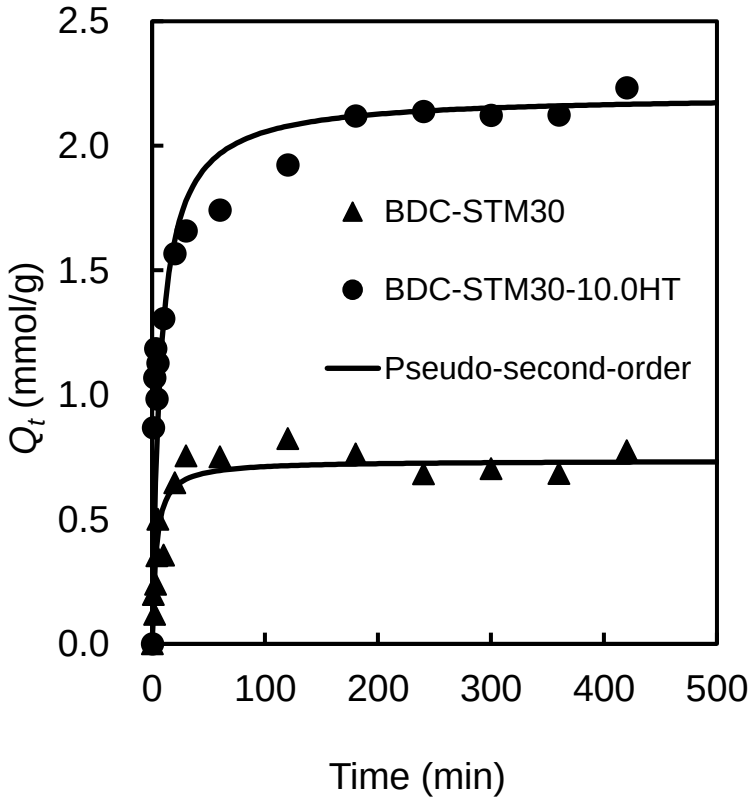

Fig. 5-5. Cr(VI) adsorption kinetic by BDC-STM30 and BDC-STM30-10.0HT.

5.3.6 Regeneration experiment

In order to evaluate the recoverability of N-doped BDC-STM30-10.0HT activated carbon, five cycles of adsorption-desorption experiments were carried out. **Fig.5-6** shows the adsorption capacity of BDC-STM30-10.0HT for Cr(VI) as the function of the adsorption-desorption cycles. After five times regenerations, the adsorption capacity of BDC-STM30-10.0HT still had 54% of the initial adsorption capacity for Cr(VI), that it had better regeneration ability than our previously study [38].

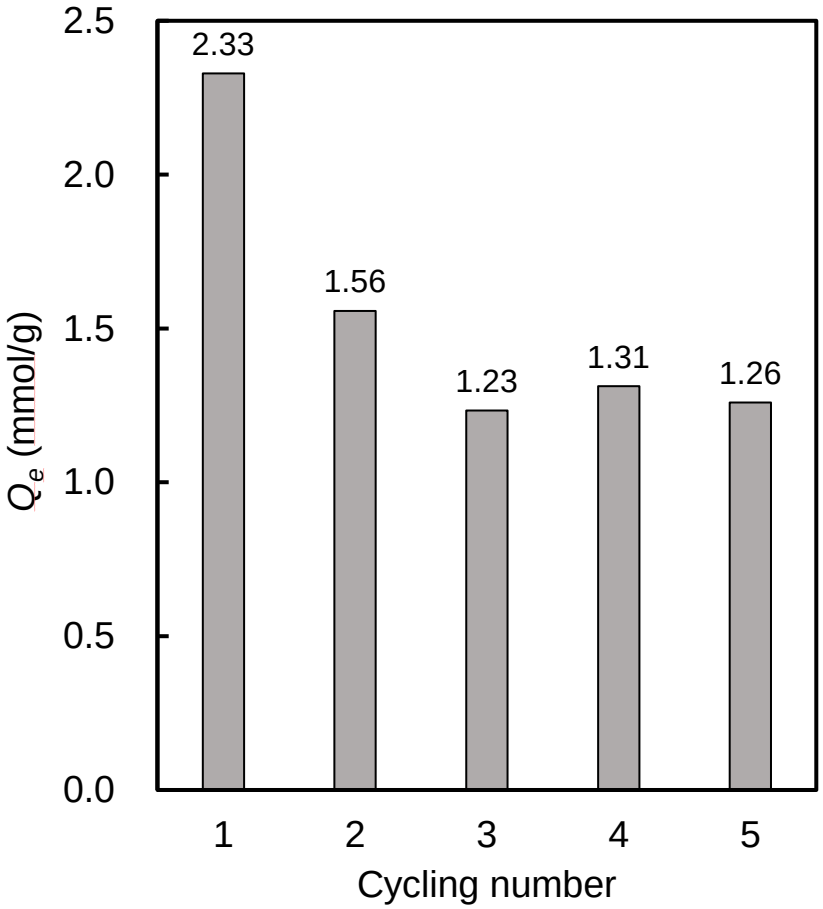

Fig. 5-6. The regeneration adsorptive performance of BDC-STM30-10.0HT after five cycles.

5.3.7 Adsorption mechanism

To understand the mechanism of Cr(VI) removal by BDC-STM30-10.0HT, the

BDC-STM30-10.0HT was analyzed by XPS after reacting with 8 mmol/L of Cr(VI) solution for 24 h at pH 2 and pH 9. As shown in **Fig. 5-7**, the Cr 2p3/2 peaks were fitted into two components at 577.1 eV and 579.5 eV, which might be due to Cr(VI) and Cr(III), respectively [39]. At pH 2, 79.6% of the adsorbed chromium existed in trivalent form, and the remaining 20.4% was present as Cr(VI). In contrast, 30.3% of the adsorbed chromium was reduced to trivalent chromium at pH 9, and 69.7% of the adsorbed chromium was present as Cr(VI). It was found that most of Cr existed in the form of Cr(III) rather than Cr(VI) on the BDC-STM30-10.0HT surface at pH 2. The existence of Cr(III) was originated from the reduction of Cr(VI) by the π electrons of the carbocyclic six-membered ring. At pH 9, the existing form of Cr(VI) becomes CrO_4^{2-}, and the oxidation ability becomes weak, implying that most of Cr was adsorbed directly as Cr(VI), and a small part was reduced to Cr(III).

The FT-IR spectra measurement was also performed to investigate the interaction between BDC-STM30-10.0HT and the adsorbed Cr(VI) at pH 2. In **Fig. 5-8**, the peak locate at about 1612 cm^{-1} of BDC-STM30-10.0HT before Cr(VI) adsorption assign C=N [40]. This indicates that there was quaternary nitrogen on BDC-STM30-10.0HT. After Cr(VI) adsorption, new peaks centered at 576 cm^{-1} and 1267cm^{-1} can be observed, which is assigned to Cr-O and C-OH [41]. This proves that Cr(VI) was effectively adsorbed on the surface of activated carbon. This is consistent with the results of the XPS analysis. After adsorption, the surface of activated carbon was oxidized to produce a large number of C-OH functional groups.

Based on the evidence presented in this work, the mechanisms that control the

sorption of Cr(VI) on the pristine and N-doped activated carbon are illustrated in **Scheme 5-1**.

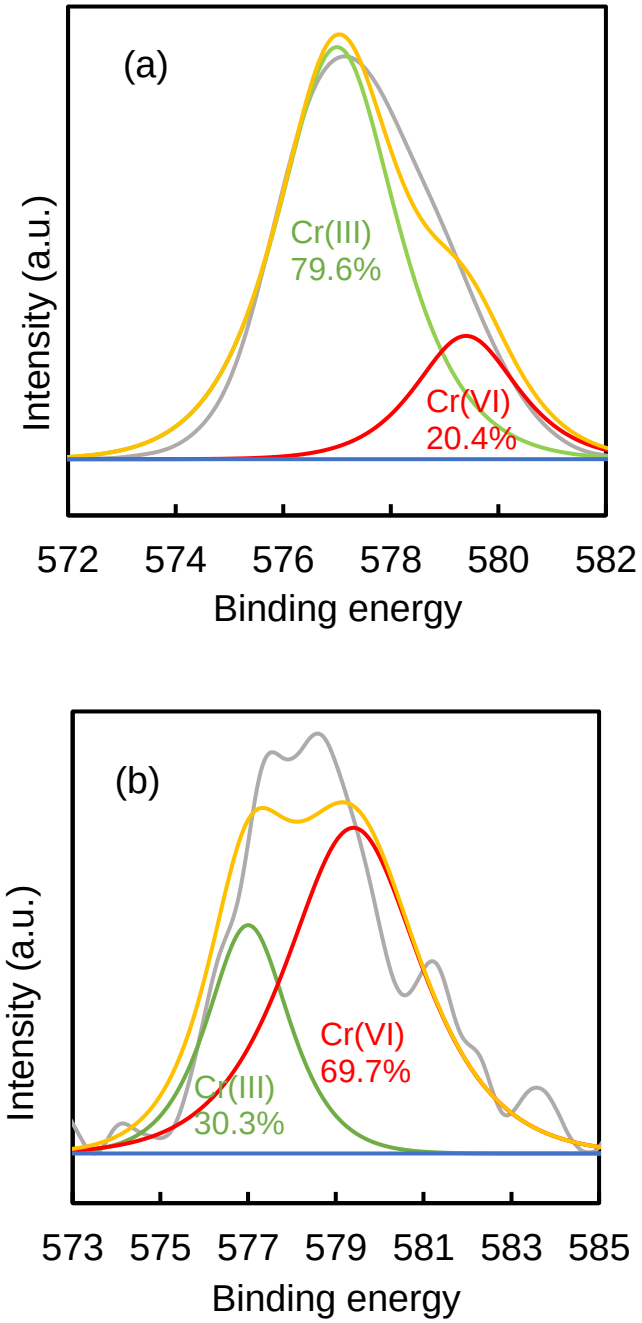

Fig. 5-7. Cr 2p3/2 spectrum of BDC-STM30-10.0HT after Cr(VI) adsorption at pH 2 (a) and pH 9 (b)

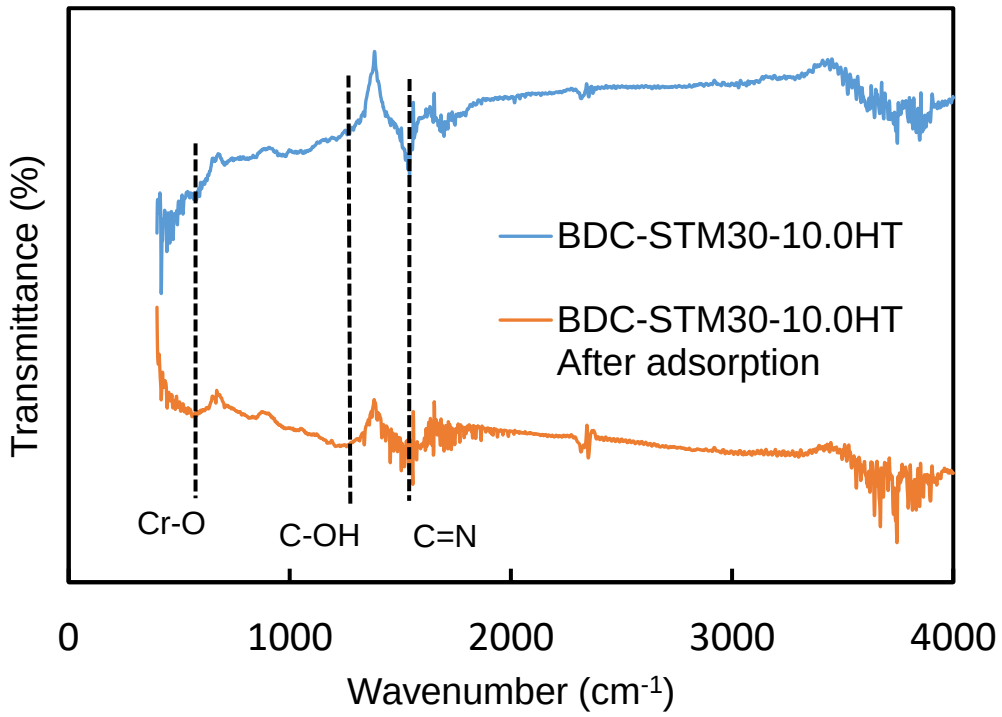

Fig. 5-8. FTIR spectra of BDC-STM30-10.0HT before and after adsorption.

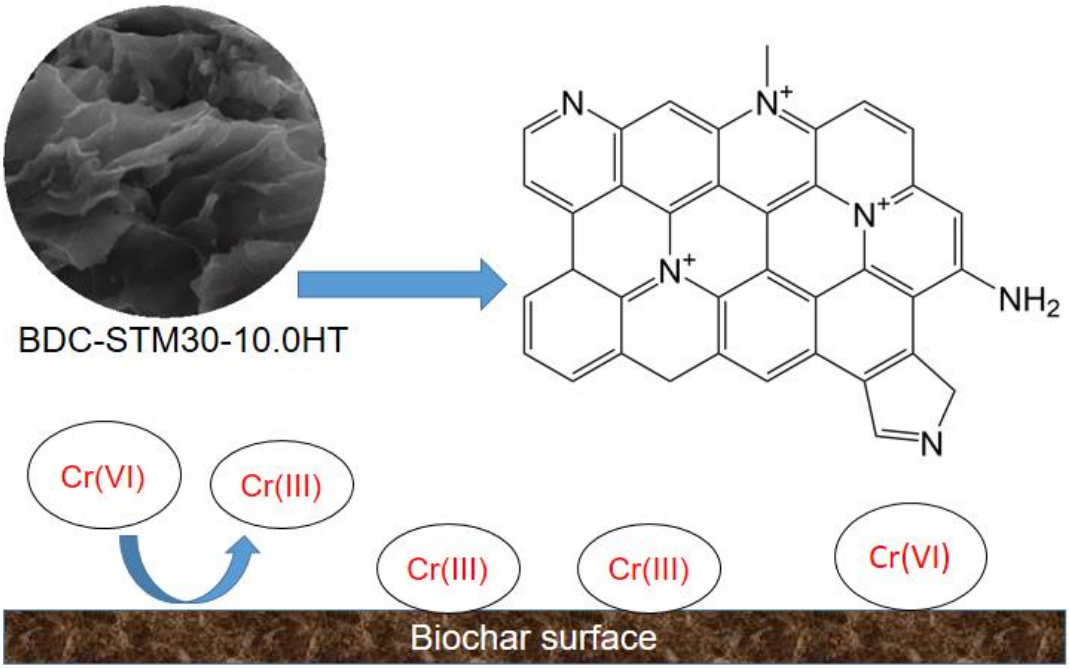

Scheme 5-1. The proposed adsorption mechanisms of Cr(VI) onto BDC-STM30-10.0HT

4. Conclusion

In conclusion, we have successfully developed novel N-doped bean dregs activated carbon adsorbent BDC-STM30-10.0HT for heavy metal Cr(VI) removal in this study. We found that the quaternary nitrogen content of the N-doped activated carbon increased more than 18 times by 1000℃ heating, and the Cr(VI) removal experiments showed that BDC-STM30-10.0HT had a high adsorption capacity (3.30 mmol/g) of Cr(VI), which was far greater than BDC-STM30. The highest adsorption capacity of Cr(VI) by BDC-STM30-10.0HT was at pH 2. Moreover, BDC-STM30-10.0HT exhibits excellent reusable adsorption performance, after five regeneration experiments, and BDC-STM30-10.0HT showed superior recyclability. Therefore, BDC-STM30-10.0HT is expected to be a promising adsorbent for the efficient removal of Cr(VI) from wastewater.

References

[1] Y.L. Liu, Y.T. Li, J.F. Huang, Y.L. Zhang, Z.H. Ruan, T. Hu, J.J. Wang, W.Y. Li, H.J. Hu, G.B. Jiang, An advanced sot-gel strategy for enhancing interfacial reactivity of iron oxide nanoparticles on rosin biochar substrate to remove Cr(VI), Sci. Total Environ. 690 (2019) 438-446.

[2] H. Shen, Y.-T. Wang, Simultaneous chromium reduction and phenol degradation in a coculture of Escherichia coli ATCC 33456 and Pseudomonas putida DMP-1, Appl. Environ. Microbiol. 61 (1995) 2754-2758.

[3] H. Dong, J. Deng, Y. Xie, C. Zhang, Z. Jiang, Y. Cheng, K. Hou, G. Zeng,

Stabilization of nanoscale zero-valent iron (nZVI) with modified biochar for Cr (VI) removal from aqueous solution, J. Hazard. Mater. 332 (2017) 79-86.

[4] A. Shakya, T. Agarwal, Removal of Cr (VI) from water using pineapple peel derived biochars: Adsorption potential and re-usability assessment, J. Mol. Liq. 293 (2019) 111497.

[5] J.F. Huang, Y.T. Li, J.H. Wu, P.Y. Cao, Y.L. Liu, G.B. Jiang, Floatable, macroporous structured alginate sphere supporting iron nanoparticles used for emergent Cr(VI) spill treatment, Carbohydr. Polym. 146 (2016) 115-122.

[6] C. Lei, Y.Q. Sun, E. Khan, S.S. Chen, D.C.W. Tsang, N.J.D. Graham, Y.S. Ok, X. Yang, D.H. Lin, Y.J. Feng, X.D. Li, Removal of chlorinated organic solvents from hydraulic fracturing wastewater by bare and entrapped nanoscale zero-valent iron, Chemosphere 196 (2018) 9-17.

[7] M. Bansal, D. Singh, V. Garg, A comparative study for the removal of hexavalent chromium from aqueous solution by agriculture wastes' carbons, J. Hazard. Mater. 171 (2009) 83-92.

[8] B. Sajjadi, T. Zubatiuk, D. Leszczynska, J. Leszczynski, W.Y. Chen, Chemical activation of biochar for energy and environmental applications: a comprehensive review, Rev. Chem. Eng. 35 (2019) 777-815.

[9] C. Zhang, G.M. Zeng, D.L. Huang, C. Lai, M. Chen, M. Cheng, W.W. Tang, L. Tang, H.R. Dong, B.B. Huang, X.F. Tan, R.Z. Wang, Biochar for environmental management: Mitigating greenhouse gas emissions, contaminant treatment, and potential negative impacts, Chem. Eng. J. 373 (2019) 902-922.

[10] J. He, Y. Xiao, J.C. Tang, H.K. Chen, H.W. Sun, Persulfate activation with sawdust biochar in aqueous solution by enhanced electron donor-transfer effect, Sci. Total Environ. 690 (2019) 768-777.

[11] Y.L. Zhao, R.Y. Zhang, H.B. Liu, M.X. Li, T.H. Chen, D. Chen, X.H. Zou, R.L. Frost, Green preparation of magnetic biochar for the effective accumulation of Pb (II): Performance and mechanism, Chem. Eng. J. 375 (2019) 10.

[12] J.W. Wu, T. Wang, Y.S. Zhang, W.P. Pan, The distribution of Pb(II)/Cd(II) adsorption mechanisms on biochars from aqueous solution: Considering the increased oxygen functional groups by HCl treatment, Bioresour. Technol. 291 (2019) 7.

[13] J.H. Park, J.J. Wang, S.H. Kim, S.W. Kang, C.Y. Jeong, J.R. Jeon, K.H. Park, J.S. Cho, R.D. Delaune, D.C. Seo, Cadmium adsorption characteristics of biochars derived using various pine tree residues and pyrolysis temperatures, J. Colloid Interface Sci. 553 (2019) 298-307.

[14] J.J. Zhang, J.G. Shao, Q.Z. Jin, Z.Q. Li, X. Zhang, Y.Q. Chen, S.H. Zhang, H.P. Chen, Sludge-based biochar activation to enhance Pb(II) adsorption, Fuel 252 (2019) 101-108.

[15] Y.Y. Liu, S.P. Sohi, S.Y. Liu, J.J. Guan, J.Y. Zhou, J.W. Chen, Adsorption and reductive degradation of Cr(VI) and TCE by a simply synthesized zero valent iron magnetic biochar, J. Environ. Manage. 235 (2019) 276-281.

[16] Y.Y. Chen, B.Y. Wang, J. Xin, P. Sun, D. Wu, Adsorption behavior and mechanism of Cr(VI) by modified biochar derived from Enteromorpha prolifera, Ecotoxicol. Environ. Saf. 164 (2018) 440-447.

[17] D. Jiang, B. Chu, Y. Amano, M. Machida, Removal and recovery of phosphate from water by Mg-laden biochar: Batch and column studies, Colloids Surf., A 558 (2018) 429-437.

[18] J.H. Kwak, M.S. Islam, S. Wang, S.A. Messele, M.A. Naeth, M.G. El-Din, S.X. Chang, Biochar properties and lead(II) adsorption capacity depend on feedstock type, pyrolysis temperature, and steam activation, Chemosphere 231 (2019) 393-404.

[19] M.M. Mian, G.J. Liu, B. Yousaf, B. Fu, R. Ahmed, Q. Abbas, M.A.M. Munir, R.J. Liu, One-step synthesis of N-doped metal/biochar composite using NH_3-ambiance pyrolysis for efficient degradation and mineralization of Methylene Blue, J. Environ. Sci. 78 (2019) 29-41.

[20] X.Y. Xu, Y.L. Zheng, B. Gao, X.D. Cao, N-doped biochar synthesized by a facile ball-milling method for enhanced sorption of CO2 and reactive red, Chem. Eng. J. 368 (2019) 564-572.

[21] W.C. Yu, F. Lian, G.N. Cui, Z.Q. Liu, N-doping effectively enhances the adsorption capacity of biochar for heavy metal ions from aqueous solution, Chemosphere 193 (2018) 8-16.

[22] M.M. Mian, G.J. Liu, B. Yousaf, B. Fu, H. Ullah, M.U. Ali, Q. Abbas, M.A.M. Munir, L. Ruijia, Simultaneous functionalization and magnetization of biochar via NH3 ambiance pyrolysis for efficient removal of Cr (VI), Chemosphere 208 (2018) 712-721.

[23] P. Yoo, Y. Amano, M. Machida, Adsorption of nitrate onto nitrogen-doped activated carbon fibers prepared by chemical vapor deposition, Korean J. Chem. Eng. 35 (2018) 2468-2473.

[24] Y. Teng, E.H. Liu, R. Ding, K. Liu, R.H. Liu, L. Wang, Z. Yang, H.X. Jiang, Bean dregs-based activated carbon/copper ion supercapacitors, Electrochim. Acta 194 (2016) 394-404.

[25] Y. Teng, K. Liu, R.H. Liu, Z. Yang, L. Wang, H.X. Jiang, R. Ding, E.H. Liu, A novel copper nanoparticles/bean dregs-based activated carbon composite as pseudocapacitors, Mater. Res. Bull. 89 (2017) 33-41.

[26] B. Wang, Y.B. Zhai, T.F. Wang, S.H. Li, C. Peng, Z.X. Wang, C.T. Li, B.B. Xu, Fabrication of bean dreg-derived carbon with high adsorption for methylene blue: Effect of hydrothermal pretreatment and pyrolysis process, Bioresour. Technol. 274 (2019) 525-532.

[27] W.F. Qi, Y.X. Zhao, X.Y. Zheng, M. Ji, Z.Y. Zhang, Adsorption behavior and mechanism of Cr(VI) using Sakura waste from aqueous solution, Appl. Surf. Sci. 360 (2016) 470-476.

[28] J.R. Pels, F. Kapteijn, J.A. Moulijn, Q. Zhu, K.M. Thomas, Evolution of nitrogen functionalities in carbonaceous materials during pyrolysis, Carbon 33 (1995) 1641-1653.

[29] Y.Q. Yang, N. Chen, C.P. Feng, M. Li, Y. Gao, Chromium removal using a magnetic corncob biochar/polypyrrole composite by adsorption combined with reduction: Reaction pathway and contribution degree, Colloids Surf., A 556 (2018) 201-209.

[30] N. Ballav, A. Maity, S.B. Mishra, High efficient removal of chromium(VI) using glycine doped polypyrrole adsorbent from aqueous solution, Chem. Eng. J. 198 (2012)

536-546.

[31] A. Alizadeh, G. Abdi, M.M. Khodaei, M. Ashokkumar, J. Amirian, Graphene oxide/Fe3O4/SO3H nanohybrid: a new adsorbent for adsorption and reduction of Cr(VI) from aqueous solutions, RSC Adv. 7 (2017) 14876-14887.

[32] L.Y. Dong, Y. Jin, T. Song, J.S. Liang, X. Bai, S.M. Yu, C.Y. Teng, X. Wang, J.J. Qu, X.M. Huang, Removal of Cr(VI) by surfactant modified Auricularia auricula spent substrate: biosorption condition and mechanism, Environ. Sci. Pollut. Res. 24 (2017) 17626-17641.

[33] J.G. Shang, J.C. Pi, M.Z. Zong, Y.R. Wang, W.H. Li, Q.H. Liao, Chromium removal using magnetic biochar derived from herb-residue, J. Taiwan Inst. Chem. Eng. 68 (2016) 289-294.

[34] Y.T. Han, X. Cao, X. Ouyang, S.P. Sohi, J.W. Chen, Adsorption kinetics of magnetic biochar derived from peanut hull on removal of Cr (VI) from aqueous solution: Effects of production conditions and particle size, Chemosphere 145 (2016) 336-341.

[35] S.S. Zhu, X.C. Huang, D.W. Wang, L. Wang, F. Ma, Enhanced hexavalent chromium removal performance and stabilization by magnetic iron nanoparticles assisted biochar in aqueous solution: Mechanisms and application potential, Chemosphere 207 (2018) 50-59.

[36] J.Y. Song, Q.L. He, X.L. Hu, W. Zhang, C.Y. Wang, R.F. Chen, H.Y. Wang, A. Mosa, Highly efficient removal of Cr(VI) and Cu(II) by biochar derived from Artemisia argyi stem, Environ. Sci. Pollut. Res. 26 (2019) 13221-13234.

[37] K.L. Tan, B.H. Hameed, Insight into the adsorption kinetics models for the removal

of contaminants from aqueous solutions, J. Taiwan Inst. Chem. Eng. 74 (2017) 25-48.

[38] B. Chu, M. Yamoto, Y. Amano, M. Machida, Adsorption, reduction and regeneration behavior of high surface area activated carbon in removal of Cr(VI), Desalin. Water Treat. 136 (2018) 395-404.

[39] B. Stypula, J. Stoch, The characterization of passive films on chromium electrodes by XPS, Corros. Sci. 36 (1994) 2159-2167.

[40] T. Altun, E. Pehlivan, Removal of Cr(VI) from aqueous solutions by modified walnut shells, Food Chem. 132 (2012) 693-700.

[41] W.C. Cheng, C.C. Ding, X.X. Wang, Z.Y. Wu, Y.B. Sun, S.H. Yu, T. Hayat, X.K. Wang, Competitive sorption of As(V) and Cr(VI) on carbonaceous nanofibers, Chem. Eng. J. 293 (2016) 311-318.

Chapter 6 Preparation of bamboo-based oxidized biochar for simultaneous removal of Cd(II) and Cr(VI) from aqueous solution

6.1 Introduction

Cd(II) and Cr(VI) are the common highly toxic heavy metals, which widely exist in printing and dyeing wastewater, electroplating wastewater and another industrial wastewater [1, 2]. Cadmium has adverse effects on human health, including pulmonary insufficiency, renal dysfunction, cancer, disease and hypertension [3]. Cadmium exists in water mainly in the main form of Cd(II) (Cd^{2+}). Unlike cadmium, the main forms of chromium in aqueous solution are Cr(III) (Cr^{3+}, $Cr(OH)_2^+$) and Cr(VI) ($HCrO_4^-$, CrO_4^{2-}, $Cr_2O_7^{2-}$) [4, 5], and Cr(VI) is approximately 100 times highly more toxic than Cr(III) [6]. Cr(VI) is easily adsorbed by the human body, and has a great toxicity to human kidney, stomach and liver [7]. Cd(II) and Cr(VI) ions are both extremely toxic metals that usually exist simultaneously in electroplating, paint pigmentations, and printing and dyeing and wastewater [8, 9]. The existence of pollutants exhibit complicated interactions in adsorption behaviors [10]. Thus it is important to remove these heavy metals before discharging into environment.

Existing methods for removal of Cr(VI) and Cd(II) from water include chemical precipitation [11, 12], membrane filtration [13, 14], ion exchange [15, 16], adsorption [17] and biological processes [18, 19]. Adsorption method is known to be an easy, low cost and high efficiency method for the treatment of heavy metals such as Cd(II) and Cr(VI) [20]. Surface adsorption is mainly dominated by electrostatic interaction,

hydrogen bonding, π-π stacking and pore-filling [21]. In the adsorption method, the selection of adsorbent is decisively important. Widely-used adsorbents such as biochar, zeolites, and molecular sieves generally have a large specific surface area. Among them, biochar derived from biomass has been proved to be a universal adsorbent for heavy metal because of its favorable physicochemical properties and relatively low cost [22-24]. Moso bamboo is abundant, especially in Asia. It is characterized by the rapid growth (getting mature within 3-5 years only) compared with other plants, and thus is regarded as cheaply available biochar material [25].

However, most of the biochar have low surface area due to the lack of porous structure. In order to overcome this shortcoming, $ZnCl_2$ is generally used as a surface active agent to increase the specific surface area and the adsorption ability of biochar [26]. The higher specific surface area also allows the biochar surface to have a higher positive charge, which facilitates the adsorption of various anions, (e.g., $Cr_2O_7^{2-}$, CrO_4^{2-}, NO_3^-, and PO_4^{2-}) [27]. Biochar not only has a porous structure, but also has some oxygen-containing functional groups on its surface. These oxygen-containing functional groups provide a prevalence of negative charges on the biochar which have the ability to adsorb cations (e.g., Cu^{2+}, Cd^{2+}, Pb^{2+}, and Ni^{2+}) [28]. Although the surface of biochar contains a certain amount of oxygen-containing functional groups, the number of the functional groups is small. Therefore, the oxygen-containing functional groups can be introduced to the surface of the biochar by oxidation method [29].

At present, there are many studies on the adsorption of Cd(II) or Cr(VI) by biochar [30, 31], but this biochar was commonly used to remove Cd(II) or Cr(VI) separately

rather than simultaneously [32]. Because the adsorption potentials of Cd(II) and Cr(VI) are different, this becomes the main factor restricting their simultaneous adsorption. In previous studies, simultaneous removal of Pb(II) and Cr(VI) by a novel sewage sludge-derived biochar immobilized nanoscale zero-valent iron (SSB-nZVI) was reported [33]. The change in pH is important in the adsorption process, however, it is often neglected. Furthermore, the presence of one metal ion in the solution may affect the adsorption of another metal ion. Hence, it is crucial to study the interaction of two ions in adsorption.

In this work, Cd(II) and Cr(VI) were selected as two representative heavy metals. The bamboo-based biochar was prepared, which was then modified by $ZnCl_2$ and oxidized by $(NH_4)_2S_2O_8$ solution for the removal of Cd(II) and Cr(VI). The main objectives of this paper are: (1) to assess the production and surface properties of bamboo-based oxidized biochar; (2) to evaluate the removal of Cd(II) and Cr(VI) under different conditions; (3) to explore the possibility of Cd(II) and Cr(VI) simultaneous adsorption; (4) to study the interaction between Cd(II) and Cr(VI) during adsorption; (5) to demonstrate the adsorption mechanism of the prepared biochar for removal of Cd(II) and Cr(VI) in water.

6.2 Materials and methods

6.2.1 Preparation of oxidized biochars

The feedstock for the production of biochar was willow residues pruned from moso bamboo. Moso bamboo obtained in Aichi prefecture, Japan, was cut into chips (8 mm*10 mm*5 mm, W*L*T) and used as a precursor for preparation of adsorbent.

The bamboo chips were dried in an oven at 110°C for 1 h. In this study, using the $ZnCl_2$ as an activator, the prepared bamboo chips were impregnated with $ZnCl_2$ solution at a ratio of 3 g-$ZnCl_2$/g-bamboo, and then the mixture was dried in an oven at 110°C overnight. The resulting mixture was pyrolyzed for 1 h at 500°C under N_2 atmosphere in a tubular furnace. The prepared biochar was placed in 1 M HCl solution and stirred for 1 h, rinsed in a Soxhlet extractor for 24 h, and dried overnight at 110°C. The obtained samples were referred to as BZ.

The prepared biochars were oxidized in order to load the oxygen-containing functional groups. Using $(NH_4)_2S_2O_8$ solution as an oxidant, BZ (1.0 g) was added into 0.6 kg/L $(NH_4)_2S_2O_8$ solution (50 mL) in a flask, and placed in 30°C water for continuously stirring for 6-48 h. After that, the resulting samples were filtered and washed with hot deionized water for several times until the filtrate pH became neutral, followed by drying in an oven at 110°C overnight. The obtained samples were referred to as BZ-APS*x*h, where *x* is the number of hours for oxidation.

6.2.2 Characterization

The specific surface area (S_{BET}), mesopore volume (V_{meso}) and micropore volume (V_{micro}) of the prepared biochar were calculated based on N_2 adsorption/desorption isotherms at −196°C using Bellsorp-mini II (MicrotracBEL, Co., Ltd., Japan) surface area analyzer. The surface morphology of the biochar was observed by Hitachi S-4800 SEM (Hitachi, Japan). The elemental composition of C, H and N of the adsorbents was determined with Perkin Elmer 2400 II (Perkin Elmer Japan, Co., Ltd., Japan), and O

content was obtained by difference. X-ray photoelectron spectroscopy (XPS) analysis was performed using an ULVAC-PHI Model-1800 spectrometer. FTIR spectrophotometer (IRAffinity-1, SHI-MADZU, Japan) was used to analyze surface functional groups of adsorbents. The concentrations of Cr(VI) and Cd(II) solution after batch experiments were determined with atomic absorption spectrometer novAA300 (Analytik Jena AG, Germany).

6.2.3 Batch adsorption

Batch Cr(VI) adsorption experiments were conducted to examine the adsorption and reduction performance of the prepared biochar as adsorbents. Potassium dichromate ($K_2Cr_2O_7$) and cadmium nitrate ($Cd(NO_3)_2$) were used for preparing the stock solution of Cr(VI) and Cd(II). All batch experiments were carried out in Erlenmeyer flasks. A 0.02 g of the BZ-APS was put into a flask containing 20 mL of solution (Cr(VI) and/or Cd(II)) with various initial concentrations. The flasks were agitated in a water bath shaker at 25°C by the speed of 100 rpm. Sampling and filtration were carried out after a certain contact time.

The effect of oxidation time of the oxidized biochar on the removal of Cr(VI) and Cd(II) was determined by using BZ-APS6h, BZ-APS12h, BZ-APS24h, and BZ-APS48h at concentrations of 1000 mg/L in a mixed solution of Cr(VI) and Cd(II) under natural pH condition (pH 6). The concentrations of Cr(VI) and Cd(II) in solution were 4 mmol/L each.

The effect of solution pH on Cr(VI) and Cd(II) adsorption was examined by

mixing 20 mg of adsorbent with 20 mL of 1.5 mmol/L Cr(VI) and Cd(II) solution. The mixed solution had different pH values, ranging from 2 to 7. The initial pH of phosphate solution was adjusted by 0.1 M HCl and 0.1 M NaOH.

To study the adsorption isotherms, 20 mg of the BZ-APS24h was mixed with 20 mL of either Cr(VI) (0.1-7.7 mmol/L) or Cd(II) (0.1-2.2 mmol/L) at natural pH (pH 6), and then shaken at 100 rpm for 24 h at 25°C, 35°C and 45°C. And to study the kinetics of the adsorption process, 0.1 g of the BZ-APS24h was mixed with 20 mL of 4 mmol/L Cr(VI) and 4 mmol/L Cd(II) solution under natural pH (pH 6), followed by shaking at 100 rpm.

6.3 Results and discussion

6.3.1 Physicochemical characteristics of biochars

The elemental composition of oxidized biochar with different oxidation time was shown in **Table 6-1**. It can be seen from **Table 6-1** that the oxygen content of the non-oxidized BZ was 7.9%. After 6-48 hours of oxidation, the content of oxygen in biochar increases proportionally from 22.4% up to 30.1%. This indicates that oxygen functional groups would be loaded with the increase of oxidation time, on the biochar.

The morphologies of the BZ and the BZ-APS24h prepared are shown in **Fig. 6-1**. It could be seen that nearly no porous structure was observed from a smooth surface of the BZ. The surface of the BZ-APS24h had a relatively fluffy porous structure, which was rougher than that of the BZ. This may be attributed to the destruction of the surface structure of oxidized biochar.

The nitrogen adsorption-desorption isotherm curve of the BZ-APS24h is shown in

Fig. 6-2, and a type I isotherm was observed, which indicates the mainly microporous structure existence. The specific surface area (BET) and micro-/mesoporous structure of the biochar are shown in **Table 6-2**. It can be seen that the surface of the biochar before and after oxidation differed greatly. With the increase of oxidation time, the specific surface area of oxidized biochar decreased from 1730 m^2/g to 928 m^2/g, and total pore volume decreased from 1.61 cm^3/g to 0.47 cm^3/g. This principally is due to the fact that with increase of oxidation time, more oxygen-containing functional groups were loaded to the surface of biochar. But the plugging pore structure by increase of these functional groups is conducive to the removal of Cd(II).

The functional groups on oxidized biochar were analyzed by XPS. Detailed XPS survey of the regions for C1s of BZ and BZ-APS24h is shown in **Fig. 6-3**. For the C1s XPS spectrum of the BZ, a strong peak appeared at 285.4 eV, which is attributed to C-C (77%), and the other peaks located at 286.7 and 288.4 eV are assigned to the C-O (13%) and C=O (6%), respectively. After oxidation, the C-O (21%) and C=O (12%) peaks of the BZ-APS24h contain obvious increment compared with BZ. This indicates that the functional groups on the surface of oxidized biochar are mostly –COOH, with a small amount of -OH.

Table 6-1 Elemental composition of each prepared biochar

Sample	C (%)	H (%)	N (%)	O* (%)
BZ	90.4	1.5	0.2	7.9
BZ-APS6h	76.2	1.2	0.2	22.4
BZ-APS12h	75.0	1.2	0.2	23.6
BZ-APS24h	72.9	1.3	0.2	25.6
BZ-APS48h	68.3	1.4	0.2	30.1

* Calculated by difference

Table 6-2 Textural and surface properties of each prepared biochar

Sample	S_{BET} (m^2/g)	V_{total} (cm^3/g)	V_{micro} (cm^3/g)	V_{meso} (cm^3/g)
BZ	1730	1.61	1.55	0.06
BZ-APS6h	1480	1.06	1.02	0.04
BZ-APS12h	1350	0.95	0.93	0.02
BZ-APS24h	1120	0.62	0.61	0.01
BZ-APS48h	928	0.47	0.45	0.02

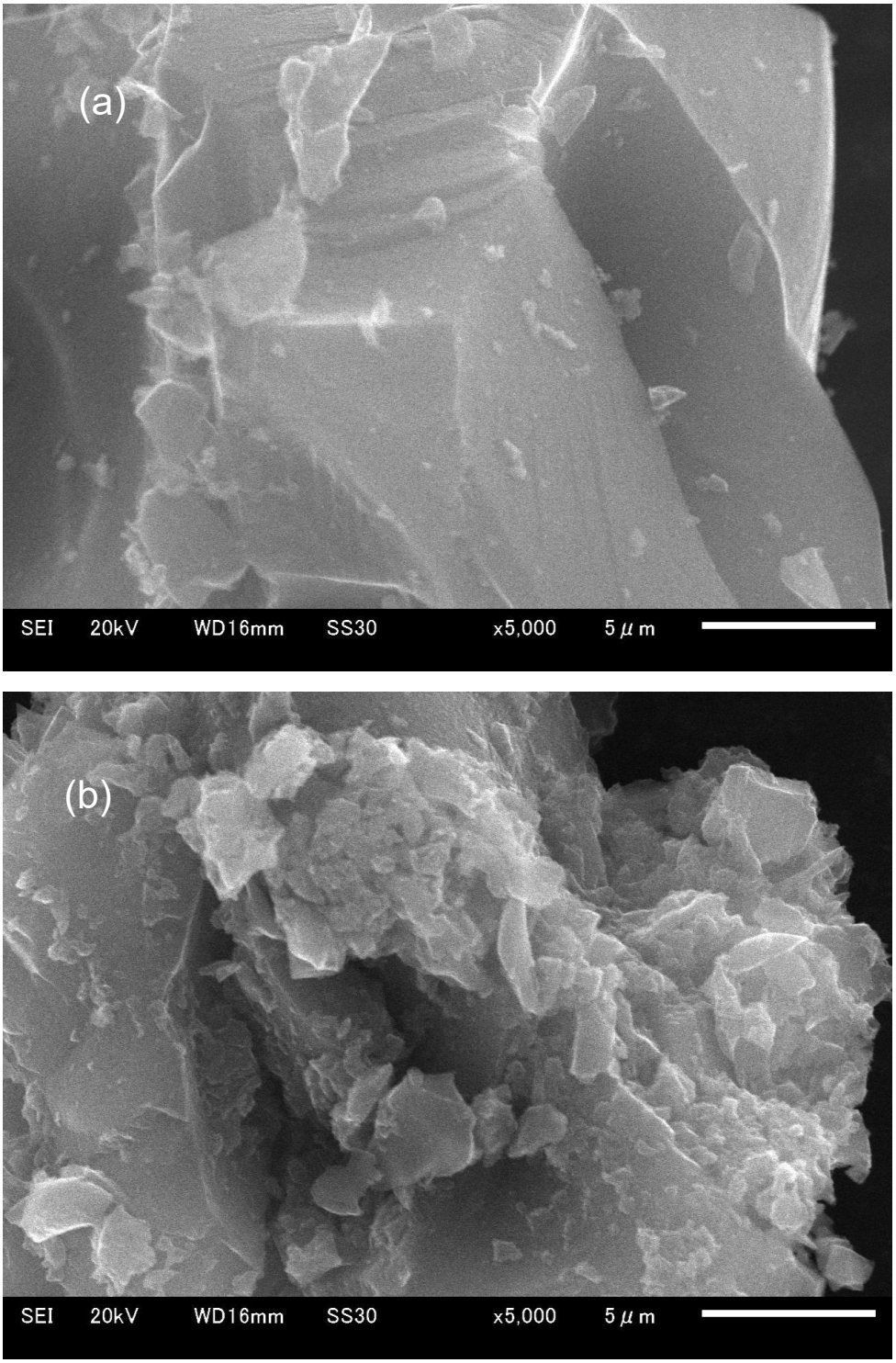

Fig.6-1 SEM images of BZ (a) and BZ-APS24h (b).

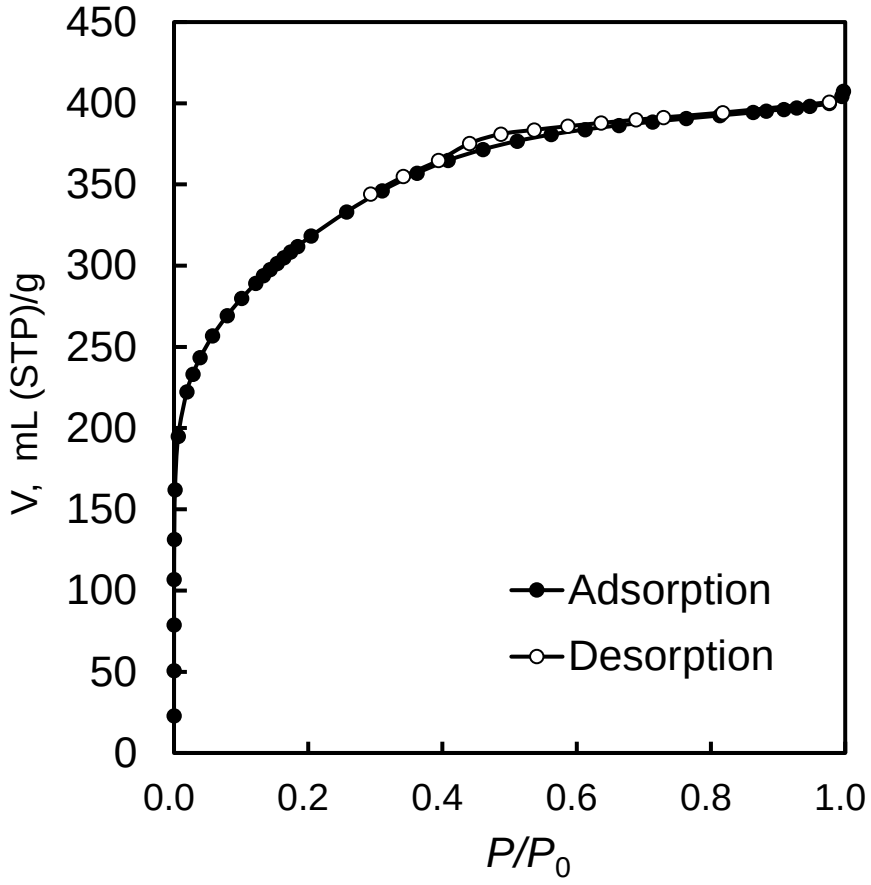

Fig.6-2 Nitrogen adsorption isotherm of BZ-APS24h.

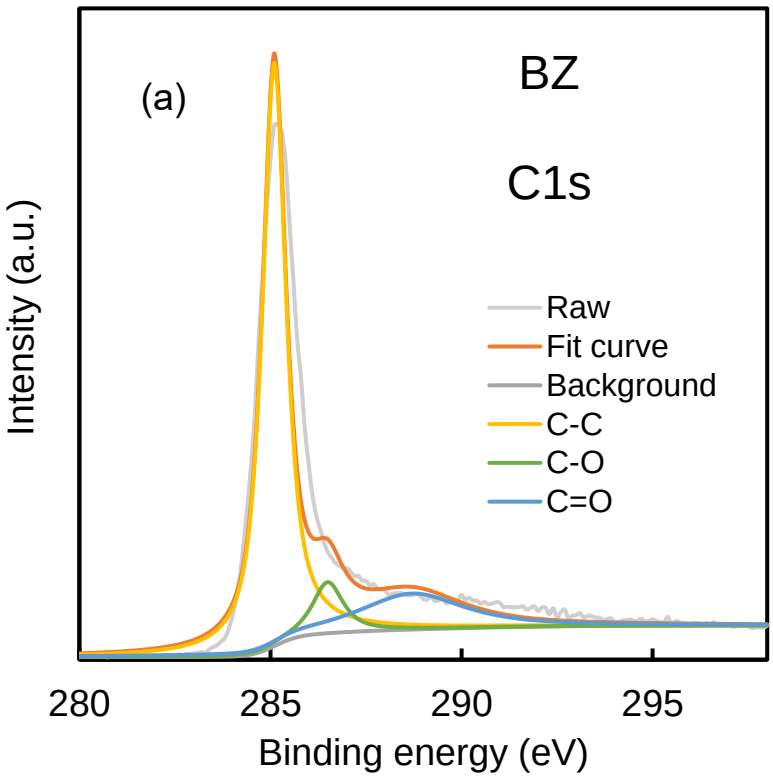

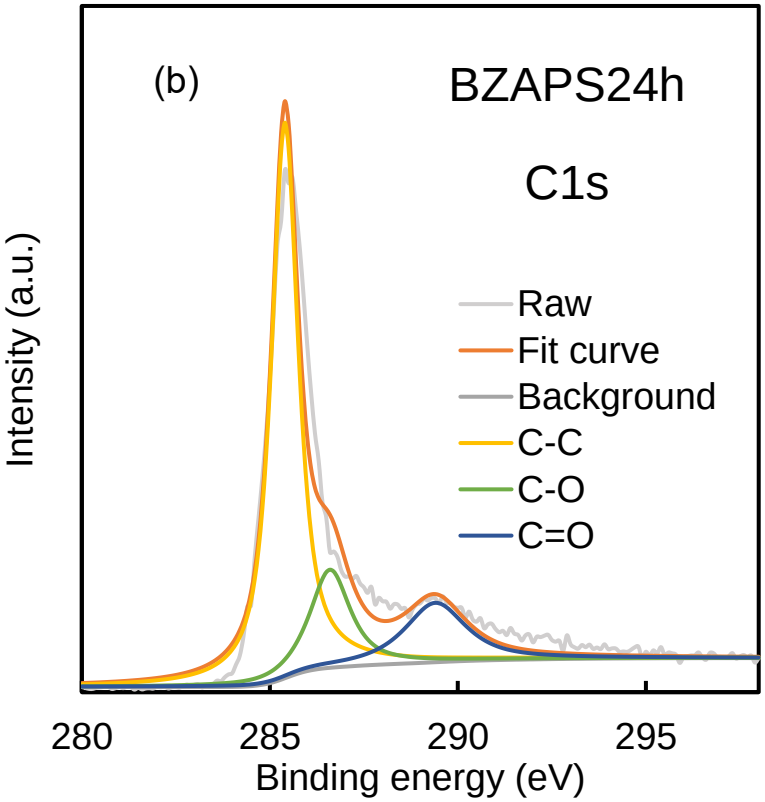

Fig.6-3 XPS survey spectra of BZ (a) and BZ-APS24h (b).

6.3.2 Effect of initial oxidation time

From **Tables 6-1** and **6-2**, it can be understood that the increase of oxidation time caused the increase of surface functional groups on the oxidized biochar, so their adsorption capacity for Cr(VI) and Cd(II) should be different. **Fig. 6-4** shows the adsorption capacity of Cr(VI) and Cd(II) with different oxidation times. It was observed that when oxidation time increased from 6 h to 24 h, the adsorption capacity of Cr(VI) and Cd(II) increased; when the oxidation time increased from 24 h to 48 h, the adsorbed amount of Cd(II) remained unchanged, but the adsorbed amount of Cr(VI) decreased. Meanwhile, the equilibrium pH of the solution decreased with the increase of oxidation time of biochar. The existence of chromium in the solution after adsorption was measured **Fig. 6-4(a)**. The results show that the adsorption performance of oxidized biochar for mixed solution of Cr(VI) and Cd(II) reached the highest point when the oxidation time was 24 hours. At the same time, the existence of chromium in the solution after adsorption was measured and the results are shown in **Fig. 6-4(b)**. It can be inferred that the remaining chromium in the solution was mainly Cr(VI), and no Cr(VI) was reduced to Cr(III) under these conditions.

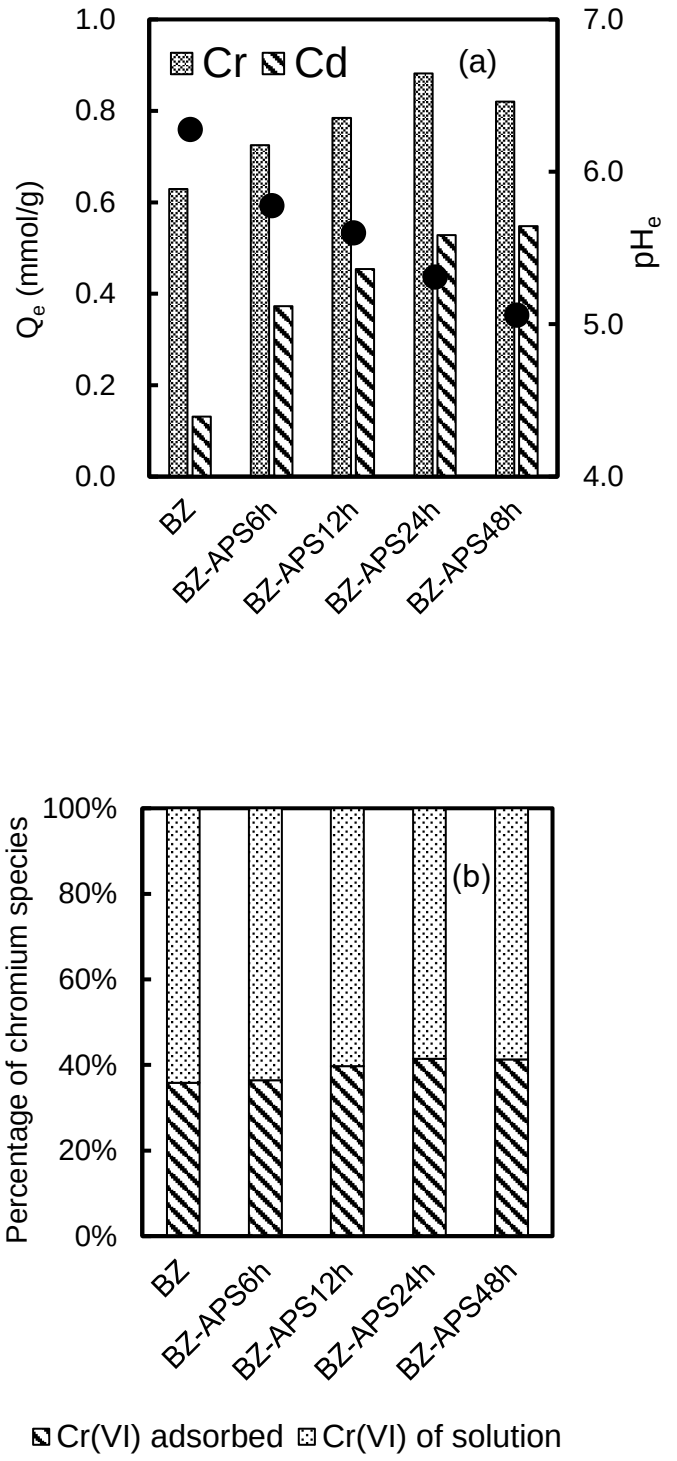

Fig. 6-4 Simultaneous removal of Cd(II) and Cr(VI) by different materials.

6.3.3 Effect of solution pH

Initial solution pH has an significant impact on the removal efficiency of Cr(VI) and Cd(II) in aqueous solution. Cadmium species are found to be present in deionized water in the forms of Cd^{2+}, $Cd(OH)^{+}$, $Cd(OH)_2^0$, $Cd(OH)_2(s)$, etc [34]. Cd^{2+} begins to precipitate when pH > 7, thus, the effect of pH was studied within the range from 2 to 7. The effects of solution pH on Cr(VI) adsorption, Cd(II) adsorption and co-adsorption of Cr(VI) and Cd(II) with oxidized biochar BZ-APS24h samples were investigated as shown in **Fig. 6-5**.

For adsorption of Cr(VI), the adsorbed amount of Cr(VI) on BZ-APS24 decreased as pH increased from 2 to 7. This is because the solution pH value significantly affected the structure of the adsorbents, the surface charges of the adsorbent and the surface-reactive functional groups in the solution. Cr(VI) exists in different ionic forms in aqueous solution. When solution pH is greater than 6, it presents as CrO_4^{2-}; when pH is ranging from 1.0 – 6.0, it exists as $Cr_2O_7^{2-}$ and $HCrO_4^{-}$ [35], which are favorably adsorbed by BZ-APS24h at low pH because of the electrostatic attraction. When the initial pH was from 2 to 6, equilibrium solution pH was found to increase. Increase in pH can be explained by solute–sorbent binding reactions. When the oxo groups on the surface of the biochar are in contact with the solution, the following reaction occurs [36]:

$$C_xO + HCrO_4^- + 2H_2O \rightarrow C_xO_2H_3CrO_3^+ + 2OH^- \quad (6\text{-}1)$$

$$CrO_4^{2-} + 2H^+ \rightarrow Cr_2O_7^{2-} + H_2O \ . \quad (6\text{-}2)$$

On the contrary, for adsorption of Cd(II) alone, the adsorbed amount increased as

the pH increased from 2 to 5. When the initial pH was changed from 5 to 7, the equilibrium pH of the solution dropped to 3.5-4, while the adsorption amount did not significantly change. In the adsorption process of Cd(II) on biochar, Cd(II) ions were exchanged with protons on the surface carboxy group or other functional groups of the oxidized biochar, causing the decrease in the solution pH; when the pH of the solution dropped to a certain level, the ion exchange was no longer progressed. Through the adjustment of the equilibrium pH of the solution by adding NaOH to the solution, the effect of equilibrium pH on the adsorption amount of Cd(II) was obtained, as shown in **Fig. 6-5(c)**. It can also be seen from **Fig. 6-5(c)** that the equilibrium pH had a greater effect on Cd(II) adsorption than initial pH. As the equilibrium pH increased, the adsorbed amount of Cd(II) increased. The higher pH may lead to the transformation of −COOH groups present in the biochar into $-COO^-$, which was conductive to the adsorption of Cd^{2+}.

Fig. 6-5(d) shows the effect of initial pH in mixed solution of Cr(VI) and Cd(II). It could be clearly seen that the co-adsorption of Cd(II) and Cr(VI) was the same as adsorption of the Cr(VI) or Cd(II), and the pH change before and after adsorption was not significant. With the increase of the initial pH, the adsorbed amount of Cd(II) in the mixed solution gradually increased, while the adsorbed amount of Cr(VI) gradually decreased. Usually, the pH in natural water is about 6. Therefore, the initial pH value of 6 was selected for the further studies on Cr(VI) and Cd(II) ions adsorption.

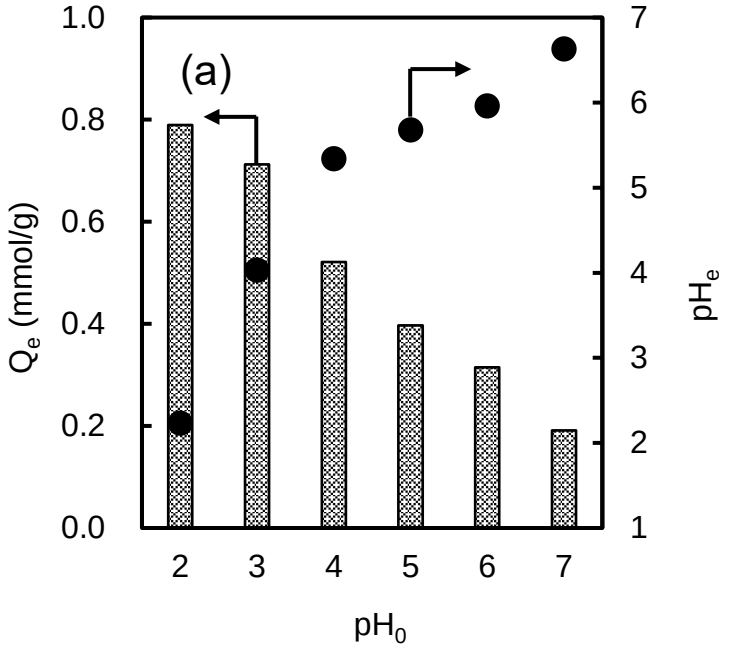
(a)
1.0
0.8
0.6
0.4
0.2
0.0
Q_e (mmol/g)
7
6
5
4
3
2
1
pH_e
2
3
4
5
6
7
pH_0

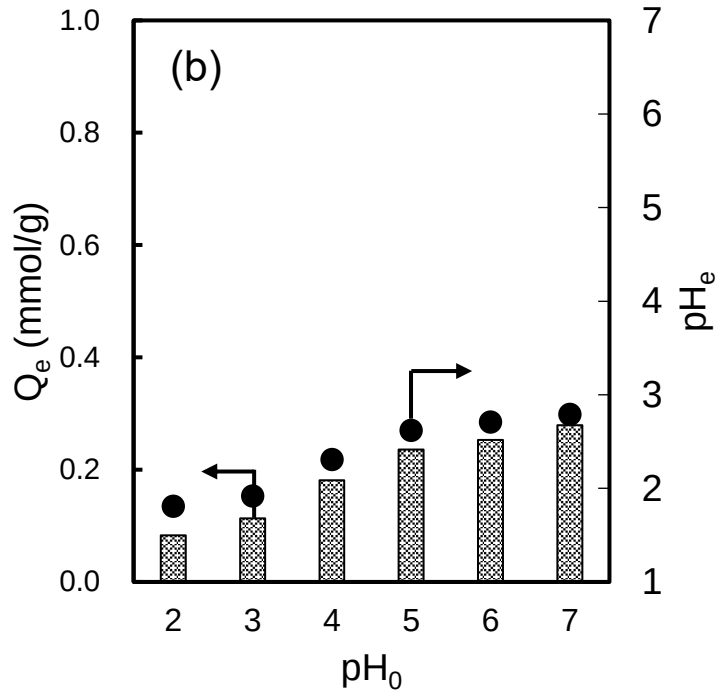
(b)
1.0
0.8
0.6
0.4
0.2
0.0
Q_e (mmol/g)
7
6
5
4
3
2
1
pH_e
2
3
4
5
6
7
pH_0

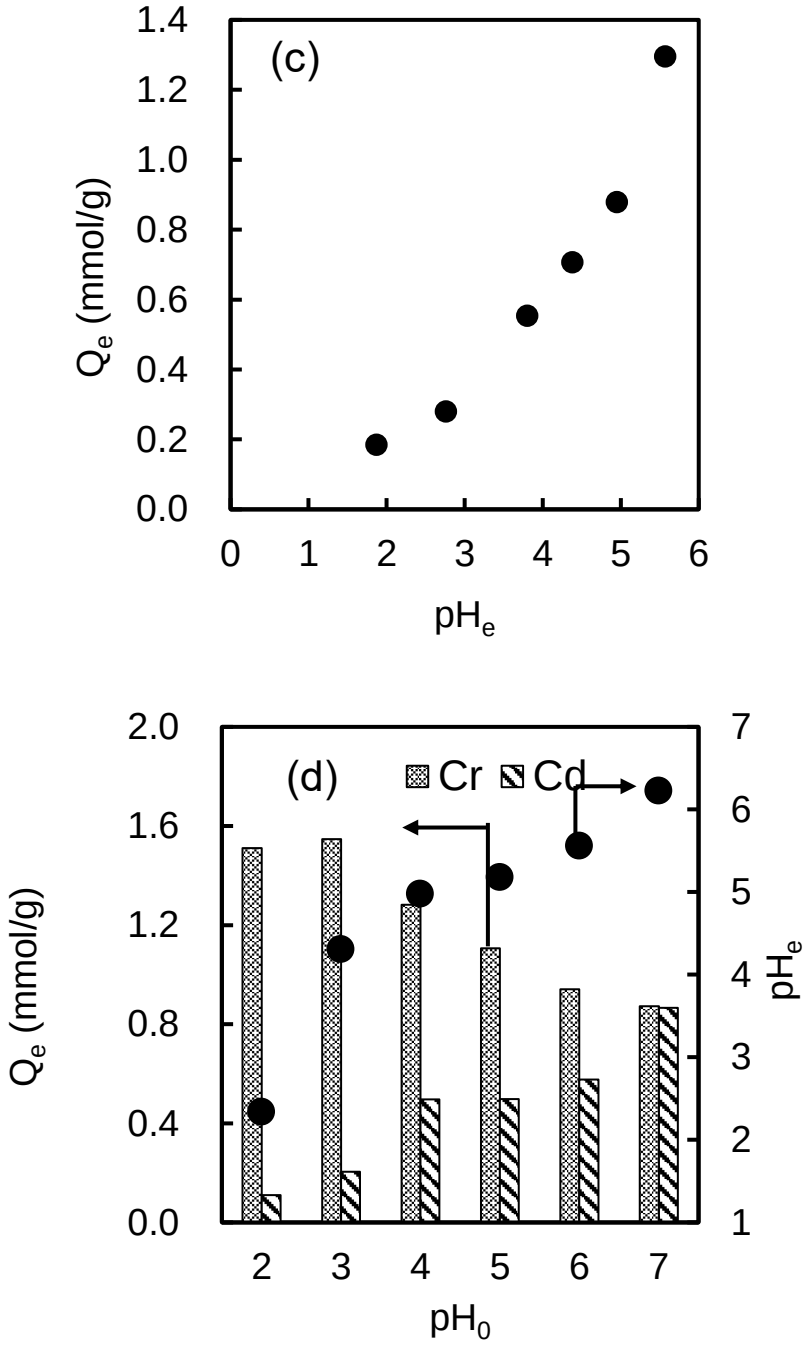

Fig. 6-5 Effect of initial pH value on Cr(VI) removal (a); effect of initial pH value on Cd(II) removal (b); effect of equilibrium pH value on Cd(II) removal (c); effect of initial pH value on Cd(II) and Cr(VI) simultaneous removal (d).

6.3.4 Effect of contact time and adsorption kinetics

The contact time between the adsorbate and the adsorbent is an important factor affecting the water treatment. It can be seen from **Fig. 6-5** that the pH of the solution changes with the adsorption, so it is important to study the change of pH with time during the adsorption process. **Fig. 6-6** shows the time course of removal efficiency of Cr(VI) and Cd(II) together with the change of pH. It can be seen that both the Cd(II) and Cr(VI) adsorption equilibriums can be reached within 180 min in Cd(II) solution, Cr(VI) solution and mixed solution of Cd(II) and Cr(VI) mixed solution. As shown in **Fig. 6-6(a1)** and **Fig. 6-6(a2)**, for the removal of Cd(II) alone, the pH of the solution dropped from 6.1 to 3.3 since the start of adsorption is due to the exchange of Cd^{2+} and H^{+} ions during adsorption. When the adsorption reached equilibrium, the pH of the solution tended to be stable at 3.3. In contrast, it can be seen from **Fig. 6-6(b1)** and **Fig. 6-6(b2)** that for the removal of Cr(VI) alone, the pH of the solution first decreased from 6.1 to 5.5 and then gradually increased to 5.7, which was a less significant change compared with the adsorption of Cd(II) alone. In the mixed solution of Cd(II) and Cr(VI), **Fig. 6-6(c1)** indicates that both Cr(VI) and Cd(II) were well adsorbed, and **Fig. 6-6(c2)** indicates that the pH of the solution dropped rapidly from 6.1 to 4.4 within 20 minutes, then gradually rose to 5.0 from 20 minutes to 480 minutes. This is mainly due to that the adsorption of cadmium first led to a decrease in pH, and then the adsorption of chromium caused the rise of pH.

The results of the kinetic analysis are shown in **Tables 6-3** and **6-4**. The pseudo-first-order model has lower correlation coefficient (R^2) compared to that of the pseudo-

second-order models, and all R^2 values are greater than 0.99 for pseudo-second-order models. This indicates that the pseudo-second-order kinetic model is more appropriate than pseudo-first-order kinetic model in describing the adsorption process of Cd(II) and Cr(VI) onto BZ-APS24h. These facts suggest that the adsorption behavior is mainly governed by diffusion control mechanism in Cd(II) solution, Cr(VI) solution and mixed solution of Cd(II) and Cr(VI) [37, 38].

Table 6-3 Kinetic parameters for single Cd(II) and Cr(VI) adsorption

	Pseudo-first-order			Pseudo-second-order		
	Q_e (mmol/g)	k_1 (min^{-1})	R^2	Q_e (mmol/g)	k_2 (g/mmol • min)	R^2
Cd(II)	1.34	0.07	0.766	0.26	0.67	0.996
Cr(VI)	1.78	0.06	0.812	0.60	3.25	0.997

Table 6-4 Kinetic parameters for simultaneous Cd(II) and Cr(VI) adsorption

	Pseudo-first-order			Pseudo-second-order		
	Q_e (mmol/g)	k_1 (min^{-1})	R^2	Q_e (mmol/g)	k_2 (g/mmol • min)	R^2
Cd(II)	1.42	0.24	0.964	0.47	0.52	0.999
Cr(VI)	2.76	0.14	0.721	0.84	0.19	0.999

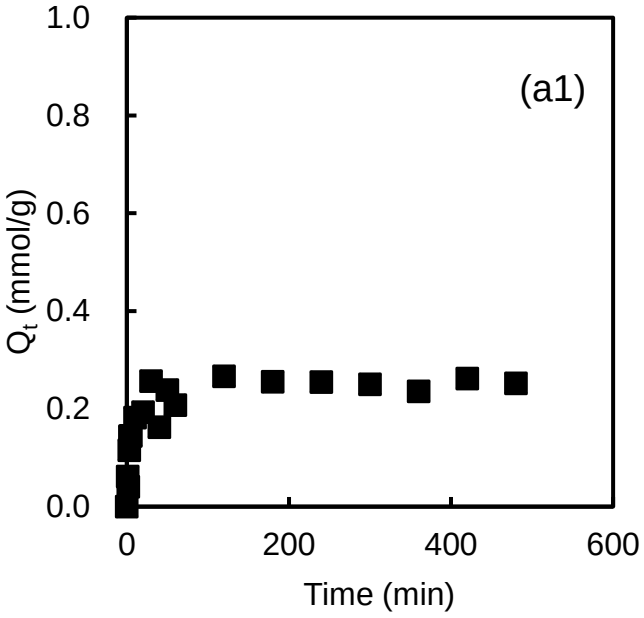
(a1)
1.0
0.8
0.6
0.4
0.2
0.0
Q_t (mmol/g)
0
200
400
600
Time (min)

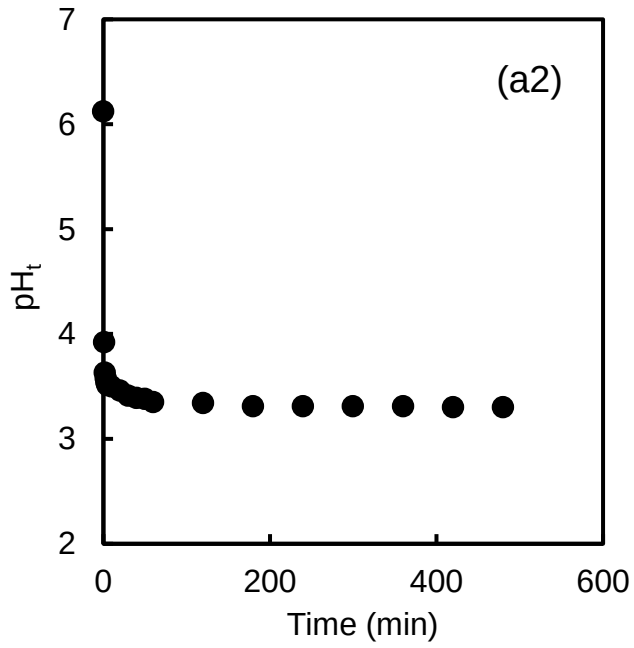
(a2)
7
6
5
4
3
2
pH_t
0
200
400
600
Time (min)

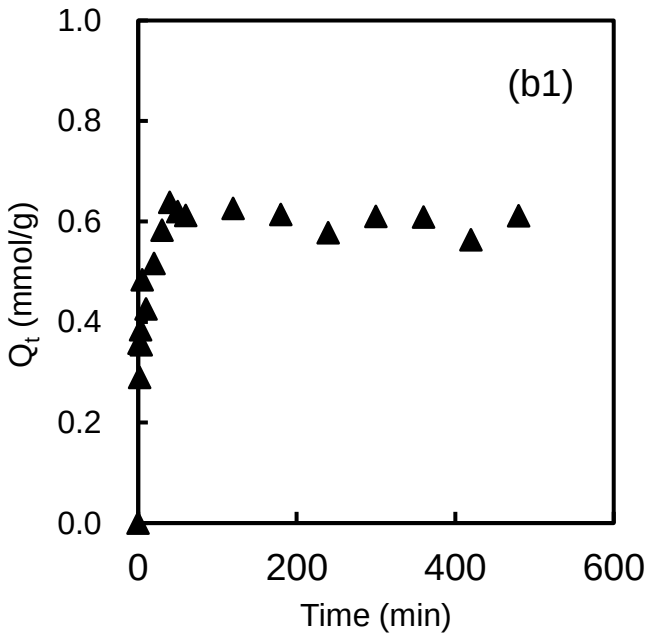
(b1)
1.0
0.8
0.6
0.4
0.2
0.0
Q_t (mmol/g)
0
200
400
600
Time (min)

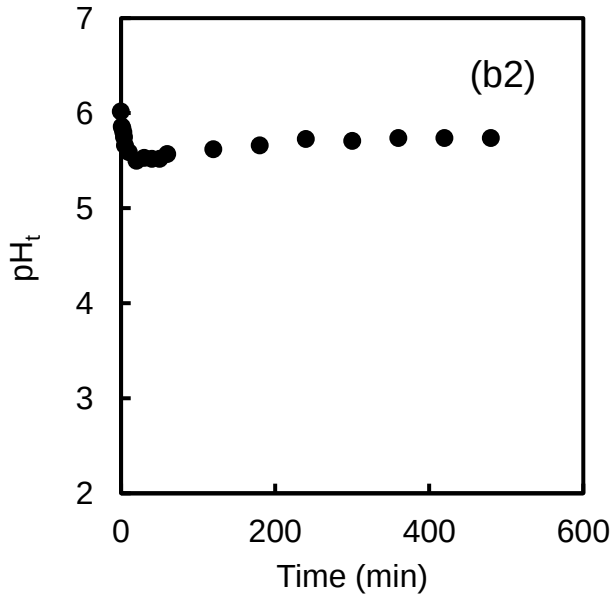
(b2)
7
6
5
4
3
2
pH_t
0
200
400
600
Time (min)

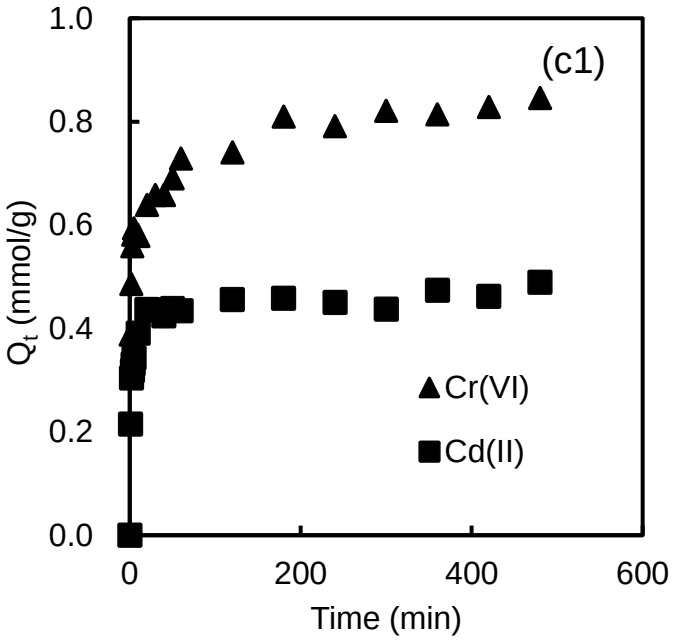

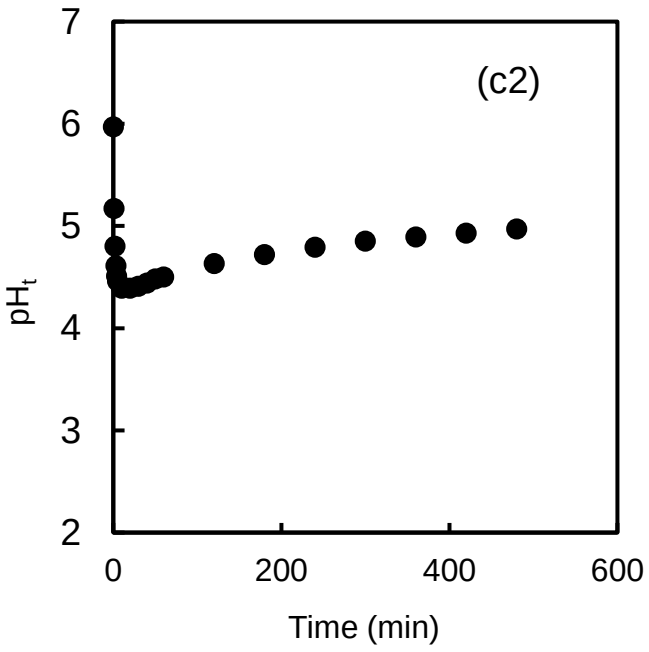

Fig.6-6 Effect of contact time: (a1) changes in adsorption quantities in single Cd(II) removal; (a2) changes in solution pH for single Cd(II) removal; (b1) changes in adsorption quantities for Single Cr(VI) removal; (b2) changes in solution pH for Single Cr(VI) removal; (c1) changes in adsorption quantities for Cd(II) and Cr(VI) simultaneous removal; (c2) changes in solution pH for Cd(II) and Cr(VI) simultaneous removal.

6.3.5 Equilibrium adsorption isotherms

The adsorption isotherms of individual Cr(VI) and Cd(II) on BZ-APS24h are shown in **Fig. 6-7**. Langmuir and Freundlich models were applied to investigate the adsorption process of Cr(VI) and Cd(II) at 25°C, 35°C and 45°C. The different isotherm constants determined are shown in **Tables 6-5** and **6-6**. The Langmuir model was more fitted than the Freundlich model, with R^2 ranging from 0.989 to 0.998 for the BZ-APS24h. The Langmuir isotherm is usually used to describe the mono-layer adsorption on a homogenous surface. Therefore, the adsorption of Cr(VI) and Cd(II) on the BZ-APS24h should be monolayer, showing uniform surface properties [39].

By comparing the maximum adsorption capacity (X_m) at different temperatures, it can be seen that the adsorption amount of Cd(II) decreased with the increase of temperature, and the maximum adsorption amount of Cr(VI) increased with the increase of temperature. This indicates that the adsorption of Cr(VI) by oxidized biochar is an endothermic reaction, while the adsorption of Cd(II) is an exothermic reaction. This result is consistent with the previous reports [40, 41].

Table 6-5 Langmuir and Freundlich adsorption isotherm parameters of Cd(II) in aqueous solution

	Langmuir model			Freundlich model		
Temperature	X_m (mmol/g)	K_1 (L/mmol)	R^2	K_f ([mmol/g][mmol/L])^n	*1/n*	R^2
25℃	0.27	33.9	0.998	0.022	0.27	0.787
35℃	0.21	28.5	0.996	0.027	0.16	0.944
45℃	0.15	25.6	0.989	0.012	0.09	0.916

Table 6-6 Langmuir and Freundlich adsorption isotherm parameters of Cr(VI) in aqueous solution

	Langmuir model			Freundlich model		
Temperature	X_m (mmol/g)	K_1 (L/mmol)	R^2	K_f ([mmol/g][mmol/L])^n	*1/n*	R^2
25℃	0.65	8.36	0.998	0.20	0.17	0.976
35℃	0.76	9.43	0.998	0.28	0.19	0.972
45℃	0.86	11.19	0.997	0.35	0.21	0.934

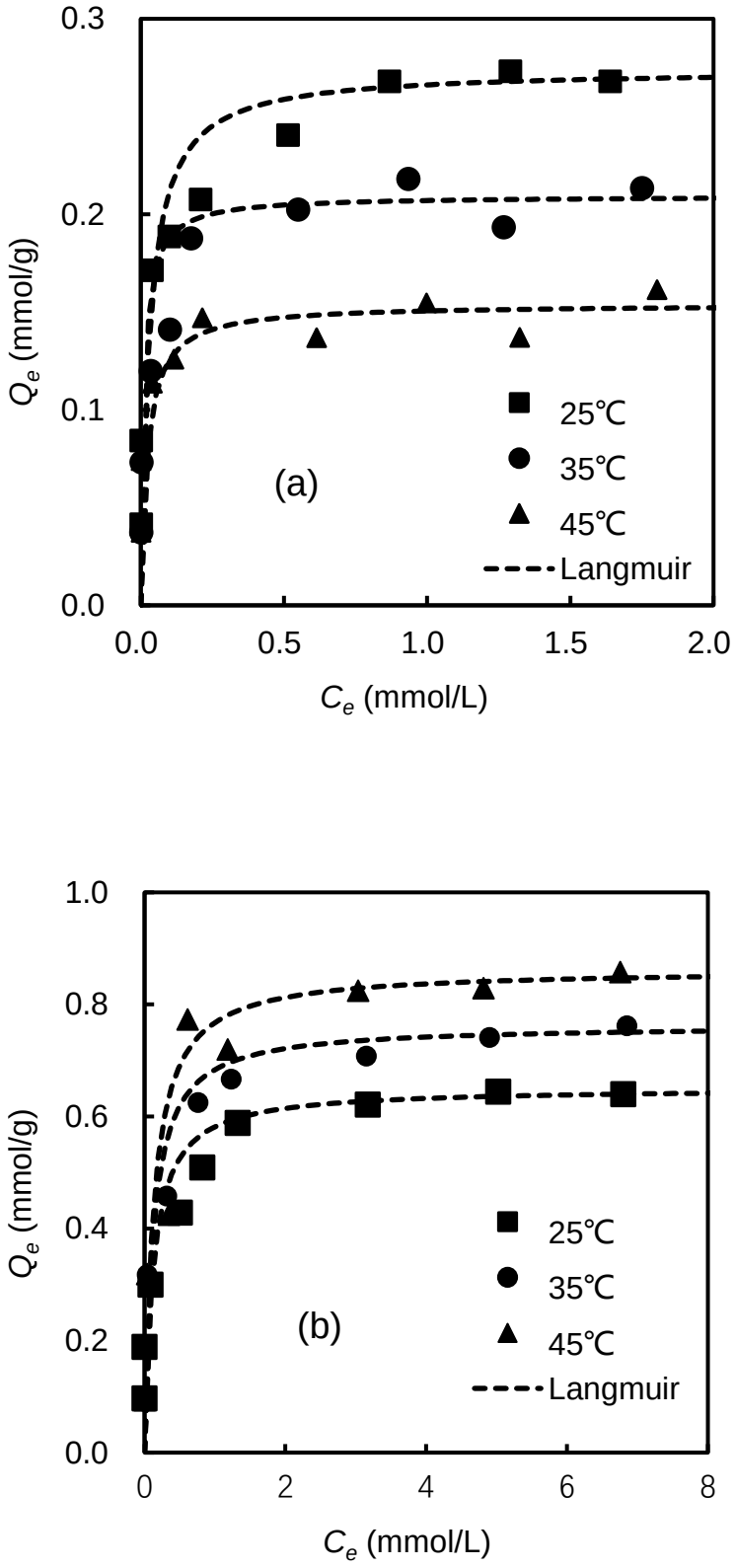

Fig. 6-7 Adsorption isotherms of Cd(II) onto BZ-APS24h (a) and BZ-APS24h (b).

6.3.6 Mutual influence of Cd(II) and Cr(VI)

Fig. 6-8(a) shows the results of adsorption experiments for Cr(VI) solution containing different concentrations of Cd(II). As the Cd(II) concentration in the solution increased from 0 to 400 mg/L, the adsorbed amount of Cr(VI) increased from 0.62 to 0.97 mmol/g, and the equilibrium pH dropped from 5.5 to 4.1. This may be due to that the adsorption of Cd(II) led to a decreased solution pH that was favorable for the adsorption of Cr(VI), so the presence of Cd(II) is beneficial to the adsorption of Cr(VI) on oxidized biochar. Similarly, the solution pH rose due to the adsorption and reduction of Cr(VI), as the Cd(II) concentration in the solution increased from 0 to 400 mg/L, the equilibrium pH went up from 3.0 to 5.3, and the adsorbed amount of Cr(VI) increased from 0.28 to 0.79 mmol/g, as shown in **Fig. 6-8(b)**. This indicates that the presence of Cr(VI) is contributed to the adsorption of and Cd(II), this is because the adsorption of Cr(VI) results in the increase of solution pH, and the increase of pH is favorable for the adsorption of Cd(II).

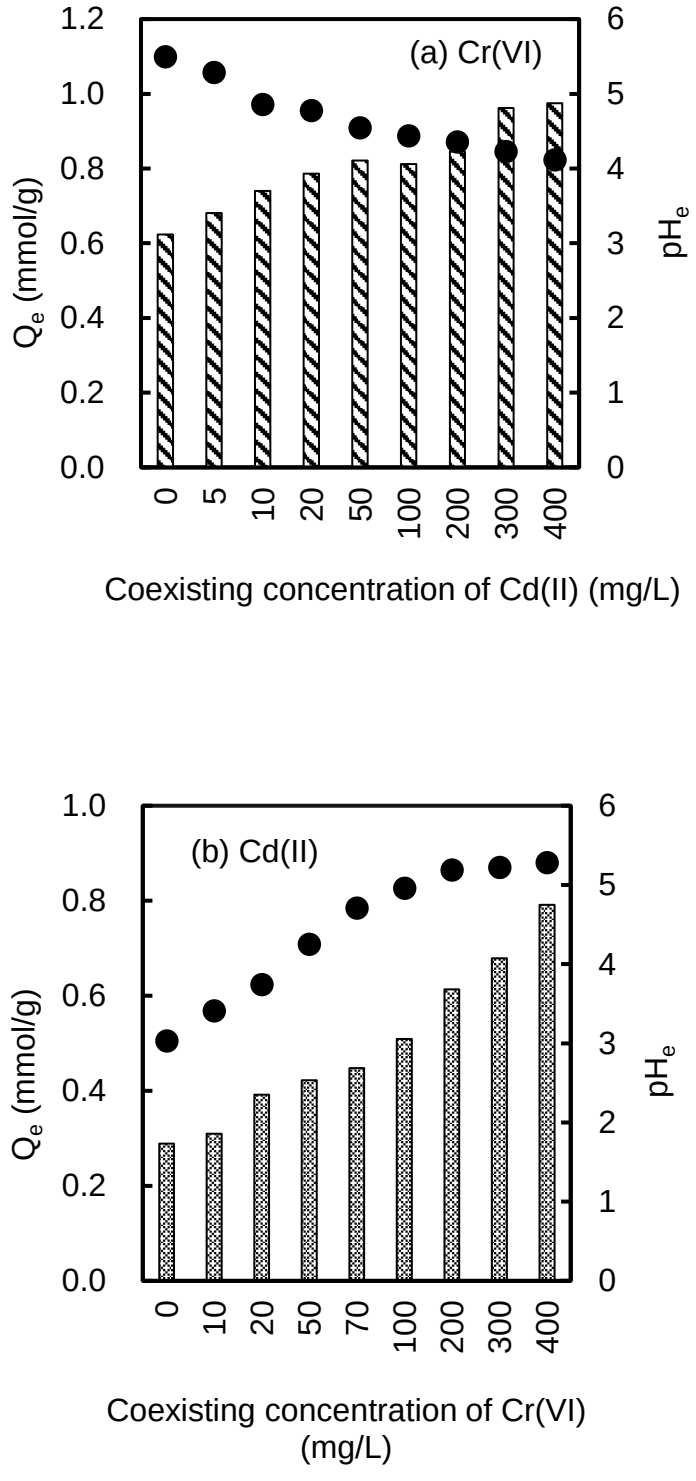

Fig. 6-8 Mutual influence of coexisting Cd(II) and Cr(VI): adsorption of (a) Cr(VI) and (b) Cd(II).

6.3.7 Possible adsorption mechanism

The oxygen functional groups of biochar play a vital role in the adsorption process. The adsorption of Cd(II) onto the BZ-APS24h mainly depends on the oxygen functional groups. As shown in **Fig. 6-9**, the FTIR analysis reveals the surface functional groups of prepared biochar. The peak located at about 1612 cm^{-1} and 3564 cm^{-1} might assign O=C-O and -OH [42], respectively. It can be seen that the peak of -COOH on BZ-APS24h was larger than that on BZ. After the simultaneous adsorption of Cd(II) and Cr(VI), the peaks at -COOH and -OH of BZ-APS became larger. This is due to the strong oxidability of Cr(VI), and the surface of biochar was oxidized in the process of adsorption.

In order to determine the adsorption mechanism, XPS analysis of BZ-APS24h after Cr(VI) and Cd(II) adsorption was performed. As shown in **Fig. 6-10(a)**, the Cd3d5 spectrum was divided into only one peak in 406 eV, which indicates that Cd(II) was adsorbed on the surface of biochar by Cd^{2+} ions. As shown in **Fig. 6-10(b)**, for the removal of Cr(VI), two peaks appeared at 577.8 and 580.4 eV in the Cr2p3/2 region, which might be due to Cr(VI) and Cr(III), respectively [43]. It was found that most of Cr existed in the form of Cr(III) rather than Cr(VI) on the BZ-APS24h surface. The existence of Cr(III) is originated from the reduction of Cr(VI) by the π electrons of the carbocyclic six-membered ring [44]. Based on the analysis in **Fig. 6-6**, it can be concluded that the adsorption rate of Cd(II) was faster, so Cd^{2+} was first exchanged with H^{+} of the -COOH on the surface of the BZ-APS24h, resulting in a drop in the pH of the solution. At the same time, due to the drop in pH of the solution, which became

conducive to the adsorption of Cr(VI). The adsorption of Cr(VI) was also carried out simultaneously. A portion of Cr(VI) was directly adsorbed on the surface of biochar, and another portion of Cr(VI) was reduced to Cr(III). OH^- ions are released during the reduction and adsorption of Cr(VI), and the H^+ ions released during Cd(II) adsorption are neutralized.

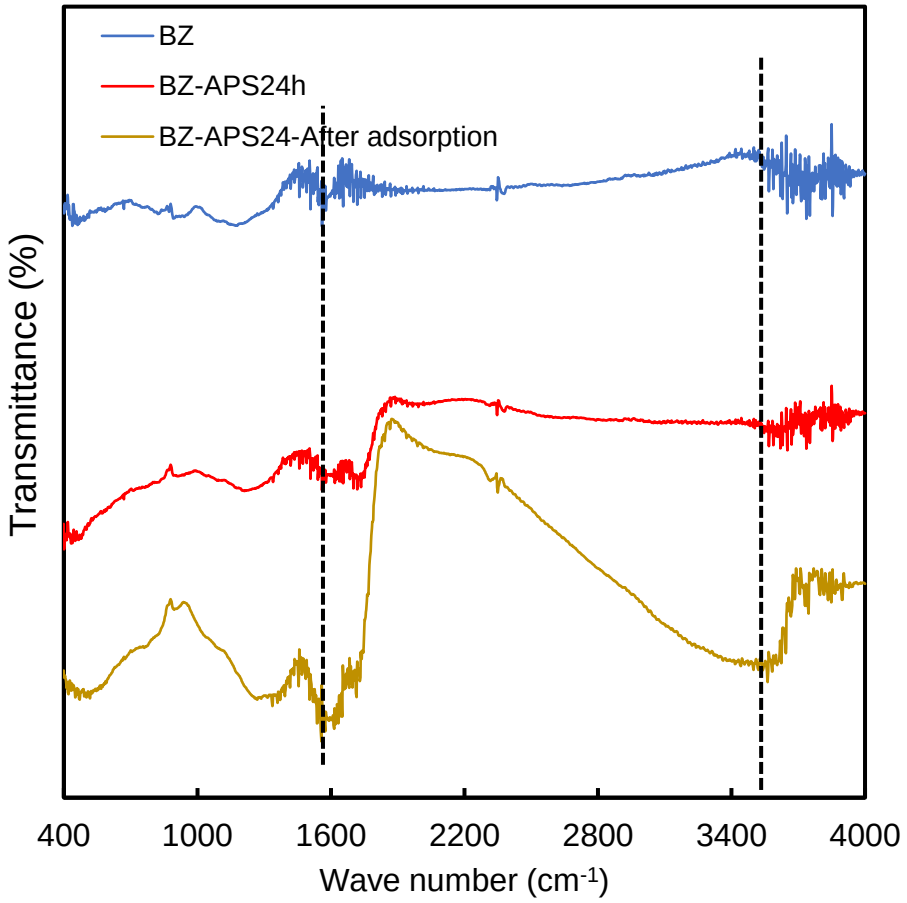

Fig. 6-9 FTIR spectra of BZ, BZ-APS24h and BZ-APS24h after adsorption

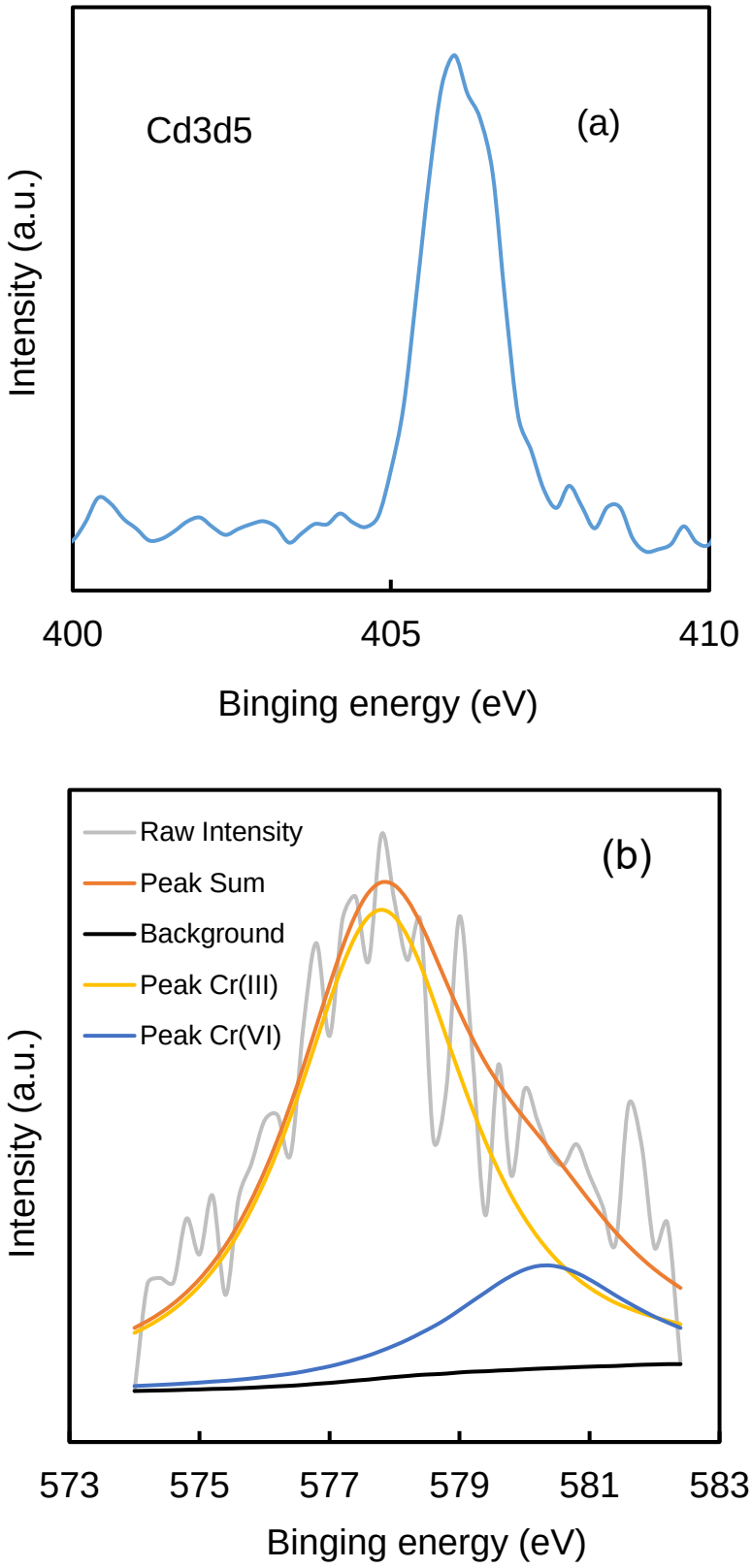

Fig. 6-10 XPS survey spectra of Cd3d5 (a) and Cr2p3/2 (b) for the BZ-APS24h after adsorption.

6.4 Conclusion

In summary, oxidized biochar (BZ-APS24h) was successfully prepared using bamboo. The prepared BZ-APS24h is rich in oxygen-containing functional groups and reserves a high specific surface area. The BZ-APS24h exhibited excellent adsorption performance for the removal Cd(II) and Cr(VI), with adsorption capacity of 0.65 mmol/g (33.8 mg/g) for removal of Cr(VI) removal, and 0.27 mmol/g (30.3 mg/g) for removal of Cd(II) at 25°C. BZ-APS24h is capable of simultaneously adsorbing Cd(II) and Cr(VI) in a mixed solution of Cd(II) and Cr(VI). The pH of the solution has a great influence on the adsorption process. Cd(II) adsorption causes a decrease in pH, while adsorption of Cr(VI) causes an increase in pH. Acidic pH is favorable for the adsorption of Cr(VI), while neutral pH is favorable for the adsorption of Cd(II). The coexistence of Cd(II) and Cr(VI) can promote the adsorption of the other ion. Thus, BZ-APS24h is demonstrated to be an excellent adsorbent for simultaneous removal of Cd(II) and Cu(VI) from aqueous solution.

References

[1] K. Selvi, S. Pattabhi, K. Kadirvelu, Removal of Cr(VI) from aqueous solution by adsorption onto activated carbon, Bioresour. Technol. 80 (2001) 87-89.

[2] F.Y. Wang, H. Wang, J.W. Ma, Adsorption of cadmium (II) ions from aqueous solution by a new low-cost adsorbent—Bamboo charcoal, J. Hazard. Mater. 177 (2010) 300-306.

[3] Y.S. Ok, A.R. Usman, S.S. Lee, S.A.A. El-Azeem, B. Choi, Y. Hashimoto, J.E. Yang,

Effects of rapeseed residue on lead and cadmium availability and uptake by rice plants in heavy metal contaminated paddy soil, Chemosphere 85 (2011) 677-682.

[4] W. Qi, Y. Zhao, X. Zheng, M. Ji, Z. Zhang, Adsorption behavior and mechanism of Cr (VI) using Sakura waste from aqueous solution, Appl. Surf. Sci. 360 (2016) 470-476.

[5] X. Lv, J. Xu, G. Jiang, X. Xu, Removal of chromium (VI) from wastewater by nanoscale zero-valent iron particles supported on multiwalled carbon nanotubes, Chemosphere 85 (2011) 1204-1209.

[6] H. Shen, Y.-T. Wang, Simultaneous chromium reduction and phenol degradation in a coculture of Escherichia coli ATCC 33456 and Pseudomonas putida DMP-1, Appl. Environ. Microbiol. 61 (1995) 2754-2758.

[7] X. Yi, F. Xiao, X. Zhong, Y. Duan, K. Liu, C. Zhong, A Ca^{2+} chelator ameliorates chromium (VI)-induced hepatocyte L-02 injury via down-regulation of voltage-Dependent anion channel 1 (VDAC1) expression, Environ. Toxicol. Pharmacol. 49 (2017) 27-33.

[8] Q. Chen, J. Zheng, L. Zheng, Z. Dang, L. Zhang, Classical theory and electron-scale view of exceptional Cd (II) adsorption onto mesoporous cellulose biochar via experimental analysis coupled with DFT calculations, Chem. Eng. J. 350 (2018) 1000-1009.

[9] X. Zhang, L. Lv, Y. Qin, M. Xu, X. Jia, Z. Chen, Removal of aqueous Cr (VI) by a magnetic biochar derived from Melia azedarach wood, Bioresour. Technol. 256 (2018) 1-10.

[10] S.J. Ye, G.M. Zeng, H.P. Wu, C. Zhang, J. Liang, J. Dai, Z.F. Liu, W.P. Xiong, J. Wan, P.A. Xu, M. Cheng, Co-occurrence and interactions of pollutants, and their impacts on soil remediation-A review, Crit. Rev. Env. Sci. Technol. 47 (2017) 1528-1553.

[11] A.A. Nezhad, M. Alimoradi, M. Ramezani, Highly efficient removal of Cd (II) ions by composite of GO and layered double hydroxide composite, Mater. Res. Express 6 (2018) 015015.

[12] Y. Huang, X. Lee, F.C. Macazo, M. Grattieri, R. Cai, S.D. Minteer, Fast and efficient removal of chromium (VI) anionic species by a reusable chitosan-modified multi-walled carbon nanotube composite, Chem. Eng. J. 339 (2018) 259-267.

[13] S.P. Verma, B. Sarkar, Simultaneous removal of Cd (II) and p-cresol from wastewater by micellar-enhanced ultrafiltration using rhamnolipid: Flux decline, adsorption kinetics and isotherm studies, J. Environ. Manage. 213 (2018) 217-235.

[14] L. Li, J. Zhang, Y. Li, C. Yang, Removal of Cr (VI) with a spiral wound chitosan nanofiber membrane module via dead-end filtration, J. Membr. Sci. 544 (2017) 333-341.

[15] L. Alvarado, I.R. Torres, A. Chen, Integration of ion exchange and electrodeionization as a new approach for the continuous treatment of hexavalent chromium wastewater, Sep. Purif. Technol. 105 (2013) 55-62.

[16] L. Dong, L.a. Hou, Z. Wang, P. Gu, G. Chen, R. Jiang, A new function of spent activated carbon in BAC process: Removing heavy metals by ion exchange mechanism, J. Hazard. Mater. 359 (2018) 76-84.

[17] R. Xiao, J.J. Wang, R. Li, J. Park, Y. Meng, B. Zhou, S. Pensky, Z. Zhang, Enhanced sorption of hexavalent chromium [Cr (VI)] from aqueous solutions by diluted sulfuric acid-assisted MgO-coated biochar composite, Chemosphere 208 (2018) 408-416.

[18] L. Shen, Z. Jin, D. Wang, Y. Wang, Y. Lu, Enhance wastewater biological treatment through the bacteria induced graphene oxide hydrogel, Chemosphere 190 (2018) 201-210.

[19] Y. Zuo, G. Chen, G. Zeng, Z. Li, M. Yan, A. Chen, Z. Guo, Z. Huang, Q. Tan, Transport, fate, and stimulating impact of silver nanoparticles on the removal of Cd (II) by Phanerochaete chrysosporium in aqueous solutions, J. Hazard. Mater. 285 (2015) 236-244.

[20] L. Ling, W.-J. Liu, S. Zhang, H. Jiang, Achieving high-efficiency and ultrafast removal of Pb (II) by one-pot incorporation of a N-doped carbon hydrogel into FeMg layered double hydroxides, J. Mater. Chem.A 4 (2016) 10336-10344.

[21] S. Ye, M. Yan, X. Tan, J. Liang, G. Zeng, H. Wu, B. Song, C. Zhou, Y. Yang, H. Wang, Facile assembled biochar-based nanocomposite with improved graphitization for efficient photocatalytic activity driven by visible light, Appl. Catal., B 250 (2019) 78-88.

[22] B. Jiang, Y. Lin, J.C. Mbog, Biochar derived from swine manure digestate and applied on the removals of heavy metals and antibiotics, Bioresour. Technol. 270 (2018) 603-611.

[23] S. Ye, G. Zeng, H. Wu, C. Zhang, J. Dai, J. Liang, J. Yu, X. Ren, H. Yi, M. Cheng,

Biological technologies for the remediation of co-contaminated soil, Crit. Rev. Biotechnol. 37 (2017) 1062-1076.

[24] S.J. Ye, G.M. Zeng, H.P. Wu, J. Liang, C. Zhang, J. Dai, W.P. Xiong, B. Song, S.H. Wu, J.F. Yu, The effects of activated biochar addition on remediation efficiency of co-composting with contaminated wetland soil, Resour. Conserv. Recycl. 140 (2019) 278-285.

[25] D. Jiang, B. Chu, Y. Amano, M. Machida, Removal and recovery of phosphate from water by Mg-laden biochar: Batch and column studies, Colloids Surf., A 558 (2018) 429-437.

[26] Y. Su, X. Sun, X. Zhou, C. Dai, Y. Zhang, Zero-valent iron doped carbons readily developed from sewage sludge for lead removal from aqueous solution, J. Environ. Sci. 36 (2015) 1-8.

[27] R. Li, L. Zhang, P. Wang, Rational design of nanomaterials for water treatment, Nanoscale 7 (2015) 17167-17194.

[28] M.F. El-Banna, A. Mosa, B. Gao, X. Yin, Z. Ahmad, H. Wang, Sorption of lead ions onto oxidized bagasse-biochar mitigates Pb-induced oxidative stress on hydroponically grown chicory: Experimental observations and mechanisms, Chemosphere 208 (2018) 887-898.

[29] M. Machida, B. Fotoohi, Y. Amamo, T. Ohba, H. Kanoh, L. Mercier, Cadmium (II) adsorption using functional mesoporous silica and activated carbon, J. Hazard. Mater. 221 (2012) 220-227.

[30] W.J. Yin, Z.Z. Guo, C.C. Zhao, J.T. Xu, Removal of Cr(VI) from aqueous media

by biochar derived from mixture biomass precursors of Acorus calamus Linn. and feather waste, J. Anal. Appl. Pyrolysis 140 (2019) 86-92.

[31] Q. Tao, Y.X. Chen, J.W. Zhao, B. Li, Y.H. Li, S.Y. Tao, M. Li, Q.Q. Li, Q. Xu, Y.D. Li, H.X. Li, B. Li, Y.L. Chen, C.Q. Wang, Enhanced Cd removal from aqueous solution by biologically modified biochar derived from digestion residue of corn straw silage, Sci. Total Environ. 674 (2019) 213-222.

[32] D. Wang, G. Zhang, Z. Dai, L. Zhou, P. Bian, K. Zheng, Z. Wu, D. Cai, Sandwich-like nano-system for simultaneous removal of Cr(VI) and Cd(II) from water and soil, ACS Appl. Mater. Interfaces 10 (2018) 18316-18326.

[33] Z.-H. Diao, J.-J. Du, D. Jiang, L.-J. Kong, W.-Y. Huo, C.-M. Liu, Q.-H. Wu, X.-R. Xu, Insights into the simultaneous removal of Cr^{6+} and Pb^{2+} by a novel sewage sludge-derived biochar immobilized nanoscale zero valent iron: Coexistence effect and mechanism, Sci. Total Environ. 642 (2018) 505-515.

[34] V.C. Srivastava, I.D. Mall, I.M. Mishra, Adsorption of toxic metal ions onto activated carbon: Study of sorption behaviour through characterization and kinetics, Chem. Eng. Process. Process Intensif. 47 (2008) 1269-1280.

[35] M. Goswami, L. Borah, D. Mahanta, P. Phukan, Equilibrium modeling, kinetic and thermodynamic studies on the adsorption of Cr(VI) using activated carbon derived from matured tea leaves, J. Porous Mater. 21 (2014) 1025-1034.

[36] S. Mor, K. Ravindra, N. Bishnoi, Adsorption of chromium from aqueous solution by activated alumina and activated charcoal, Bioresour. Technol. 98 (2007) 954-957.

[37] Y. Zhou, Q. Jin, T. Zhu, Y. Akama, Adsorption of chromium (VI) from aqueous

solutions by cellulose modified with β-CD and quaternary ammonium groups, J. Hazard. Mater. 187 (2011) 303-310.

[38] M. Bhaumik, A. Maity, V. Srinivasu, M.S. Onyango, Enhanced removal of Cr (VI) from aqueous solution using polypyrrole/Fe_3O_4 magnetic nanocomposite, J. Hazard. Mater. 190 (2011) 381-390.

[39] K.Y. Foo, B.H. Hameed, Insights into the modeling of adsorption isotherm systems, Chem. Eng. J. 156 (2010) 2-10.

[40] J. Sun, Z. Zhang, J. Ji, M. Dou, F. Wang, Removal of Cr6+ from wastewater via adsorption with high-specific-surface-area nitrogen-doped hierarchical porous carbon derived from silkworm cocoon, Appl. Surf. Sci. 405 (2017) 372-379.

[41] Y. Shi, T. Zhang, H. Ren, A. Kruse, R. Cui, Polyethylene imine modified hydrochar adsorption for chromium (VI) and nickel (II) removal from aqueous solution, Bioresour. Technol. 247 (2018) 370-379.

[42] P.F.R. Ortega, J.P.C. Trigueiro, M.R. Santos, A.M.L. Denadai, L.C.A. Oliveira, A.P.C. Teixeira, G.G. Silva, R.L. Lavall, Thermodynamic Study of Methylene Blue Adsorption on Carbon Nanotubes Using Isothermal Titration Calorimetry: A Simple and Rigorous Approach, J. Chem. Eng. Data 62 (2017) 729-737.

[43] D. Park, Y.-S. Yun, J.H. Jo, J.M. Park, Mechanism of hexavalent chromium removal by dead fungal biomass of Aspergillus niger, Water Res. 39 (2005) 533-540.

[44] M. Li, Y. Gong, A. Lyu, Y. Liu, H. Zhang, The applications of populus fiber in removal of Cr(VI) from aqueous solution, Appl. Surf. Sci. 383 (2016) 133-141.

Chapter 7 Conclusions and outlooks

7.1 Conclusions

In this study, bamboo and bean dregs as biomass materials were developed as raw materials of activated carbon to adsorb Cd(II) and Cr(VI). Meanwhile, commercially available activated carbon CGP was also activated to increase the adsorption capacity of Cr(VI). This study has mainly achieved the following conclusions.

(1) Activated carbon BAP with high specific surface area (1470 m^2/g) and high mesopore volume (1.64 cm^3/g) can be prepared by NaOH pretreatment and H_3PO_4 activation of bamboo. After oxidation of BAP, more oxygen-containing functional groups were supported on the surface. The Na-intercalated oxidized activated carbon BAP1-Na could keep the pH of the solution constant during the adsorption process, and it was very effective for the removal of Cd(II). Compared with BAC, BAP1-Na has a faster adsorption rate for Cd(II), which is attributed to the high mesoporous volume of BAP. After studying the effect of pH on the solution, it was found that the equilibrium pH of the solution had a great influence on the adsorption amount. With the increase of pH, the adsorption amount of Cd(II) on activated carbon decreased.

(2) The specific surface area of the commercially available activated carbon CGP can be greatly improved by KOH activation, thereby greatly increasing the adsorption amount of Cr(VI). The activated carbon CGP-K3-800 adsorbent prepared by KOH activation has an adsorption capacity of 4.99 mmol/g, which is 1.64 times that of CGP. By studying the effect of pH, it was found that CGP-K3-800 had better adsorption under acidic conditions. The adsorption reaction is in accordance with the Langmuir model,

and the increase in temperature can enhance the adsorption capacity of CGP. CGP-K3-800 exhibits better regeneration performance than CGP. As the reuse time increases, the surface of the activated carbon is gradually oxidized, which leads to a gradual decrease in the reducing ability. At the same time, this also shows that the activated carbon after oxidation still has a strong adsorption capacity for Cr(VI).

(3) Nitrogen-doped biochar adsorbent BZ-9.5AG-30min was successfully prepared by using $ZnCl_2$ activation and ammonia treatment to remove heavy metal Cr(VI). Cr(VI) removal experiments show that BZ-9.5AG-30min has a higher Cr(VI) adsorption capacity (4.31 mmol/g), which is much higher than previously reported. The effect of pH indicates that the maximum adsorption capacity of BZ-9.5AG-30min for Cr(VI) is pH2. The adsorption reaction accords with the Langmuir model, and the kinetic analysis shows that the adsorption of Cr(VI) is good by the pseudo second-order model fitted by BZ-9.5AG-30min. After five times regeneration experiments, BZ-9.5AG-30min has good recyclability. Therefore, BZ-9.5AG-30min is expected to be a promising adsorbent for effectively removing hexavalent chromium from wastewater.

(4) The biochar adsorbent BDC-STM30-10.0HT was successfully prepared using bean dregs as a raw material to remove heavy metal Cr(VI). The activation method uses an environmentally friendly steam activation method. Cr(VI) removal experiments show that BDC-STM30-10.0HT has a high adsorption capacity (3.30 mmol/g), which is much higher than BDC-STM30. This may be due to an increase in specific surface area and quaternary nitrogen content. The pH of the solution showed a significant effect on the adsorption of Cr(VI), and the adsorption capacity under acidic conditions was

better. After five times regeneration experiments, BDC-STM30-10.0HT exhibited excellent reusable adsorption properties.

(5) Oxidized biochar (BZ-APS24h) was prepared using bamboo. The prepared BZ-APS24h is rich in oxygen-containing functional groups and retains a high specific surface area. BZ-APS24h can adsorb both Cd(II) and Cr(VI) at the same time, and both exhibit excellent adsorption properties. The adsorption capacities of Cr(VI) and Cd(II) alone were 0.65 mmol/g (33.8 mg/g) and 0.27 mmol/g (30.3 mg/g), respectively. By studying the influence of adsorption time, it is found that the pH value of the solution has a great influence on the adsorption process. Adsorption of Cd(II) leads to a decrease in pH, while adsorption of Cr(VI) leads to an increase in pH. The acidic pH value is favorable for the adsorption of Cr(VI), while the neutral pH value is favorable for the adsorption of Cd(II). Therefore, BZ-APS24h proved to be an excellent adsorbent for simultaneously removing Cd(II) and Cr(VI) from an aqueous solution.

7.2 Outlooks

In this study, bamboo, bean dregs and commercially available activated carbon CGP were used as raw materials to prepare adsorbents to remove heavy metal ions Cd(II) and Cr(VI) in aqueous solution. Different activation methods have been used to achieve a better adsorption effect. However, due to time and condition constraints, further research is needed on the adsorption mechanism. Therefore, it is recommended to conduct further research from the following recommendations:

(1) In the study of Cr(VI) adsorption, only the specific surface area, nitrogen

content and quaternary nitrogen content of activated carbon were investigated for the adsorption of Cr(VI), but the effect on oxygen content was not discussed in detail. Future studies can investigate the effects of oxygen content and the adsorption of oxygen-containing functional groups on Cr(VI) adsorption.

(2) It is conceivable to study the simultaneous adsorption of more heavy metal ions. Due to time constraints, only the simultaneous adsorption of heavy metal ions Cd(II) and Cr(VI) was investigated. In the future research, it is possible to consider adding more kinds of heavy metal ions to study the interaction between ions at the same time of adsorption.

(3) The test water in this study is an ideal and artificial solution prepared from chemicals, and the research on the adsorption of heavy metals in the actual wastewater is insufficient. In order to make the research more practical, actual wastewater can be used for research in future research.

Publication

Journal

[1] B. Chu, Y. Amano, M. Machida, Isotherm, Kinetic and Thermodynamic Studies for Adsorption of Cd(II) from Aqueous Solution onto Mesoporous Bamboo Activated Carbon, Journal of Environmental Chemistry, Vol.27, No.4, pp.163-169, 2017

[2] B. Chu, M. Yamoto, Y. Amano, M. Machida, Adsorption, reduction and regeneration behavior of high surface area activated carbon in removal of Cr(VI), Desalination and Water Treatment 136 (2018) 395-404.

[3] B. Chu, Y. Amano, M. Machida, Preparation of bamboo-based oxidized biochar for simultaneous removal of Cd(II) and Cr(VI) from aqueous solutions, Desalination and Water Treatment 168 (2019) 269-281.

[4] B. Chu, Y. Amano, M. Machida, Preparation of bean dreg derived N-doped activated carbon with high adsorption for Cr(VI), Colloids and Surfaces A: Physicochemical and Engineering Aspects (In Press)

[5] B. Chu, Y. Amano, M. Machida, Adsorption behavior of Cr(VI) by N-doped biochar derived from bamboo, Water Practice and Technology (In Press)

Conference

Bei CHU, Yoshimasa AMANO, Motoi MACHIDA, The adsorption of Cd(II) by bamboo-based oxidized biochar, Internatiol Symposium on Adsorption 2019